Unraveling the migration and search strategies of the slime mold *Physarum polycephalum*

Lucas Tröger
Technische Universität München
Doctoral thesis
Munich 2024

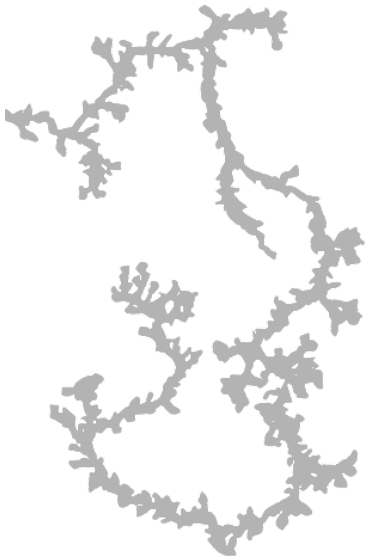

Technische Universität München
TUM School of Natural Sciences

Unraveling the migration and search strategies of the slime mold *Physarum polycephalum*

Lucas Walter Tröger

Vollständiger Abdruck der von der TUM School of Natural Sciences der Technischen Universität München zur Erlangung eines

Doktors der Naturwissenschaften (Dr. rer. nat.)

genehmigten Dissertation.

Vorsitz: Prof. Dr. Julia Herzen

Prüfende der Dissertation:

1. Prof. Dr. Karen Alim
2. Prof. Dr. Friedrich C. Simmel

Die Dissertation wurde am 22.10.2024 bei der Technischen Universität München eingereicht und durch die TUM School of Natural Sciences am 18.11.2024 angenommen.

Acknowledgements

I am grateful to Karen Alim for her unwavering enthusiasm towards my research. Her constant support, advice and guidance have been instrumental in my growth as a researcher and person.

I would like to thank Florian Goirand for his interest in my experiments, which gave my research a new direction, and for his advice, which has greatly supported me.

I am also indebted to several other people: Thanks to Raphaël Voituriez for giving me the opportunity to spend some time in his research group at the Sorbonne Université and for the pleasant collaboration, as well as to Samuel Bell, Julien Brémont, Theresa Jakuszeit and Marc Besse. Thanks to Mathieu Le Verge-Serandour for sharing all his knowledge, which is immense. Thanks to Diana Lenski, a former master's student and by now PhD student in the BPM group, for working with me on the search strategies of *Physarum*. Thanks to Evelyn Packeiser for always taking great care of the lab. Thanks also to the rest of the BPM group and alumni for creating a nice atmosphere, good discussions and much fun: Adrian Büchl, Agnese Codutti, Arne Rosenberg, Daniel Drissler, Elias Huber, Emily Eichenlaub, Fabian Drexel, Fabian Henn, Fatemeh Mirzapour-Shafiyi, Jan Jedryszek, João Ramos, Johnny Tong, Karim Ajmail, Kaspar Wachinger, Katharina Weber, Komal Bhattacharyya, Lara Szeimies, Leonie Karr, Lisa Schick, Marta Conti, Mathias Höfler, Mirna Kramar, Mona Byberg Michelsen, Nico Schramma, Nico Schramma2, Nora Deiringer, Siyu Chen, Sophia Hampe, Swarnavo Basu, Thomas Kunzendorf, Timea Unold, and Valentin Pauli.

Finally, big thanks to Agathe Jouneau and my family for all their support.

Abstract

The survival of a species, from single cells to animals, depends on the fitness of its individuals. To survive and reproduce, organisms face challenges such as finding food, mates, and shelter, which can be classified as search problems. Evolution has produced various means of locomotion, from the amoeboid crawling of microscopic cells to swimming fish and flying insects, which result from complex biological processes at different scales. At the largest scale, these processes lead to exploration of the environment, which can be guided by external cues but involves stochasticity. Is there an emerging order or even search strategies beyond this stochastic motion? And if so, how can we describe them? Statistical physics has developed tools that allow us to quantify the stochasticity of migration trajectories, identify the underlying mechanisms, and model them. Here, we want to ask whether the slime mold *Physarum polycephalum*, a unicellular organism of remarkable size, which is said to show smart behavior, also has search strategies. If so, how does it achieve them and what are the consequences of its large cell size in this context?

To address these questions, we experimentally studied and quantified the migration behavior of *P. polycephalum* plasmodia on the time scale of days in the absence and presence of chemicals like nutrients, individually and collectively. We developed a data-driven model to describe the dynamics of migrating cells. With this, we showed that *P. polycephalum* performs a run-and-tumble movement and achieves superdiffusive migration through self-avoiding behavior mediated by the repellent slime trail it deposits. Our model matches the statistics of the experimental trajectories from migration in the absence and presence of nutrients. Varying organism size, we found that the long-term superdiffusion arises from self-avoidance determined by cell size. This highlights a potential evolutionary advantage for larger plasmodia, which may have driven *P. polycephalum* to evolve into one of the largest cells we know.

Further, we tested the influence of the environment's chemical composition on its migration, with a special focus on its ability to climb a gradient of nutrients, known as chemotaxis. We found that large cells perform more efficient chemotaxis than small cells, once more hinting at an advantage of larger cells. Further, we identified a connection between the environment-dependent morphology of *P. polycephalum* and its migration behavior. We quantified an additional migration phase, which is characterized by protrusion oscillations.

Finally, we investigated the collective dynamics of many plasmodia interacting through their slime trails. Self-interacting random walks are known to exhibit complex dynamics like aging and nontrivial persistence, which influence search efficiency. Our preliminary results provide insights into the search strategy of *P. polycephalum* in a competitive scenario, and the statistical properties of interacting self-avoiding walks.

In summary, we used a physics-based approach to study the search behavior of *P. polycephalum*. We found that it has a rich repertoire of such behaviors, from self-avoiding run-and-tumble motion during free migration to guided migration in chemical gradients and aging dynamics during competitive migration. Our quantification and theoretical descriptions allowed us to interpret them and show that *P. polycephalum*, although unicellular, developed fascinating search dynamics.

Zusammenfassung

Das Überleben einer Art, von einzelnen Zellen bis hin zu Tieren, hängt von der Fitness ihrer Individuen ab. Um zu überleben und sich fortzupflanzen, stehen Organismen vor Herausforderungen wie der Suche nach Nahrung, Partnern und Unterschlupf, die man als Suchprobleme bezeichnen kann. Die Evolution hat verschiedene Arten der Fortbewegung hervorgebracht, vom amöboiden Kriechen mikroskopischer Zellen bis hin zu schwimmenden Fischen und fliegenden Insekten, die das Ergebnis komplexer biologischer Prozesse auf verschiedenen Größenskalen sind. Auf der größten Skala führen diese Prozesse zur Erkundung der Umwelt, die durch äußere Anhaltspunkte geführt werden kann, aber Stochastizität beinhaltet. Gibt es eine emergente Ordnung oder sogar Suchstrategien jenseits dieser stochastischen Bewegung? Und wenn ja, wie können wir sie beschreiben? Die statistische Physik hat Instrumente entwickelt, die es uns ermöglichen, die Stochastizität von Migrationstrajektorien zu quantifizieren, die zugrunde liegenden Mechanismen zu ermitteln und sie zu modellieren. Hier wollen wir fragen, ob der Schleimpilz *Physarum polycephalum*, ein einzelliger Organismus von bemerkenswerter Größe, dem intelligentes Verhalten nachgesagt wird, ebenfalls Suchstrategien hat. Wenn ja, wie erreicht er diese und welche Konsequenzen hat seine große Zellgröße in diesem Zusammenhang?

Um diese Fragen zu beantworten, haben wir das Migrationsverhalten von *P. polycephalum* Plasmodien auf der Zeitskala von Tagen in der Ab- und Anwesenheit von Chemikalien wie Nährstoffen, einzeln und gemeinsam, experimentell untersucht und quantifiziert. Wir entwickelten ein datengestütztes Modell, um die Dynamik der migrierenden Zellen zu beschreiben. Damit konnten wir zeigen, dass *P. polycephalum* eine Run-and-Tumble-Bewegung ausführt und eine superdiffusive Migration durch selbstmeidendes Verhalten erreicht, das durch die repulsive Schleimspur vermittelt wird, die es hinterlässt. Unser Modell stimmt mit den statistischen Daten der experimentellen Trajektorien der Migration in Ab- und Anwesenheit von Nährstoffen überein. In Abhängigkeit von der Größe des Organismus haben wir festgestellt, dass die langfristige Superdiffusion aus einem zellgrößenabhängigen Selbstmeidungsverhalten resultiert. Dies weist auf einen potenziellen evolutionären Vorteil für größere Plasmodien hin, der *P. polycephalum* dazu gebracht haben könnte, sich zu einer der größten uns bekannten Zellen zu entwickeln.

Des Weiteren haben wir den Einfluss der chemischen Zusammensetzung der Umgebung auf die Migration der Zellen untersucht, mit besonderem Augenmerk auf ihre Fähigkeit, einen Nährstoffgradienten zu erklimmen, die so genannte Chemotaxis. Wir fanden heraus, dass große Zellen eine effizientere Chemotaxis durchführen als kleine Zellen, was einmal mehr auf einen Vorteil größerer Zellen hindeutet. Darüber hinaus haben wir einen Zusammenhang zwischen der umweltabhängigen Morphologie von *P. polycephalum* und seinem Migrationsverhalten festgestellt. Wir haben eine zusätzliche Migrationsphase quantifiziert, die durch Protrusionsoszillationen gekennzeichnet ist.

Schließlich untersuchten wir die kollektive Dynamik mehrerer Plasmodien, die über ihre Schleimspuren interagieren. Es ist bekannt, dass selbst-interagierende Zufallsbewegungen komplexe Dynamiken wie Alterung und nicht-triviale Persistenz aufweisen, die die Sucheffizienz beeinflussen. Unsere vorläufigen Ergebnisse geben Einblicke in die Suchstrategie von *P. poly-*

cephalum in einem kompetitiven Szenario und in die statistischen Eigenschaften interagierender selbstmeidender Pfade.

Zusammengefasst haben wir einen physikalischen Ansatz verwendet, um das Suchverhalten von *P. polycephalum* zu untersuchen. Wir fanden heraus, dass es über ein reichhaltiges Repertoire an solchen Verhaltensweisen verfügt, von der selbstmeidenden Run-and-Tumble-Bewegung während der freien Migration über die geführte Migration in chemischen Gradienten bis hin zur Alterungsdynamik während der kompetitiven Migration. Unsere Quantifizierung und theoretischen Beschreibungen ermöglichten es uns, sie zu interpretieren und zu zeigen, dass *P. polycephalum*, obwohl einzellig, eine faszinierende Suchdynamik entwickelt hat.

Contents

1 Motivation

Imagine you are lost in the mountains with no GPS and no network. Time is pressing because it will soon be dark. You have to rely on your navigational skills to find your way home or hope that you will be found quickly so that you do not have to spend the night out. In both cases, a good strategy will increase your chances of getting home soon. But what is the best strategy for lost hikers to get home or for the rescue team to find them?

Having a good search strategy can save lives - be it the life of a person lost on a hike in the mountains or the life of a starving cell searching for food. The right strategy will heavily depend on the context: in the case of victim search with unmanned aerial vehicles (UAVs), the success of a search is dependent on a set of parameters like the quality of the signal collected by the UAVs, their energy resources, the environmental circumstances, including hazards, and the processing of information by the UAVs [1]. In general, this statement applies to any type of search problem. Just replace the UAVs by another type of searcher, like an animal, a sperm cell or a protein, and the victim by another type of goal, like prey, an egg cell or a specific site on a DNA strand [2–4].

Search problems have attracted the attention of physicists because they can be treated mathematically and optimized solutions can be found [5–7]. They are often formulated in the following way: what is the best strategy to exploit food sources that are distributed in patches in the environment [7, 8]? There is a conflict between exploitation and exploration. Patches contain a finite amount of food so that they will be depleted, but moving to new patches is energy-intensive, so exploitation and exploration must be balanced. The optimization of the movement between the patches is an interesting problem by itself: what is a good strategy to find a target when it is far and the searcher has no information about its position? This type of problem can be approached using random walk theory from statistical physics [6]. Search problems are abundant in nature and their solutions in the form of search strategies have an intriguing application in cells: how do these simple organisms without processing units like CPUs or neurons manage to fulfill their tasks like finding food, mates, or shelter? Examples are the parasite *Plasmodium sporozoites* finding the best spots to enter blood vessels to initiate malaria infection [9], human dermal keratinocytes finding other cells of the same type to close a wound in the skin [10, 11], and dinoflagellates hunting down their prey [12]. Is there a strategy behind their success? Or do cells simply rely on random motion to reach their goals? And if there is a strategy, is it optimized, for example by minimizing the search time [13–15]?

An early study of cell motility was performed by Przibram in the early 20th century [16, 17], who described the motion of *Paramecium*, a unicellular ciliate, as random like the Brownian motion of molecules. However, his methods were imprecise [10], and a couple of years later, Fürth showed that the description was ignoring the presence of persistence, but he still considered it a random process [18]. Only much later, researchers became aware of correlation in the movement of living organisms and started to call it strategic [19]. Nowadays, we know that cells span a range of different search strategies. Bacteria like *Escherichia coli* perform a run-and-tumble motion [20], cellular slime molds like *Dictyostelium discoideum* employ persistent random motion [21], and the dinoflagellate *Oceanisphaera marina* can switch between Brownian motion and Lévy walks depending on the availability of prey in its surroundings [12]. The adaptation of the search strategy in the last example nicely illustrates that the best search strategy for a cell depends on its environment. Many scenarios are possible: search can be performed in the absence of external cues [21] or in the presence of such cues, for example chemical gradients [20]. There can be one or many targets, and targets can have various distributions [22–24].

Different search strategies will have different success [14, 19, 23, 25, 26]. But is there an overall optimal strategy? Statistical physics and random walk theory have been used as a framework to tackle this question [7]. The short answer is no. A given search strategy will perform differently in different environments, and the best strategy for a given environment depends on its properties, like, for example, the target distribution [14, 15, 23, 27], but also on the amount of information the searcher has about its environment [7]. It has been shown that a switching between different strategies, known as intermittent behavior can optimize search, even in a constant environment [22, 28]. In this context, it is interesting that different organisms have developed similar search strategies [29]. It appears that natural selection may drive a converging evolution of search strategies, balancing out performance and fitness costs – an observation that bridges different kingdoms of life [29]. This makes it interesting to study the search strategies of an organism on the verge between unicellularity and multicellularity, the slime mold *Physarum polycephalum*, which shows apparent smart behavior and problem-solving abilities [30].

2 Background and outline

In this chapter, we review the biology and behavior of *Physarum polycephalum*, as well as some theoretical concepts necessary for the global understanding of this thesis. More specific background information is given as introductions to the individual chapters.

2.1 Biology of the slime mold *Physarum polycephalum*

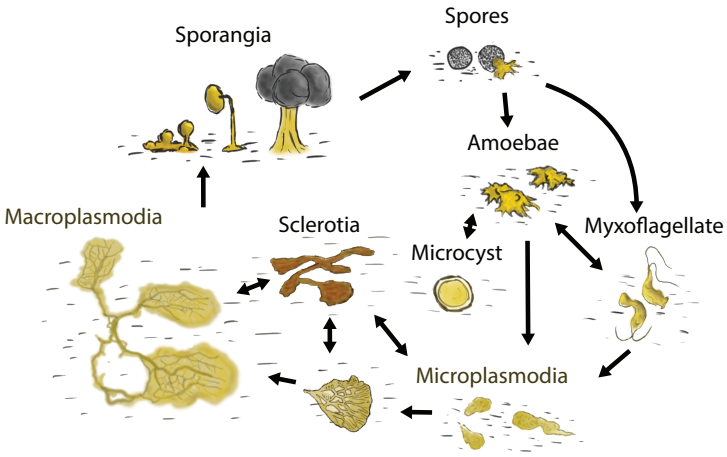

Figure 1: Life cycle of *P. polycephalum*. Spores germinate and evolve into amoebae or flagellates, depending on the conditions. These fuse to become microplasmodia which grow to macroplasmodia. Starvation induces differentiation into sporangia which produce new spores. Adapted from Reference 30, which is licensed under CC BY 4.0 (Copyright © 2024 by the authors).

Physarum polycephalum shares traits with plants, animals and fungi, but it belongs to neither of them [31]. It is a myxomycete or true slime mold, which is an organism with a unique life cycle [32, 33] (Figure 1). Starting from a zygote in the form of a uninucleate amoeba, a single cell grows into a large multinucleate mass as it feeds, called a plasmodium, in which only the nuclei divide, not the cell itself. A single cell of *P. polycephalum* typically contains hundreds

of millions of nuclei [34] – a rule of thumb may be billions of nuclei per square centimeter of plasmodium [35]. These divide almost simultaneously every 10 hours in a plasmodium [34, 36]. Under certain conditions, including the presence of light [37], the plasmodium can differentiate into fruiting bodies, or sporangia, containing haploid spores, which give rise to amoeba of the next generation [32]. During this life cycle, *P. polycephalum* may also take on other forms such as myxoflagellates, microcysts, or sclerotia, which are adaptations to specific external conditions [30].

All of this life cycle can be followed in the lab in sterile liquid culture [31, 38], which makes this organism appealing to developmental biologists. Furthermore, plasmodia are large, so they are visible by the unaided eye, and their properties can be easily studied [31]. Biophysicists are particularly interested in its rich behavior during its plasmodial stage, where it forms an actively moving cell that is covered in a layer of slime [39]. The production of this extracellular material, which is only present during the plasmodial stage of its life cycle, is why it is called a slime mold [40]. The plasmodium's morphology is size-dependent: small plasmodia consist of one or two leading protrusions and a trailing tube (Figure 2), while large plasmodia are organized into a back part consisting of a network of tubes and a fan-like frontal part [41].

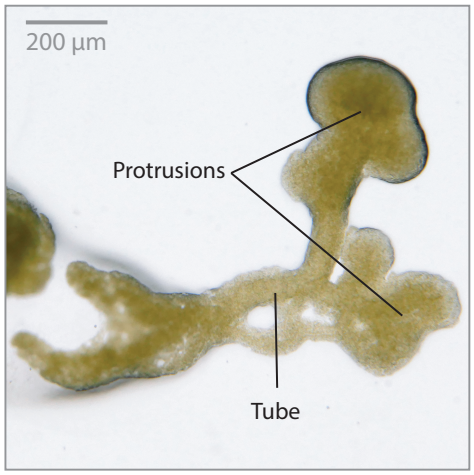

Figure 2: Plasmodial form of *P. polycephalum*. Brightfield image on 1.5% agar. The migration front consists of protrusions connected by a trailing tube.

The tube walls are a poroelastic structure with membrane invaginations called the ectoplasm, which enclose a viscous fluid called the endoplasm [30] (Figure 3). The endoplasm is subject to shuttle-streaming [42, 43], driven by the contractions of the both filamentous and fibrillar actomyosin mesh in the ectoplasm [44]. This shuttle-streaming transports nutrients, chemicals and organelles like nuclei back and forth throughout the whole cell [30], with peak flow velocities reaching up to $1\,\mathrm{mm/s}$ [45]. The actomyosin contractions form a peristaltic wave whose wavelength scales with organism size [46, 47].

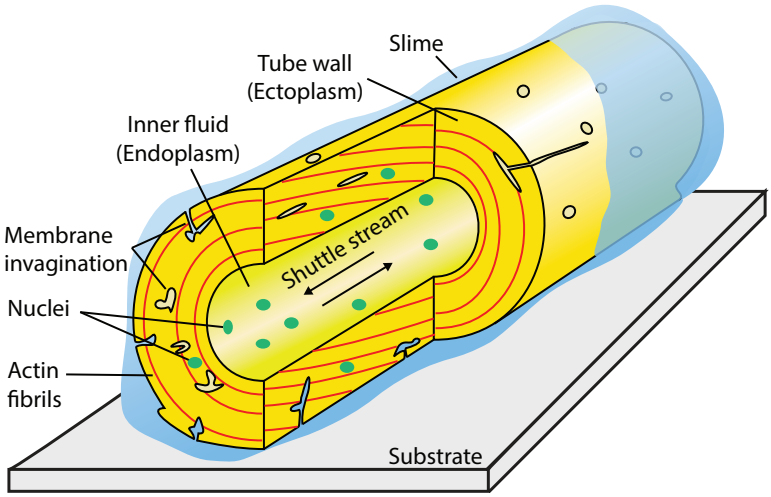

Figure 3: Cross-section of a plasmodial tube covered with a layer of slime and composed of the invaginated tube wall, containing actin fibrils, and the liquid endoplasm, engaged in shuttle-streaming and transporting organelles like nuclei. Adapted from Reference 30, which is licensed under CC BY 4.0 (Copyright © 2024 by the authors).

The shuttle streaming in turn drives migration of the plasmodium by a net transfer of cell mass from the trailing end to the front of the cell [39, 46]. It is referred to as amoeboid migration, the ancestral type of movement of probably many eukaryotes [48]. Symmetry breaking to initiate movement occurs in cells with a diameter of at least $100\,\mu\mathrm{m}$, below which migration is not possible [49]. The means of adhesion to the substrate during migration is not well understood, although a few studies have reported the existence of focal adhesion points in the form of actin fibrils that connect to the substrate [30, 50].

The morphology of the migrating cell depends on the size of the plasmodium [41], the environmental conditions [51, 52], the nutritional state of the plasmodium [53], and its migration phase [54]. During movement, the cell shape is not fixed, but changes periodically in a mixture of oscillations of several different periods [41, 55–57]. The shuttle streaming plays an important role in several of the abilities and behaviors that have gained *P. polycephalum* the epithet ‘smart’ [30], some of which are described in the following section.

2.2 Abilities and behavior of *Physarum polycephalum*

Studying the behavior of *P. polycephalum* has gained popularity since the experiments by Nakagaki and others. They challenged a huge plasmodium to solve a maze by connecting the entrance and exit of the maze, where agar blocks containing nutrients were deposited as a food source. *P. polycephalum* found the shortest path between them [58]. In two subsequent studies, they tested if it can form a connection path minimizing the exposure to light and design a network connecting the most important stations of the Tokyo railway system. *P. polycephalum* managed also these tasks, showing some features of optimality [59, 60]. The growing interest in the problem-solving abilities of *P. polycephalum* has led researchers to expose it to many other optimization challenges, which it solved, such as the traveling salesman problem [61], the two-armed bandit problem [62], and speed-accuracy trade-off decisions [63]. Choosing the right diet [64] and anticipating periodic events [65] are among its abilities, too. *P. polycephalum* has also been reported to exhibit habituation and learning [66–72]. Its flexible network morphology allows it to adapt efficiently to its environment [73] and to encode memory in its network architecture [74].

As mentioned above, migration occurs in plasmodia larger than $100\,\mu\mathrm{m}$ [49]. The speed and morphology of migrating plasmodia depend on plasmodium size, with small plasmodia having few branches and migrating slowly with speeds of the order of $1\,\mathrm{mm/h}$, and large plasmodia forming a reticulated network and migrating rapidly with speeds around $1\,\mathrm{cm/h}$ [41]. Large, starving plasmodia can even reach speeds of $3\,\mathrm{cm/h}$, only pausing during the phase of nuclei division [39]. In general, there are large variations in speed during migration [41, 75], with oscillations having periods of 2 and 20 minutes [41]. Small plasmodia show different phases of movement, resembling a run-and-tumble motion, where they alternate between phases of fast, persistent motion and phases of reorientation with only little movement, so that persistent motion is only present on short time scales [76–78].

Another striking behavior is the use of the extracellular material it produces, the slime, as a way of marking the places it has already visited, similar to the idea of Hansel and Gretel in the fairy tale of the same name. The slime covering the plasmodium is left behind during migration, marking areas already visited and serving as an external memory [79–81]. This allows *P. polycephalum* to preferentially explore novel, unexploited areas. The following paragraphs summarize the properties and function of the extracellular slime and draw a connection to self-avoiding walks.

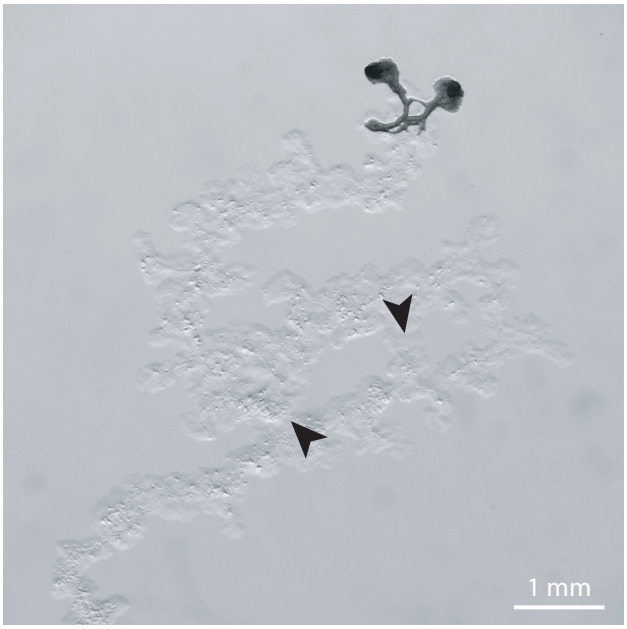

Figure 4: Brighfield image of a migrating plasmodium leaving behind a transparent slime track on a 1.5% agar substrate. Arrow heads mark events where the plasmodium has avoided the previously deposited slime trail.

Plasmodia of *P. polycephalum* are covered by a slimy substance, called glycocalyx [39]. It mainly consists of macromolecules called exopolysaccharides (EPS), which are secreted by the plasmodia [82]. This happens via exocytosis of slime-filled vesicles at the advancing front of a plasmodium and contributes to protrusion formation [83, 84]. During migration, this slime is left behind the plasmodium, leaving a slime track [39] (Figure 4). Notably, the composition of the glycocalyx differs from the one of the slime tracks [82]. Both glycocalyx and slime tracks contain monosaccharides, so sugars, like galactose, glucose and rhamnose, proteins and various sulphate groups. However, the proportions are different. The glycocalyx contains mainly glucose, rhamnose and proteins, whereas the slime tracks are mainly made up out of rhamnose and contain more water. The glycocalyx contains thin filaments, possibly actin fibers, parallel to plasma membrane like a sheath [85, 86], which are also present in the slime tracks left behind the cell [85].

The two versions of slime also have different functions. Despite the high content in carbon, the glycocalyx is not metabolized by starving plasmodia and hence does not serve as a carbon source [40]. Interestingly, the glycocalyx shows antimicrobial activity, especially against *C. albicans*, in contrast to the slime tracks [82]. Therefore, its main purpose is probably to protect the organisms against the environment including bacteria [40]. Furthermore, it may serve the

transport and uptake of substances [86], and it has been shown to suppress cytokinesis, the division of the cell into two daughter cells, which might play an important role in the formation of the non-dividing, multinucleate plasmodium [87]. Finally, it is helping in the recognition of other plasmodia due to its extension around the cell [86, 88]: the sensing of other individuals is not restricted to direct contact. Instead, *P. polycephalum* is able to sense other individuals from a distance [88]. The mechanism for this might be an extension of the glycocalyx around plasmodia for a distance of up to 1 mm from the cell [88]. This allorecognition is constricted to intraspecies interactions [89].

To our current knowledge, the function of the slime tracks is only to serve as a cue for *P. polycephalum*. Reid and others investigated the response of *P. polycephalum* to its extracellular slime [79, 80]. When given the choice between two possible paths with oat flakes at the end, *P. polycephalum* decides depending on the slime content of the different paths. *P. polycephalum* strongly avoids areas covered in slime when given an alternative route without slime. When no free area is available, *P. polycephalum* does not avoid the slime. From this, the authors concluded that the slime serves as a cue for already explored areas [79]. Further they found that the mean migration speed does not change in an environment which is fully covered in slime compared to a blank environment. Smith-Ferguson and others investigated if *P. polycephalum* can differentiate between its own slime and the slime of another strain or even another species, *Didymium bahiense*, and between fresh and old slime [81]. They found that *P. polycephalum* does not react differently to slime of different age and does not discriminate between the slime of different strains part of the same species, but it prefers the slime of another species over its own.

Abilities like navigation, decision-making, memory and learning, have led researchers to attribute basal cognition to *P. polycephalum* [72]. It has also been speculated that the slime, as an external memory, may be a possible evolutionary precursor to internal spatial memory in animals [90]. In this thesis, we investigate a not-yet-appreciated feature of the external memory: it increases space exploration efficiency by making the migration of plasmodia a self-avoiding walk.

2.3 Random walks

A self-avoiding walk is a special type of random walk. Before we discuss this special case, we first introduce random walks in general. They have been used extensively in statistical physics to describe the trajectories of particles undergoing repeated collisions, the shape of polymers [91], and the stochastic motions of living organisms [7]. A well-known version of a random walk is diffusion or Brownian motion, the random motion of molecules in a gas or liquid due to thermal agitation [92]. The molecules constantly bump into each other and change direction, instead of moving in a straight line, which would be ballistic motion.

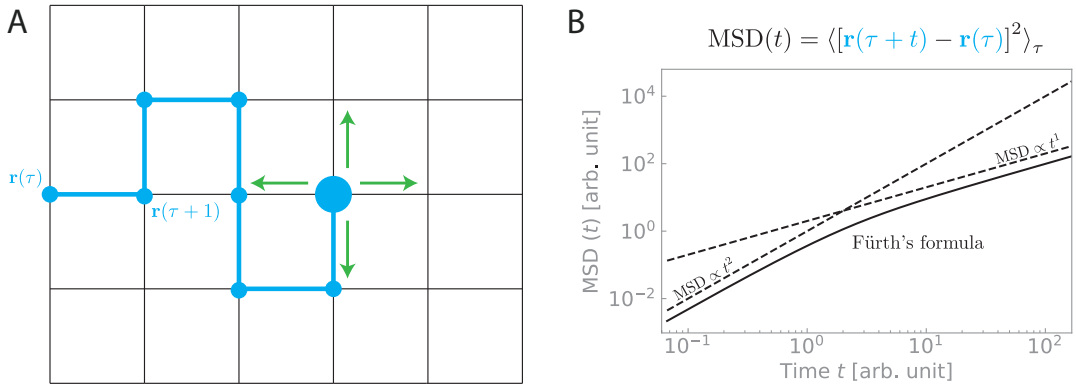

Figure 5: (A) Random walk on a grid. Small, blue circles indicate past positions $\mathbf{r}(\tau)$ and the large, blue circle indicates the current position. Green arrows indicate the possibilities for the next step. In the case of a self-avoiding walk, the arrows pointing to the left and down would be forbidden since these positions have already been visited. (B) Mean squared displacement (MSD) of different types of motion. The MSD of a persistent random walk can be described by Fürth's formula (solid line) which interpolates between ballistic (MSD $\propto t^2$) and diffusive motion (MSD $\propto t^1$).

A theoretical description of a diffusing particle can be generated by the following algorithm [92]: A particle moves in two dimensions and takes a step left, right, up, or down with equal probability every t_{step} seconds, moving at a constant speed v, such that a step has a length $l = vt_{\mathrm{step}}$. So, it is effectively moving on a grid (Figure 5A). The particle has no memory of its past, so it can return to previously visited positions. The consequence is that the expectation value of its position after any time t is its starting position, which can be formulated mathematically in the following way [92]: Consider a particle moving in two dimensions, starting from the origin.

With $\mathbf{r}(n)$ being the position of the particle after n steps, and $\mathbf{l}(n)$ the preceding step, we can formulate an iteration rule according to the movement described before:

$$\mathbf{r}(n) = \mathbf{r}(n-1) + \mathbf{l}(n).$$

A displacement $\mathbf{l}(n)$ can take on one of the four values $(l, 0)$, $(-l, 0)$, $(0, l)$, or $(0, -l)$ with equal probability, such that they will cancel out on average. Therefore, the mean position of the particle after n steps is given by

$$\langle \mathbf{r}(n) \rangle = \langle \mathbf{r}(n-1) + \mathbf{l}(n) \rangle = \langle \mathbf{r}(n-1) \rangle + \langle \mathbf{l}(n) \rangle = \langle \mathbf{r}(n-1) \rangle,$$

with $\langle ... \rangle$ denoting the average over all possible trajectories. This means that if we let it perform its random walk several times, the average end position will be the starting position because of the symmetry of the walk. To quantify how far it is spreading, one uses the mean squared displacement $\mathrm{MSD} = \langle \mathbf{r}^2 \rangle$, which gives a positive number. In many cases, it can be neatly expressed as a power law, $\langle \mathbf{r}^2 \rangle = Dt^\beta$, with D the generalized diffusion coefficient, t the time and β the power law exponent [93]. What is the MSD of our diffusing particle? Using the same iteration rule as before, we can write

$$\langle \mathbf{r}^2(n) \rangle = \langle [\mathbf{r}(n-1) + \mathbf{l}(n)]^2 \rangle = \langle \mathbf{r}^2(n-1) \rangle + \langle 2\mathbf{r}(n-1)\mathbf{l}(n) \rangle + \langle \mathbf{l}^2(n) \rangle.$$

Since $\mathbf{r}(n-1)$ and $\mathbf{l}(n)$ are independent variables, the mean in the second term factorizes such that $\langle 2\mathbf{r}(n-1)\mathbf{l}(n) \rangle = 2\langle \mathbf{r}(n-1) \rangle \langle \mathbf{l}(n) \rangle = 0$. The last term computes as $\langle \mathbf{l}^2(n) \rangle = 2l^2$, where the factor of 2 is due to the two-dimensional motion. So, in total,

$$\langle \mathbf{r}^2(n) \rangle = \langle \mathbf{r}^2(n-1) \rangle + 2l^2 = \langle \mathbf{r}^2(0) \rangle + 2nl^2 = 2nl^2.$$

Writing $n = t/t_{\mathrm{step}}$, with t the time spent on the random walk, we find that the MSD of the diffusing particle is proportional to the time

$$\langle \mathbf{r}^2(n) \rangle = 2\frac{l^2}{t_{\mathrm{step}}}t,$$

so the power law exponent is $\beta = 1$. For simple diffusion in d dimensions, the MSD can be expressed as $\langle \mathbf{r}^2 \rangle = 2dDt$, where $D = l^2/2t_{\mathrm{step}}$ is the regular diffusion constant and the factor of 2 is commonly introduced for a simpler notation of Fick's equations of diffusion [92].

Here, we focus on the two-dimensional case since it is the migration space of *P. polycephalum*. It is also the dimension for which the random walk was first introduced by Pearson [94]. An important special case of a random walk is the persistent random walk, where the

motion of the random walker has a certain persistence length due to a short term memory that is not present in diffusion [15]. Therefore, its movement has longer streaks of straight motion than diffusive motion (Figure 6A,B). This is, for example, the case for swimming bacteria like *E. coli*, which move on a relatively straight line for a certain time (called *run*) before changing directions (called *tumble*) [92]. In this case, the time until the next change of direction is distributed exponentially [92]. Another example of a persistent random walk is an active microswimmer which moves forward by self-propulsion but slowly changes its directions due to, e. g., rotational diffusion [95]. Here, the random walk is not taking place on a grid but in continuous space. This version is also known as correlated random walk because the direction of successive steps is correlated by a distribution of turning angles (i. e. reorientations after each step) peaked around zero [19]. To characterize on which scales the movement appears straight, one can define a persistence length $l_\mathrm{P} = v_0/(2D_\mathrm{rot})$, where D_rot is the effective rotational diffusion constant. Above this length scale, the random walker looses orientation and the motion will effectively be diffusive on long time scales [18, 21, 96].

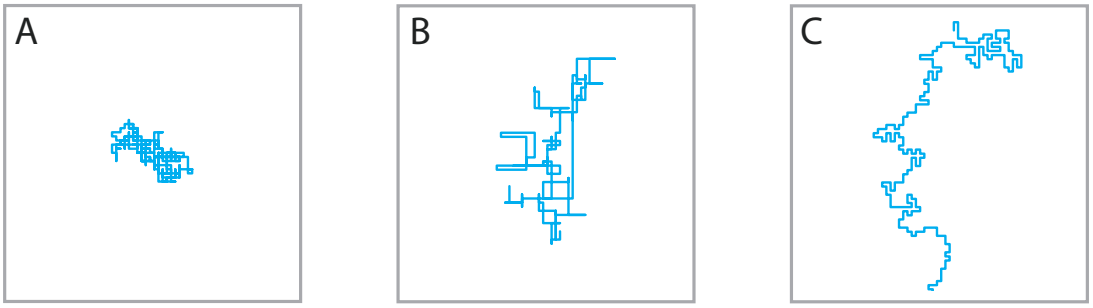

Figure 6: Comparison of different types of random walks (400 steps). (A) Random motion or diffusion. (B) Persistent random walk with a persistence time of 2 steps. (C) Self-avoiding walk.

The MSD of a persistent random walk is described by Fürth's formula [18, 97]: $\langle r^2 \rangle \propto \alpha t + e^{-\alpha t} - 1$, with $1/\alpha$ the persistence time, which can be converted into a persistence length by multiplying with a characteristic velocity. This formula was derived by Ornstein and Fürth independently of each other [98]. For large t, the formula simplifies to the MSD of simple diffusion or random motion, whereas for small t, we get an MSD scaling with the time squared, so ballistic or straight motion. This can be neatly illustrated by plotting the MSD against time in a log-log plot, where the slope of the MSD is given by its power law exponent (Figure 5B). Inbetween the limit cases of diffusive and ballistic motion is a regime where the power law exponent lies between 1 and 2, which is known as superdiffusive motion. Motion characterized by an exponent smaller than 1 is called subdiffusion. To summarize, different definitions of a random walk lead to different scaling behavior of the MSD with time. One can therefore use

the MSD to estimate if a given trajectory is closer to random motion, characterized by a power law exponent of $\beta = 1$, or closer to straight motion, characterized by a power law exponent of $\beta = 2$.

There are also several random walks that are superdiffusive at large t, like Lévy flights/walks and fractional Brownian motion [93]. Lévy walks have been used extensively to describe the motion of biological organisms [6]. In contrast to the run-and-tumble motion, where run lengths are exponentially distributed, Lévy walks are characterized by a power law distribution of step lengths. This makes the Lévy walk scale invariant and leads to a superdiffusive MSD exponent, where the exact value depends on the power law exponent of the step length distribution [6].

Another superdiffusive random walk is the self-avoiding walk. A self-avoiding walk (SAW) is a random walk with the additional rule to not return to any previous position [99] (Figure 6C). They appear for example in fractal geometries [100] and trails of sea urchins [101]. The power law exponent of the MSD has not yet been calculated due to the mathematical complexity that the avoidance rule introduces, but it is generally accepted to be close to $\beta = 1.5$, as estimated from numerical computations [102, 103]. The SAW model was also used by Flory to successfully describe long, flexible polymer chains, which are not intersecting with themselves due to excluded volume interactions [104]. In the following, we will refer to this description as the self-repelling chain (SRC) [105]. It captures the scaling properties of polymer chains immersed in a dilute solution of a good solvent or at high temperatures [106]. This is because the van der Waals attraction between the monomers can be neglected, so that only the hard-core repulsion between the monomers is relevant [107]. However, the statistics describing the SRC are valid only for the case of the actual chain, so an already finished 'walk'. Growing polymers, which are built step by step and actually resemble a random walk in this sense, have different conformational statistics due to different weights for individual steps of the random walk and could thus also have different scaling properties [105, 108]. Therefore, modifications of the SRC have been investigated to describe the deviating properties. By now, there are various different definitions of SAWs in the literature with subtle differences. They are briefly summarize here, together with their scaling properties, to decide on the best definition to model the self-avoiding walk of *P. polycephalum*.

A model for the linear growth of polymers was introduced by Majid and others [108]. This kinetic growth walk, which is also called genuinely self-avoiding walk (GSAW) [109], describes a growing random walk, where the probability of a step to an previously visited site is zero. This means that it only stops if it is trapped. Different configurations of this type of SAW have different probabilities to appear, which contrasts with the SRC, where all configurations have the same probability [108]. Nevertheless, this model has a critical exponent close to $\beta = 1.5$ and is thought to share also other scaling properties with the SRC [110]. Note, however, that

”only walks much longer than the average walk length before trapping are representative for the true asymptotic behavior“ [105, 111]. Amit and others proposed a variation of the SRC in which the walk can actually grow, similar to the GSAW. This so-called 'true' self-avoiding walk can intersect itself, but tries to avoid this by choosing less visited regions [112]. This is modelled by a repulsive potential which is linearly increasing with the number of visits. The power law exponent is $\beta = 1$, but the correct scaling behavior involves logarithmic corrections [113]. This means that this type of avoidance is not strong enough to keep the random walker from visiting its past trajectory again, such that on long time scales the movement is effectively diffusive. A modification of this model with a saturating potential is the self-attractive random walk with repulsive interaction, which results in a critical exponent $\beta = 1$ without logarithmic corrections [114]. Another variant is the k-tolerant walk [115]. In this case, each vertex may be visited more than once, but less than k times, which nevertheless probably preserves the scaling properties of the SRC [116]. So, the scaling remains the same if the random walker can visit its past trajectory only for a finite number of times and will effectively avoid it on long time scales. Table 1 summarizes the different scaling behaviors of the described random walks.

Type of random walk	β on long time scales
Brownian motion or diffusion	1
Persistent random walk	1
Ballistic motion	2
Fractional Brownian motion	0-2
Lévy walk	1-2
Self-repelling chain	1.5
Genuinely self-avoiding walk	1.5
True self-avoiding walk	1 (with logarithmic corrections)
Self-attractive random walk with repulsion	1
k-tolerant walk	1.5

Table 1: Different random walks and their scaling behavior.

In the case of *P. polycephalum*, the effect of its self-avoiding behavior on its migration statistics has yet been overlooked: Recent models do not take it into account and simplify the migration by describing it as a persistent random walk [77, 117]. But which of the previous SAW models is the best for this case? For a moving cell that is avoiding its past trajectory, the GSAW seems to be the best definition, as trajectories develop in time. We will use this version to model the self-avoiding migration of plasmodia of *P. polycephalum*.

2.4 Search strategies

The previously described random walks can all be seen as search strategies in the sense that they show a distinct way of exploring the migration space, which can be characterized, for example, by the MSD exponent β. Search strategies in living organisms often have the purpose of finding food (called foraging), mates or shelter. There are also scenarios where two goals need to be achieved at the same time, like in the case of planktonic organisms that hunt for algae but also want to escape fish that are chasing them [118]. Depending on the specific goal and the conditions of the search, different strategies will have different success [14, 19, 23, 25, 26]. If the aim is, for example, to find a target in some distance, Brownian motion is the best strategy when the target is close because superdiffusive random walks tend to overshoot the target [23]. But if the target is far as, for example, in low target density scenarios, superdiffusive motion, like in Lévy walks, is better than Brownian motion [14]. This result is connected to the Lévy flight foraging hypothesis, which states that living organisms must have evolved to use Lévy flights as a search strategy since they are optimal in some scenarios [6]. Indeed, many organisms have movement patterns resembling Lévy flights [119].

If the target and the searcher are confined in a certain area, a run-and-tumble walk is better than ballistic motion because tumbles can lead to reorientations close to the target, which increases the chance of finding it [26]. 'Better' means here that the search strategy is more optimal in the sense that the time to find the target, quantified by the mean first passage time, is minimized [26]. Here, also intermittent search strategies, where active search phases alternate with non-reactive displacement phases, were shown to optimize search time when targets are difficult to detect [13, 22, 28, 120]. The idea is that these targets can only be detected in a search phase with little displacement, modeled by diffusion, but that a phase of ballistic but non-reactive motion is necessary to relocate the searcher into unvisited locations [22]. This balances out the advantages and disadvantages of both phases: during ballistic movement, targets cannot be found, but it is helpful to explore new territory, while during diffusive movement, targets can be found, but it is limited in space.. Bénichou and coworkers found that search time is minimized when the average duration of the ballistic phase varies with the average duration of the diffusive phase like a power law [13]. This kind of mixed search strategy is employed, for example, by proteins searching for their specific target sites on DNA, or by foraging animals [22].

Optimal foraging theory (OFT) is another way to quantify the optimality of searching behavior. It assumes that foraging organisms aim to maximize their fitness by optimizing the balance

between the energy uptake from food and the energy expended on searching [8, 121, 122]. According to it, foraging behavior is inheritable and will evolve towards enhanced individual fitness [121]. In a review, Bartumeus and others discussed the strengths and weaknesses of OFT [7]. They highlight that OFT is based on statistical physics and random walk theory, which provide a framework to understand the search strategies of living organisms across scales, from single cells to animals. In this context, a critical open question is how much information about their targets foraging organisms can actually acquire and use, while most models of OFT assume that the searcher has all the information at hand. However, the best search strategy in a certain environment does not only depend on basic conditions like the target distribution, but also on the amount of information the searcher has about them [7]. Bartumeus and others also stress that living organisms often forage in a non-systematic way, which could be a good strategy when information is lacking. This loops back to the intermittent search strategies, which are optimal when information about targets is difficult to gather.

Besides optimization, search strategies of very different species share common features like risk aversion [29]. For example, *E. coli* does not minimize the time to reach high concentrations of nutrients, i. e. finding the shortest path, but instead maximizes the possible minimum uptake of the nutrients [123]. This kind of strategy is also called *satisficing*, as an alternative to *optimizing* [124, 125]. The advantage is that bad outcomes are minimized in uncertain environments, but it comes with the cost of underperforming in favorable environments [29]. An interesting example is also that of copepods, small crustaceans, whose persistence length of movement is adapted to the most important aim concerning their reproduction [118]: females have a much shorter persistence length than males. For males, a long persistence length increases the chance of finding a female, but also increases the risk of encountering a predator. This risk is minimized for females with a short persistence length, which keep the eggs and do not search for males.

2.5 Chemical sensing and response by cells

Bonner [126] pointed out that signals and their reception lie at the heart of social behavior, and that they must have co-evolved alongside in the transition from unicellular to multicellular life. How do cells respond to the presence of chemicals? First, a cell needs a means of sensing a chemical, which is done by chemoreceptors. Chemoreceptors are proteins or protein complexes that bind molecules from the environment and convert this signal into a message that can be further processed in the cell [127]. These receptors are distributed uniformly on the cell and do not redistribute during cell movement [128]. To detect a gradient, that is, a difference in concentration of certain molecules across space, cells have evolved different mechanisms, which is interesting from a physicist's point of view. *Spatial sensing*, where cells measure concentration differences across their cell body, is typical for many eukaryotes [129]. *Temporal sensing*, where concentration differences are measured at two successive points in the gradient during movement, is employed when cells are too small to sense the gradient spatially, like many bacteria [130]. However, bacteria can nevertheless sense spatial gradients under certain conditions, for example when gradients are very steep [131–133]. In fact, the type of gradient sensing depends on the combination of cell size, locomotion speed and gradient steepness [131, 132, 134–136]. In shallow gradients, small and fast cells preferentially employ temporal sensing because the concentration differences perceived during movement are larger than the ones perceived across the cell body, while big and slow cells employ spatial sensing because of the opposite reason [134–136]. Another putative way to measure a gradient is *pseudospatial sensing*, where a cell measures the change in concentration over time on an extending protrusion, but this mechanism lacks experimental evidence [137].

How do single cells respond when a concentration difference is sensed, and how does this depend on the signal strength? The response of the bacterium *E. coli* to a concentration gradient of chemicals, for example, is dependent on the perceived concentration changes. Its chemotactic drift velocity, which is the velocity component parallel to the gradient, is proportional to the gradient of the logarithm of the concentration [138]. This is related to the Weber-Fechner law, an empirical, psychophysical law applicable to many species and sensory modalities [139]. Developed by Weber, it was reformulated by Fechner in 1860 [140]: equal relative increments of stimuli lead to proportionally equal increments of sensation. Fechner concluded from this that the intensity of sensation is proportional to the logarithm of the stimulus intensity.

The signaling cascades triggered by the sensing of chemicals are relatively simple in prokaryotes, whereas eukaryotes display much more intricate signaling cascades [141, 142]. The response of eukaryotic cells to chemicals could be explained by intracellular signaling cycles like, for example, the LEGI system [143, 144]. We will briefly summarize this system, following Parent and Devreotes [128]: It is a hybrid model of spatial and temporal sensing that describes how a cell could process a difference in the perceived concentration at opposite sides of the cell body to achieve persistent movement in the direction of the higher concentration. The internal signaling cycle is simplified to the dynamics of two biochemical processes: a local excitation E and a global inhibition I, which are regulated by receptor occupancy. E is given by the local fraction of occupied receptors at one part of the cell, while I is given by the global, averaged fraction of occupied receptors. The difference between E and I gives rise to a response $\mathrm{R} = \mathrm{E} - \mathrm{I}$. When a cell sits in a concentration gradient, both ends will experience a rapid rise in E, accompanied by a slower rise of I, such that both ends will experience an increase in R. Both E and I plateau shortly after reaching a steady state. At the cell end facing up the gradient, which we now call the front of the cell, the steady state value $\mathrm{E}_{\mathrm{front}}$ is higher than $\mathrm{E}_{\mathrm{rear}}$ on the other cell side, while the global I is the same on both sides. This means that the front of the cell, where $\mathrm{E}_{\mathrm{front}} > \mathrm{I}$, will experience a positive response R, while the rear of the cell, where $\mathrm{E}_{\mathrm{rear}} < \mathrm{I}$, will have a negative response. Therefore, the cell can detect the direction of the gradient. This system allows cells to sense even shallow gradients with small concentration differences because the inhibition activity subtracts the ambient chemical concentration, such that the direction of the gradient can be sensed more accurately [128].

2.6 Outline of this thesis: The migration of *Physarum polycephalum* in various contexts

The following section briefly outlines this thesis by highlighting the key findings discussed in each chapter.

In *Chapter 3*, we investigate if the migration behavior of freely migrating plasmodia of *P. polycephalum* follows a search strategy and if we can describe it by a random walk model. It is based on the peer-reviewed publication "Size-dependent self-avoidance enables superdiffusion in macroscopic unicellulars", published in March 2024 in the Proceedings of the National Academy of Sciences.

To adress this, we experimentally study and quantify the migration behavior of *P. polycephalum* plasmodia on the time scale of days on 1.5% agar surfaces. We track their movement by measuring position and shape, and extract their migration statistics. Based on the data from 14 experimental trajectories, we develop a data-driven model to describe the dynamics of the migrating cells. With this, we show that *P. polycephalum* performs a self-avoiding run-and-tumble movement, where the short-term dynamics are determined by the run-and-tumble statistics. The long-term dynamics exhibit enhanced space exploration efficiency by superdiffusion of plasmodia, which arises from its self-avoiding behavior. Varying organism size, we find that the self-avoidance is size-dependent. Small plasmodia cannot always avoid slime trails, leading to frequent slime crossings, and only large plasmodia reliably avoid slime trails. Therefore, only large plasmodia show real self-avoiding behavior leading to superdiffusive migration, while small plasmodia tend to diffusive migration. This highlights a potential evolutionary advantage for larger plasmodia, which may have driven *P. polycephalum* to evolve into one of the largest cells we know.

In *Chapter 4*, we test if the migration behavior of freely migrating plasmodia is dependent on their environmental conditions. This chapter is partly based on Diana Lenski's master thesis, jointly supervised by the author and Karen Alim.

We investigate changes in the migration statistics in the presence of glucose, growth medium, salts, and acids or bases. We focus on short time scales, where the self-avoiding behavior of *P. polycephalum* has only a weak effect on the trajectory statistics. We observe environment-dependent changes in the run-and-tumble dynamics of plasmodia and their morphology. We

identify an additional migration phase besides the run phase and the tumble phase in some environments, characterized by stationary protrusion oscillations on a time scale of a few hours, which reduce the space exploration efficiency of plasmodia. They are associated with a distinct morphology of the cells, revealing the influence of morphology on the migration behavior.

In *Chapter 5*, we study the search strategy of *P. polycephalum* in a gradient of nutrients. Often in nature, chemicals are not distributed homogeneously but form gradients. Many cells are able to detect these gradients and move along them, a process called chemotaxis. Nevertheless, the underlying mechanism is not yet fully understood. It is therefore interesting to study this process in *P. polycephalum* because its large cell size requires the coordination of its randomly forming protrusions over a large spatial distance, posing an intricate problem.

We perform experiments on agar with a diffusion gradient of nutrients. We find that plasmodia have a high chemotactic index, which means they are faithfully following the gradient, but a low directionality, which means that they do not perform persistent migration. Indeed, their trajectories exhibit a high MSD exponent at long time scales but a low MSD exponent and anti-persistence at short time scales. This anti-persistent movement is associated with extended phases of protrusion oscillations similar to the ones described in Chapter 3. We show that the protrusion oscillations can be explained by a known instability based on a competition between the contraction and actin dynamics of the cell. We also find that larger plasmodia are more efficient in moving up the nutrition gradients, again highlighting the evolutionary advantage that a larger cell size might provide.

In *Chapter 6*, we investigate the collective migration strategy of a large number of plasmodia that migrate together and interact via their slime trails. The slime deposition by a single plasmodium modifies its environment and influences its further migration. With this, its migration belongs to the self-interacting random walks, known for complex dynamics like aging and nontrivial persistence. The analysis of the data includes input from Raphaël Voituriez.

We perform experiments with numbers of 25 and 49 migrating plasmodia on plain agar with starting positions arranged in a grid pattern. Analyzing their migration statistics, we find that space exploration efficiency depends on the position of plasmodia within the group, where plasmodia at the periphery have high persistence and plasmodia in the bulk low persistence. This shows how the collective effect can increase the space exploration efficiency of some individuals by sacrificing the space exploration by others. We also observe aging of the MSD and of the orienational correlation of plasmodia movements. These results provide insights into the search strategy of *P. polycephalum* in a competitive scenario.

3 Size-dependent self-avoidance – the search strategy of *Physarum polycephalum*

This chapter is based on the publication

Size-dependent self-avoidance enables superdiffusive migration in macroscopic unicellulars [145]

Lucas Tröger, Florian Goirand and Karen Alim

Proceedings of the National Academy of Sciences 121(13):e2312611121 (2024)

3.1 Summary

In this chapter, we investigate the general search behavior of the slime mold *Physarum polycephalum*. Like other cells, it faces search problems as, for example, finding food. In contrast to other unicellular organisms, *P. polycephalum* forms a remarkably large cell when searching for food, which is said to show smart behavior. Does its movement follow a search strategy? And what are the consequences of its large cell size in this context? To address these questions, we experimentally study and quantify the migration behavior of *P. polycephalum* plasmodia on the time scale of days in the absence and presence of nutrients. We develop a data-driven model to describe the dynamics of migrating cells. With this, we show that *P. polycephalum* performs a run-and-tumble movement and achieves superdiffusive migration through self-avoiding behavior mediated by the slime trail it deposits. Our model matches the statistics of the experimental trajectories from migration in the absence and presence of nutrients. In the presence of food, the run duration statistics change, only controlling the short-term migration dynamics. Varying organism size, we find that the long-term superdiffusion arises from self-avoidance determined by cell size. This highlights a potential evolutionary advantage for larger plasmodia, which may have driven *P. polycephalum* to evolve into one of the largest cells we know.

3.2 Manuscript: *Size-dependent self-avoidance enables superdiffusive migration in macroscopic unicellulars*

3.2.1 Introduction

Search problems are a widespread challenge for living organisms, from unicellular species to animals [20, 21, 146–148]. Success in finding food, mates or shelter depends on the search strategy [14, 19, 23, 25, 26]. The search of unicellulars is commonly characterized by Brownian motion on long time scales [18, 20, 21, 149], whereas more evolved life forms such as mammalian cells, insects, birds or humans show superdiffusion [2, 148, 150–155]. Strikingly, unicellulars in groups, like swarming bacteria [156], and unicellular organisms on the verge of multicellularity, like large multinucleate cells [77, 78], also show superdiffusion. Since search success is coupled to survival chances [14], the need to find effective strategies could be a driver of evolution. With the increase in cell size being the putative first evolutionary step in the critical transition from unicellular to multicellular life [32], what are the benefits of a large cell size in the context of search problems?

The mean squared displacement (MSD) measures the deviation of an organism from a reference position during its migration, quantifying how much space is explored. The MSD is typically characterized by a power law $\mathrm{MSD}(t) \propto Dt^{\beta}$ with generalized diffusion constant D, time t and exponent β [93]. Scale-invariant migration trajectories allow for a constant exponent to classify the MSD, bounded by $\beta = 1$ for Brownian motion and $\beta = 2$ for ballistic motion, where values between 1 and 2 refer to superdiffusion, as arising in Lévy walks and self-avoiding walks. For Lévy walks, the exponent is determined by the power law describing the step length distribution [6], for a self-avoiding walk in two dimensions the exponent is generally accepted to be close to $\beta = 1.5$ [103, 157]. Depending on the search task, different migration strategies lead to different success, with Brownian motion being best when search targets are close [23], but superdiffusion outperforming it when target density is low [14]. Ballistic motion is predicted to be optimal for Poisson-distributed targets but is less efficient than a run-and-tumble walk when the goal is to find a fixed target within a confinement [26]. Unicellulars already have mixed search strategies, performing ballistic motion on short time scales and Brownian motion on long time scales. Prominent examples include run-and-tumble motion and persistent random walks [18, 20, 21, 149, 158], which are characterized by a transition from ballistic motion on short time scales to Brownian motion on long time scales [18, 19, 159]. Superdiffusion on long time

scales arises, for example, from long-range correlations as found for higher life forms [19, 150], but also in crowded bacterial swarms [156] or in the giant cells of *Physarum polycephalum* [77, 78]. Yet, how the giant unicellular *P. polycephalum* generates superdiffusive motion is unclear despite its fascinating life form on the verge of multicellularity [32].

P. polycephalum is a plasmodial slime mold – a unicellular, non-dividing, multinucleate organism, devoid of the complexity of multicellular model systems. Despite the absence of a nervous system, *P. polycephalum* coordinates complex behaviors including adaptive network formation [60], speed-accuracy trade-offs during foraging [63], and nutritional decisions [64], which has earned it a reputation for being "smart" [160]. It can also escape traps by leaving a trail of slime, which it uses as an external memory to actively avoid areas it has already visited [79–81]. Its cell size is highly variable, covering a range of orders of magnitude from $100\,\mu\mathrm{m}$ to meters [160], and correlates with the average speed of locomotion, which is oscillating periodically [41]. *P. polycephalum* has proven to be highly amenable to both observation and quantification of its dynamics, as well as theoretical modeling, making it an ideal model system to, here, develop mechanistic insight into its superdiffusive motion.

In this work, we experimentally observe *P. polycephalum* plasmodia migrating in a neutral environment, perform data analysis to determine their migration characteristics and develop a data-driven model which captures *P. polycephalum*'s migration behavior. We show the robustness of our model by quantifying how the behavior changes in a nutritious migration environment. Varying organism size, we reveal the pivotal role of cell size in driving superdiffusive motion by enabling reliable self-avoidance only above a cell size of $0.65\,\mathrm{mm}^2$. Our results highlight the adaptive capabilities of *P. polycephalum*, as well as the impact of cell size on space exploration performance, suggesting the potential evolutionary advantage that this large unicellular may have.

3.2.2 Experimental setup and results

Migration shows superdiffusive MSD and anomalous persistence

We experimentally follow and quantify the migration of *P. polycephalum* plasmodia of different size and on different migration substrates. In the initial setup, plasmodia are allowed to migrate on a two-dimensional, non-nutritious substrate (1.5% agar). Using bright-field microscopy in combination with a stage-top incubator, we follow the movement of plasmodia over a period of up to 134 hours (5.6 days) while ensuring constant and homogeneous environmental conditions, namely humidity, light and temperature. We perform cell tracking and statistically analyze the centroid trajectories of individual plasmodia (Figure 7).

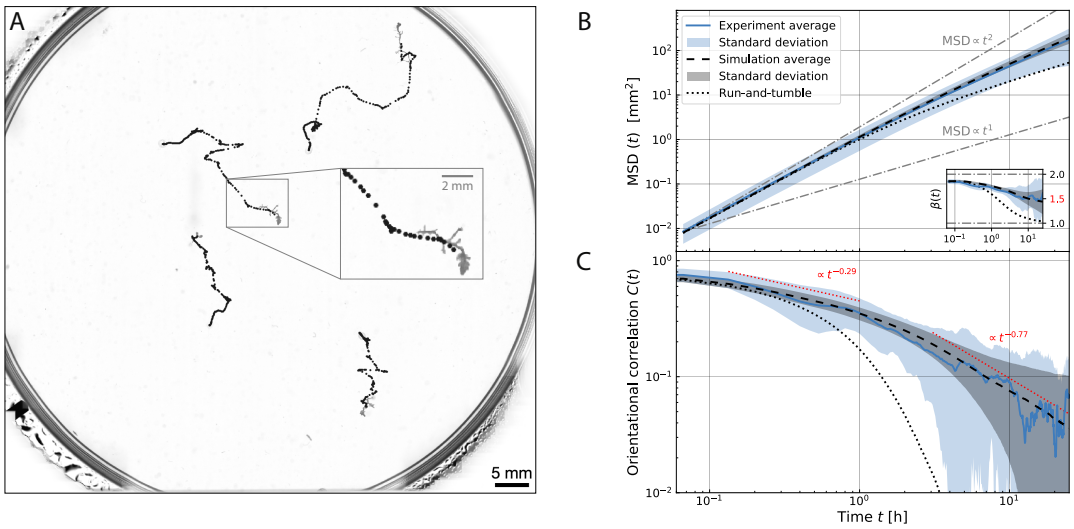

Figure 7: Migration of *P. polycephalum* shows superdiffusion and anomalous persistence. (A) Plasmodia of *P. polycephalum* on a petri dish with 1.5% agar (background subtracted image) with overlayed trajectories (one dot every 8 min, 40 h in total). (B) Log-log plot of the superdiffusive mean squared displacement (MSD) of migrating plasmodia. Blue line and shaded region represent the ensemble average over the time-averaged MSDs of 14 individual trajectories and the standard deviation, respectively. The black dashed line and shaded region shows corresponding simulation results. The black dotted line shows results from simulations without the self-avoidance, so a pure run-and-tumble. Dash-dotted lines show the MSDs of ballistic ($\propto t^2$) and diffusive motion ($\propto t^1$). Inset: Instantaneous MSD exponent $\beta(t)$. The migration is superdiffusive ($\beta > 1$) over ≈ 3 orders of magnitude in time. Red tick: Flory exponent for a self-avoiding walk in two dimensions. (C) Log-log plot of the orientational correlation $C(t)$ as a measure of persistence. The red dotted lines show power laws for comparison.

To quantify the space exploration behavior of *P. polycephalum*, we use two established measures: the time-averaged mean squared displacement, MSD,

$$\mathrm{MSD}(t) = \langle [\mathbf{r}(\tau + t) - \mathbf{r}(\tau)]^2 \rangle_\tau,$$

and the orientational correlation, C,

$$C(t) = \langle \cos\theta \rangle = \langle \hat{\mathbf{r}}(\tau + t) \cdot \hat{\mathbf{r}}(\tau) \rangle_\tau,$$

where $\mathbf{r}(\tau)$ is the position of the plasmodium's centroid at time τ with corresponding unit vector $\hat{\mathbf{r}}(\tau)$, and t is the time interval of the MSD measurement. How does the MSD of migrating *P. polycephalum* scale with t? Our statistical analysis, based on 14 experimental trajectories, shows that the MSD of plasmodia migrating on plain agar is superdiffusive over a large range of time scales (Figure 7B). However, we find that the MSD exponent β is not constant, but depends

on the time scale t. Defining the instantaneous MSD exponent $\beta(t)$ as the logarithmic derivative of the MSD

$$\beta(t) = \frac{\partial \log \mathrm{MSD}(t)}{\partial \log t},$$

we find that $\beta(t)$ is decreasing towards longer time scales (Figure 7B, inset): at the smallest time scale ($4\,\mathrm{min}$), β is close to a value of 2, signifying almost ballistic motion. At larger times, β is slowly decaying, approaching a seemingly stable value of $\beta \approx 1.5$ at the order of 10 hours, which is compatible with a self-avoiding walk. In addition to the MSD, the orientational correlation describes how well the direction of migration is aligned with respect to the direction at previous time points, thus quantifying the persistence of the migration. In the case of *P. polycephalum*, we observe that orientational correlations show a decay slower than exponential (Figure 7C), which contrasts with the exponential decay for persistent random walks [158, 161]. Thus, *P. polycephalum*'s migration shows anomalous persistence. Taken together, both experimentally observed MSD and orientational correlation cannot be explained by the standard random walk models discussed in the introduction. To understand how superdiffusivity and anomalous persistence emerge, we next quantify the migration characteristics.

The trajectories of *P. polycephalum* are reminiscent of a run-and-tumble motion [77] with phases of straight movement and phases of stationarity, after which plasmodia change their direction (Figure 7A). The stretches of straight movement are consistent with an MSD exponent close to $\beta = 2$ on small time scales, associated with ballistic migration. Another important characteristic of *P. polycephalum*'s migration is that plasmodia usually do not cross their own path. This behavior is a result of their path-marking mechanism: migrating plasmodia leave behind a slime trail which they generally avoid when encountered [79–81]. Although previously considered irrelevant in the case of very small, tadpole-shaped plasmodia [77], this avoidance could explain *P. polycephalum*'s superdiffusive behavior since self-avoiding walks are associated with a superdiffusive MSD exponent [103, 157]. Taken together, these observations suggest that the migration of *P. polycephalum* could be described by a combination of two types of random walks, i.e. as a self-avoiding run-and-tumble walk. To investigate this hypothesis, we next quantify the statistics of the migration behavior.

Quantifying Run-and-Tumble and Self-Avoiding Behavior

Closely inspecting our experimental trajectories, we distinguish *P. polycephalum*'s phases of fast, straight movement and phases of stationarity with small positional oscillations, similar to run-and-tumble [20] or intermittent behavior [28]. We discriminate the two phases, i.e. run and tumble, by measuring the local directionality, or straightness, of the movement. This quantity is defined as the ratio of the distance between two positions and the length of the plasmodium's

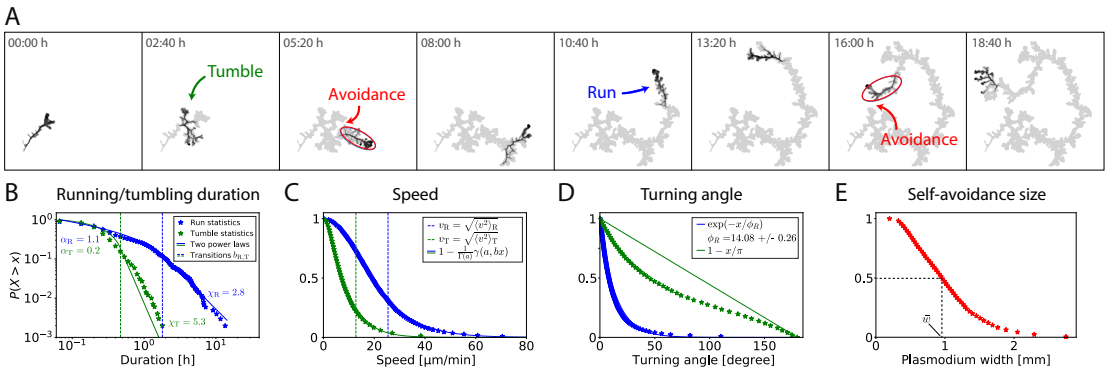

Figure 8: *P. polycephalum* performs a self-avoiding run-tumble movement during its migration. (A) Exemplary trajectory of a plasmodium with highlighted events of tumbling (green arrow), running (blue arrow) and self-avoidance (red arrows). The cumulative visited area is visualized in light gray. Overlayed ellipses are fitted to the plasmodium as an approximation for its size. Scale bar: 2 mm. (B)-(E) Parameter extraction from data for the model: Complementary cumulative distribution functions (CCDF), $P(X > x)$, of the analyzed variables, with X denoting the respective variable. Fits from maximum likelihood estimation in solid lines. (B) Run and tumble durations fitted with a combination of two power laws. (C) Speeds during runs and tumbles with fitted gamma distributions. Run statistics: $a = 2.60, b = 0.12\,\mathrm{min}^{-1}$. Tumble statistics: $a = 1.69$, $b = 0.18\,\mathrm{min}^{-1}$. Dashed lines: Root mean squared speeds. (D) Turning angles between consecutive steps during runs and tumbles. Run statistics fitted by an exponential distribution and tumble statistics approximated by a homogeneous distribution. (E) Widths of the plasmodia slime trails as a measure for the avoided space around the trajectories. The width is estimated as the width of an ellipse fitted to the plasmodium as in (A). The dashed line shows the median width of all plasmodia.

path connecting these two positions [162]. Sections of the trajectory with a directionality greater than a threshold (0.9, Materials and Methods) are identified as phases of running. Phases of arrested movement (tumbling) are characterized by a lower directionality. This method allows us to divide the trajectories into a series of two alternating phases (*Addendum*, Figure 11), which we analyze separately. We describe a single phase of running or tumbling as a series of steps, characterized by three parameters: phase duration, speeds and turning angles. We find that the distributions of running and tumbling durations are best fitted by combinations of two power laws (Figure 8B and *Addendum*, Figure 12A), according to the Akaike information criterion (*Addendum, Data analysis*). Speed distributions are well described by gamma distributions (Figure 8C). The turning-angle distribution during runs is well fitted by an exponential and the one during tumbles is close to a uniform distribution (Figure 8D).

In accordance with the literature, we observe that plasmodia generally avoid previously visited areas marked by their slime trail [79–81]. The shape and extent of the slime trail is determined by the cell shape of the migrating plasmodia, which is highly variable in time. We

describe the shape of the just forming slime trail by an ellipse fitted to the plasmodium (Figure 8A), and approximate the trail width as the median width of the fitted ellipse (Figure 8E). In our experimental observations, the distance from which the plasmodia detect the slime trail is often greater than zero (see Figure 8A, red arrows), probably due to diffusion of the unknown repellent slime component in the agar. Reid et al. found that slime from a large culture of slime mold induced an avoidance response in very large plasmodia ($1\,\mathrm{cm}^2$ cell area) for up to 6 days [80], which is much longer than the time frame considered in our analysis.

Following the quantification of migration trajectories in terms of distributions, we extract from our data that plasmodia perform a self-avoiding run-and-tumble movement governed by the following rules: a migrating plasmodium alternates between two phases of movement, running and tumbling. Running and tumbling durations are distributed according to a combination of two power laws. In each phase, the plasmodium moves with a speed characteristic for this phase, distributed according to gamma distributions. After each step, it chooses the direction of the next step according to an exponential distribution for runs and according to a uniform distribution for tumbles. As it explores its environment, the plasmodium does not come closer to its past trajectory than the median width of a plasmodium.

Model Reveals Individual Contributions of Parameters

We now use the data-derived rules and statistics to model *P. polycephalum*'s migration behavior as the combination of run-and-tumble and self-avoidance, with the aim of reproducing *P. polycephalum*'s movement in terms of the experimentally observed MSD and orientational correlation. We simplify the model by assigning constant speeds during runs and tumbles, rather than sampling from the gamma distributions. With this, the number of parameters in our model reduces to ten: the exponents $\alpha_{\mathrm{R,T}}$ and $\chi_{\mathrm{R,T}}$, and the transition points $b_{\mathrm{R,T}}$ of the combined power law distributions of running and tumbling durations, the average speeds during runs and tumbles $v_{\mathrm{R,T}}$ corresponding to the root mean squared speeds $\sqrt{\langle v_{\mathrm{R,T}}^2 \rangle}$, the average turning angle during runs ϕ_{R} and the median width of the plasmodia $\bar{w}$, which we all extract directly from the data without the need for model fitting. This is done by estimating all parameters by fitting the distributions to the data (Figure 8B-E).

Now using the ten data-derived parameters, we simulate self-avoiding trajectories as a series of runs and tumbles, which themselves consist of series of random steps characterized by a direction and by a step length, according to the described distributions. In this sense, our simulation is a kinetic process as the trajectories are built step by step in time, which differs from the classical definition of self-avoiding walks in the context of equilibrium polymers. However, the kinetic definition is believed to be in the same universality class as the classical self-avoiding walk and

Migration rule extracted from data	Model parameters	Control over MSD
Run and tumble durations distributed as two power laws		Generalized diffusion constant, MSD exponent at small time scales ($\lesssim 1\,\mathrm{h}$)
- exponent of first power law	$\alpha_{\mathrm{R,T}}$	
- exponent of second power law	$\chi_{\mathrm{R,T}}$	
- transition point between the power laws	$b_{\mathrm{R,T}}$	
Constant speed during run and tumble	$v_{\mathrm{R,T}}$	Generalized diffusion constant
Turning angles distributed exponentially during runs	ϕ_{R}	MSD exponent at short and intermediate time scales ($\lesssim 10\,\mathrm{h}$)
Self-avoidance according to plasmodium width	$\bar{w}$	MSD exponent at intermediate and long time scales ($\gtrsim 1\,\mathrm{h}$)

Table 2: Model parameters related to the migration rules extracted from the data and their control over the MSD.

to have the same critical exponents [111]. We quantify the MSD and the orientational correlation of the simulated trajectories and find that they reproduce the experimental results with excellent accuracy (Figure 7B,C), confirming that our model captures the migration behavior of *P. polycephalum* plasmodia. With the model at hand, we can vary the parameters to understand their individual contributions to the space exploration behavior (see *Addendum*, Figure 13 for parameter sweeps). The MSD is fully characterized by the generalized diffusion constant D and the time-dependent MSD exponent $\beta(t)$. We find that D depends on the speeds $v_{\mathrm{R,T}}$ but also on the average running and tumbling durations $\langle R\rangle$ and $\langle T\rangle$, which are determined by $\alpha_{\mathrm{R,T}}$, $\chi_{\mathrm{R,T}}$ and $b_{\mathrm{R,T}}$. This dependence of D can also be seen analytically: we find $D \propto \langle R\rangle\langle v_{\mathrm{R}}^2\rangle + \langle T\rangle\langle v_{\mathrm{T}}^2\rangle$ (*Addendum, Simulations*). For the MSD exponent $\beta(t)$, we find that the parameters act at different time scales. The MSD exponent at short time scales ($\lesssim 1\,\mathrm{h}$) is determined by $\langle R\rangle$ and $\langle T\rangle$ and the average turning angle during runs ϕ_{R}, with β correlating positively with $\langle R\rangle$ and negatively with $\langle T\rangle$ and ϕ_{R} (*Addendum*, Figure 13A-C). The MSD exponent at intermediate time scales ($1\,\mathrm{h} - 10\,\mathrm{h}$) is determined by ϕ_{R} and the width $\bar{w}$ of the plasmodia, with β correlating again negatively with ϕ_{R} and positively with $\bar{w}$ (*Addendum*, Figure 13C,D). The MSD exponent at long time scales ($\gtrsim 10\,\mathrm{h}$) is only determined by $\bar{w}$, which controls how fast β is converging eventually to the expected value of 1.5 for very long time scales (*Addendum*, Figures 13 and 14). Table 2 summarizes these results. The intuition behind the findings is that the straighter the movement, the higher the MSD exponent. This is the case for longer runs and a smaller average turning angle, but also for a larger plasmodium width; the width $\bar{w}$ determines the self-avoidance range, with a larger width inducing more avoidance, resulting in straighter movement. The influence of the parameters on the orientational correlation is similar to the one on the MSD exponent. Apart from the success of the model and the mechanistic insight it provides, it is not clear how robustly it describes any *P. polycephalum* plasmodium irrespective of its environment. Also, which migration parameters would change in a different environment?

Model Is Robust against Environmental Changes

To test the robustness of our model, we let plasmodia migrate on a nutritious substrate (Materials and Methods). Quantifying the MSD and orientational correlation of the obtained 9 trajectories, we do not observe significant differences from the migration behavior on plain agar on the smallest time scales ($\lesssim 10\,\mathrm{min}$), except for a larger generalized diffusion constant D. However, on larger time scales, the exponent of the MSD is higher for migration on nutritious agar, resulting in a higher MSD (Figure 9A,B). The same is true for the orientational correlation (Figure 9C). Quantification of the run-and-tumble dynamics as described in the previous section reveals that the running and tumbling durations are still distributed as power laws (*Addendum*, Figures 12B and 15), but that there are very long runs compared to migration on non-nutritious substrate: the average run duration $\langle R \rangle$ increases from $48.2\,\mathrm{min}$ to $103.2\,\mathrm{min}$, while the tumble dynamics do not change significantly, with $\langle T \rangle$ increasing from $17.9\,\mathrm{min}$ to $20.6\,\mathrm{min}$ (Materials and Methods, *Addendum*, Figure 12B). This explains both the larger generalized diffusion constant D and the higher MSD exponent β on time scales less than $1\,\mathrm{h}$, according to our analysis of the influence of the average run duration $\langle R \rangle$ on D and β. The distributions of speeds and turning angles are also largely unaffected, but the plasmodia are larger due to growth induced by the nutritious substrate, which explains the higher MSD exponent β on large time scales. We extract all model parameters from the nutritious agar dataset (*Addendum*, Figure 16) and run additional simulations with the newly extracted parameters, again yielding an excellent match with the data (Figure 9). This shows that our model is robust and we set out to investigate as a possible evolutionary advantage of *P. polycephalum* the influence of the plasmodium size on its space exploration behavior.

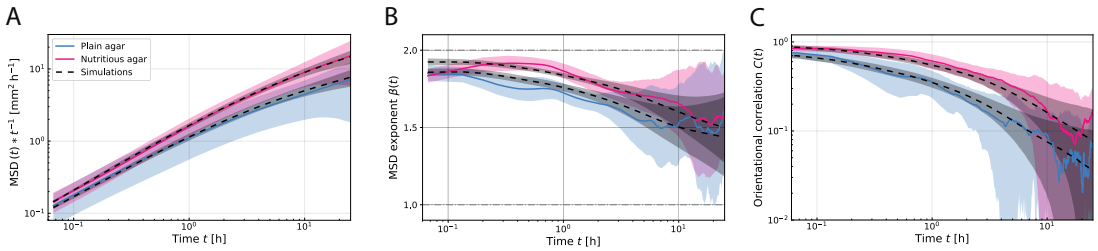

Figure 9: MSD exponent and orientational correlation of *P. polycephalum* are higher on a nutritious migration substrate, but are captured by the same type of model. (A) Log-log plot of the MSD divided by time of migrating plasmodia on non-nutritious substrate (14 trajectories) and on nutritious substrate (9 trajectories) and the MSD of the simulated trajectories. Shaded regions show the standard deviations. (B) Log-lin plot of the instantaneous MSD exponent β in experiments and simulations. (C) Log-log plot of the orientational correlation C in experiments and simulations.

Self-avoidance Critically Controlled by Organism Size

We want to experimentally test the prediction of our model that the plasmodium size influences the MSD exponent on time scales larger than 1 h. The size is an intrinsic property of the plasmodia, which we can simply vary by picking plasmodia of different size. We divide the 14 trajectories on plain agar into two equal groups (7 trajectories each), one containing plasmodia with a cell area smaller than the median cell area ($0.65\,\mathrm{mm}^2$), and the other containing larger plasmodia. Quantifying these groups separately, we find that the orientational correlation is independent of the organism size at small time scales ($\lesssim$ 1 h) (Figure 10C). MSD quantification reveals that large plasmodia have a significantly larger MSD at short time scales, meaning that they have a larger generalized diffusion constant D than small plasmodia (Figure 10A). The reason for this is that they are faster since migration speed correlates positively with cell size [41].

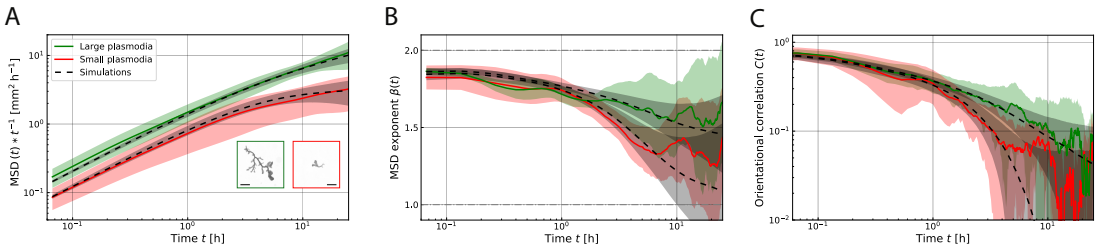

Figure 10: MSD exponent and orienational correlation of small plasmodia decrease strongly at time scales $t \gtrsim 1\,\mathrm{h}$. (A) Log-log plot of the MSD divided by time of migrating plasmodia distinguished by plasmodium size (7 small, 7 large), and the MSD of the simulated trajectories with strict self-avoidance (large plasmodia) and time-limited self-avoidance of 3 h (small plasmodia). Inset images: Example of a large and a small plasmodium, scale bars 1 mm]. Shaded regions show the standard deviations. (B) Log-lin plot of the instantaneous MSD exponent β in experiments and simulations. (C) Log-log plot of the orientational correlation C in experiments and simulations.

Most notably, the group of small plasmodia shows a strong decrease of the MSD exponent below $\beta = 1.5$ at intermediate and long time scales (Figure 10B), which is not visible in the group of large plasmodia. So, small plasmodia have a lower MSD exponent than large plasmodia at time scales larger than 1 h (*Addendum*, Figure 17), as predicted by our model. Quantification of the run-and-tumble dynamics and cell sizes for both size groups independently shows that large plasmodia have twice the width of the small plasmodia, are 29% faster and spend 31% more time in the running phase (Materials and Methods, *Addendum* Figs. 19-21). The other migration characteristics are independent of the size. We extract all model parameters from the partitioned data sets and perform additional simulations with the newly extracted parameters. Our model captures the MSD and orientational correlations of the large plasmodia (Figure 10), but overestimates those of the small plasmodia for large time scales (*Addendum*, Figure 18B).

This means that the model is missing a factor to accurately describe the migration of small plasmodia. By examining the experimental record, we find the reason for their stronger decrease in superdiffusivity: small plasmodia occasionally cross their own trajectories (four out of seven small plasmodia cross their own trajectories one to seven times in around 90 hours, see *Addendum*, Figs. 18A, 19A), revisiting previously visited areas, which makes their space exploration less efficient. This is also evident from single-cell MSDs. The individual MSDs of small plasmodia show transient regimes of diffusive motion with an exponent of $\beta = 1$, which is not the case for large plasmodia (*Addendum*, Figs. 19C and 20C). From experimental recordings, we observe that self-crossings in small plasmodia occur not before 3 hours after the deposition of the slime trail (*Addendum*, Figure 18A), suggesting a limited response to the trail. To test this, we run additional simulations in which plasmodia successively lose responsiveness to parts of the trail that are more than 3 hours in the past, allowing them to revisit regions that they have already visited before the last 3 hours. The simulation results give a good match with the experimental data (Figure 10) and suggest an MSD exponent of $\beta = 1$ on long time scales (*Addendum*, Figure 18B). The parameter describing the response time controls how fast the MSD exponent is converging towards a value of $\beta = 1$ on intermediate to long time scales (*Addendum*, Figure 18B). We also ran simulations with a crossing-associated penalty, but this does not capture the MSD exponent well (*Addendum*, Figure 18C). To directly test whether the response of plasmodia to the trail is size dependent, we experimentally examine the encounters of small and large plasmodia with the trails of small and large conspecifics. We observe that large plasmodia avoid both the trail of small and large plasmodia, in contrast to small plasmodia which avoid neither the trail of small nor large plasmodia (*Addendum*, Figs. 22 and 23). The failure of small plasmodia to respond to slime trails highlights the importance of size in enabling superdiffusive migration.

3.2.3 Discussion

We experimentally investigated and quantified the migration behavior of *P. polycephalum* plasmodia on plain agar. We found that their migration is characterized by superdiffusion and anomalous persistence on long time scales. Our analysis shows that *P. polycephalum* performs a self-avoiding run-and-tumble movement. Our data-driven model successfully captures the MSD and the orientational correlation and reveals the individual contributions of the migration parameters. Accounting for a loss of the responsiveness to the trail by small plasmodia, it teaches us that the macroscopic unicellular *P. polycephalum* achieves superdiffusive migration through size-dependent self-avoidance, which affects the MSD exponent and the orientational correlation on intermediate and long time scales.

The self-avoiding behavior is achieved by a path-marking mechanism in the form of deposited slime, which acts as an avoidance cue. Path marking as a spatial memory is known not only from Hansel and Gretel, but also from a wide range of organisms. Examples include bacteria that secrete exopolysaccharides [163], mammalian cells that deposit extracellular matrix components [164], or ants that leave pheromone trails [146, 165]. Trail formation is energetically costly, so its benefits should outweigh its costs to be evolutionarily advantageous [166]. Self-avoiding walks are a beneficial strategy in the sense that they increase the space exploration significantly [114]. Special cases of self-avoiding walks have been shown to be optimal, for example, by being more efficient than stochastic trajectories in terms of minimizing the search time [27], or by generating Lévy walks [101]. *P. polycephalum* may have developed its path-marking strategy to gain an advantage in terms of space exploration.

We observe that the type of migration behavior remains the same in a nutritious environment, underlining the robustness of our model and suggesting that this is the general mechanism by which *P. polycephalum* explores its environment. However, the migration dynamics adapt to the environment, resulting in longer run durations and therefore a higher MSD exponent on a nutritious substrate. The adaptation of the migration to the nutritional content of the environment is also observed in other cells, like bacteria [167], dinoflagellates [12], or *D. discoideum* [168]. *D. discoideum* is also known to generate gradients in homogeneous environments through the degradation of nutrients, promoting long-range chemotaxis [169]. It is possible that a similar mechanism is responsible for the longer run durations we observe for *P. polycephalum*, but we leave this for future investigation.

Migration analysis on plain agar with respect to cell size shows that small plasmodia have a lower MSD exponent than large plasmodia on long time scales and are therefore less efficient in terms of space exploration. This is due to small plasmodia crossing the slime trail. Since small plasmodia, unlike large plasmodia, fail to respond to slime trails from both small and large specimens, we suggest that there is a size threshold below which the self-avoidance mechanism no longer works well, perhaps due to a reduced ability to process information. This would also explain the previously observed Brownian motion of very small plasmodia on long time scales [77].

Our study establishes a link between cell size, long-lasting path-marking and space exploration efficiency via superdiffusion. Increasing size has been hypothesized to be the first evolutionary step in the transition from unicellular to multicellular life [32]. Our findings show that, in the case of *P. polycephalum*, a larger size is beneficial because it allows superdiffusive space exploration. This advantage could have driven *P. polycephalum* to form larger and larger cells with many nuclei [170] and thus to evolve into an organism close to multicellular life.

3.2.4 Materials and methods

Preparation and Imaging of *P. polycephalum* Plasmodial specimen were prepared from microplasmodia grown in a liquid culture using the medium by Daniel and Rusch [171] with hematin instead of chicken embryo extract [172]. Culture medium containing microplasmodia was pipetted onto an agar plate, from which individual microplasmodia with a diameter between 0.5 and $1\,\mathrm{mm}$ were selected with a $1\,\mathrm{mL}$ pipette tip and transferred to another 1.5% agar plate, with a resulting plasmodial area density of <0.01. Nutritious agar contained 10% of the culture medium.

Plasmodia (0.2 - $2\,\mathrm{mm}^2$ cell area) were imaged directly after plating under microscope light for 72 to 168 hours, with controlled temperature (24.4°C) and humidity (close to saturation). The plasmodia were imaged with a Zeiss Axio Zoom V.16 microscope equipped with a custom-made Pecon stage-top incubation system, a Hamamatsu ORCA-Flash 4.0 digital camera and a Zeiss PlanApo Z 0.5x objective, yielding a resolution of $10.83\,\mu\mathrm{m}$/pixel. A green filter ($550/50\,\mathrm{nm}$) was placed over the transmission light source of the microscope to diminish *P. polycephalum*'s response to the continuous illumination with light, since these wavelengths are known not to induce phototaxis in *P. polycephalum* [173]. In this way, plasmodia were exposed to a light intensity of only $0.078\,\mathrm{W/mm}^2$. Zeiss Zen 3.2 (blue edition) software was used for imaging. A tiled image composed of 16 tiles was acquired every $4\,\mathrm{min}$ using the Zen Tiles tool, yielding a field of view of 8.1 x $8.1\,\mathrm{cm}$. A total number of eight experiments was conducted, for examples see Supplementary Movies S1 and S2.

Image processing and analysis All tiles were converted into 8-bit TIFF files using Zeiss Zen 3.2 and their backgrounds were removed with a rolling ball algorithm. The MIST stitching algorithm [174, 175] was used to assemble the tiles into a single image. From the stitched images, we extracted plasmodium pixels using a custom-written MATLAB (The MathWorks) code, generating binary images via intensity thresholding. Subsequently, we calculated the center of mass of each plasmodium in each image to obtain the trajectories. For sufficient statistics, only trajectories with a length of at least $30\,\mathrm{h}$ were considered for the analysis.

All mean squared displacements in the main text are ensemble averages of the time-averaged squared displacements of individual trajectories. The same approach was used to calculate the orientational correlations. The instantaneous MSD exponent β is the logarithmic derivative of the MSD. Its standard deviation is computed via error propagation (*Addendum, Data analysis*). Data is shown up to the point where the standard deviation of β exceeds the boundaries given by $\beta = 1$ and $\beta = 2$.

Tumbling events were identified by calculating the directionality [162] of the migration as

Data	$\alpha_{\mathrm{R,T}}$	$\chi_{\mathrm{R,T}}$	$b_{\mathrm{R,T}}$ [min]	$v_{\mathrm{R,T}}$ $\left[\frac{\mu\mathrm{m}}{\mathrm{min}}\right]$	ϕ_{R} [rad]	$\bar{w}$ [µm]
PA	1.1, 0.2	2.8, 5.3	98, 28	24.5, 12.9	0.24	954
NA	1.1, 0.8	2.2, 4.1	132, 36	24.9, 16.7	0.25	1811
SP	1.2, 0.03	2.9, 3.6	96, 20	21.6, 11.8	0.25	674
LP	1.0, 0.2	3.1, 4.6	124, 28	27.9, 14.3	0.23	1340

Table 3: Model parameter values inferred from data sets. PA/NA = plain/nutritious agar, SP/LP = small/large plasmodia.

the ratio of the plasmodium's displacement to the total distance traveled within a time frame of 20 minutes. If the directionality was higher than the threshold value 0.9, the time point was attributed to a running event, else to a tumbling event (*Addendum*, Figure 11). The model parameters are robust against deviations of 5% from this threshold (*Addendum*, Figure 24). Note that, in principle, tumbles could be caused by encountering a slime trail, which would affect the distribution of run durations. However, we observe that only 2.4% of runs longer than $28\,\mathrm{min}$ are stopped by an encounter with a slime trail – a fraction too small to affect the distributions significantly.

The typical width of a plasmodium was estimated by the median length of the minor axis of the ellipse that has the same second moment of area as the plasmodium, which was calculated via the built-in MATLAB function *regionprops* using the property *MinorAxisLength*.

Simulations We simulated trajectories as a series of runs and tumbles, which themselves consist of series of random steps characterized by a direction and by a step length. The number of steps during a run or a tumble is determined by drawing a random number from a combination of two power laws (*Addendum, Data analysis*) with parameters $\lambda_{\mathrm{R,T}}$ and $k_{\mathrm{R,T}}$. During tumbles, directions were determined by drawing a random angle from a uniform distribution between $[-\pi,\pi]$, and speeds were fixed to v_{T}. During runs, directions were determined by drawing a random angle from an exponential distribution with mean ϕ_{R}, and speeds were fixed to v_{R}, with the additional rule that a step can only be made if it does not come closer to the previous trajectory than twice the mean plasmodium width $\bar{w}$. This rule enforces self-avoidance. All parameters used in the simulations were estimated directly from the experimental data by fitting the distributions described in the main text to the experimental data (see Table 3).

Only simulated trajectories with a minimum length of 1800 steps, corresponding to a migration duration of $120\,\mathrm{h}$, were selected to ensure the true asymptotic behavior (*Addendum, Simulations* and Figure S15). All statistics were averaged over 5000 simulated trajectories each. Simulations were performed using Python.

Data Availability Microscopy recordings data have been deposited in mediaTUM (`https://mediatum.ub.tum.de/1734713`).

3.3 Addendum: Supplementary information to the manuscript

The following is an adapted version of the

Supporting Information for: Size-dependent self-avoidance enables superdiffusive migration in macroscopic unicellulars [145]

Lucas Tröger, Florian Goirand and Karen Alim

Proceedings of the National Academy of Sciences 121(13):e2312611121 (2024)

3.3.1 Data analysis

Computation of the MSD exponent and its standard deviation via error propagation We compute the instantaneous MSD exponent β as the logarithmic derivative of the MSD

$$\beta(t) = \frac{\partial \log \mathrm{MSD}(t)}{\partial \log t}.$$

This means that the instantaneous exponent can be approximated by

$$\beta(t) = \frac{\log \mathrm{MSD}(t + t_{\min}) - \log \mathrm{MSD}(t)}{\log\left(t + t_{\min}\right) - \log\left(t\right)}, \quad \text{with } t_{\min} = 4\,\mathrm{min},$$

where $t_{\min}$ is the acquisition rate of the microscope images.

To compute the standard deviation of β, we need to propagate the error of the MSD, so its standard deviation. We assume the measurement error of the time to be negligible, which means that we only take into account the standard deviation of the MSD and write β as $\beta = c[\log(X) - \log(Y)]$, with $X = \mathrm{MSD}(t + t_{\min})$, $Y = \mathrm{MSD}(t)$ and $c = 1/(\log\left(t + t_{\min}\right) - \log\left(t\right))$. This can be approximated by $\beta \approx c * \left[\frac{1}{\langle X \rangle} X - \frac{1}{\langle Y \rangle} Y\right]$. Now, taking the variance on both sides, and using the formula for the variance of a linear combination of variables

$$Var(aX + bY) = a^2 Var(X) + b^2 Var(Y) + 2ab * Cov(X, Y),$$

we get

$$\frac{\sigma_\beta^2}{c^2} \approx \frac{\sigma_X^2}{\langle X\rangle^2} + \frac{\sigma_Y^2}{\langle Y\rangle^2} - \frac{2}{\langle X\rangle\langle Y\rangle}\sigma_{XY}.$$

We have

$$\sigma_{XY} = \langle[(X - \langle X\rangle)(Y - \langle Y\rangle)]\rangle = \langle XY\rangle - \langle X\rangle\langle Y\rangle,$$

so

$$\frac{\sigma_\beta^2}{c^2} \approx \frac{\sigma_X^2}{\langle X\rangle^2} + \frac{\sigma_Y^2}{\langle Y\rangle^2} - \frac{2\langle XY\rangle}{\langle X\rangle\langle Y\rangle} + 2.$$

Running/tumbling duration distributions To find the best model describing the distributions of running and tumbling durations, we use maximum likelihood estimation and the Akaike information criterion [176]. We find that the best model is a combination of two power laws, except for the plasmodia migrating on nutritious agar, where the best model is an exponentially truncated power law (Figs. 12, 21 and Table 4). However, simulations show the same results for both types of model (Figure 15).

The full PDF of the distribution combining two power laws is

$$f(x;\alpha,\chi,b) = A\left[x^{-\alpha}\theta(x - x_{\min})\theta(b - x) + b^{\chi-\alpha}x^{\chi}\theta(x - b)\right], \quad \text{with } x_{\min} = 4\,\text{min},$$

where

$$A = 1/\left[\frac{1}{1-\alpha}\left(b^{1-\alpha} - x_{\min}^{1-\alpha}\right) - \frac{b^{1-\alpha}}{1-\chi}\right],$$

and $\theta(x)$ is the Heaviside function. The mean is given by

$$\langle x\rangle = b\frac{\frac{1}{2-\alpha}\left[1 - (x_{\min}/b)^{2-\alpha}\right] + \frac{1}{\chi-2}}{\frac{1}{1-\alpha}\left[1 - (x_{\min}/b)^{1-\alpha}\right] + \frac{1}{\chi-1}}.$$

The complementary cumulative distribution function used in Figs. 12 and 21 is given by

$$\bar{F}(x;\alpha,\chi,b) = 1 - F(x;\alpha,\chi,b),$$

where

$$F(x;\alpha,\chi,b) = A\left\{\frac{1}{1-\alpha}\left(x^{1-\alpha} - x_{\min}^{1-\alpha}\right)\theta(b - x) + \left[\frac{1}{1-\alpha}\left(b^{1-\alpha} - x_{\min}^{1-\alpha}\right) + \frac{b^{\beta-\alpha}}{1-\beta}\left(x^{1-\beta} - b^{1-\beta}\right)\right]\theta(x - b)\right\}.$$

3.3.2 Simulations

Diffusion constant of a run-and-tumble motion We derive the generalized diffusion constant D in terms of the run-and-tumble characteristics under the assumption that the influence of the self-avoidance is negligible. Let a run-and-tumble walk of N steps consist of N_0 runs and N_0 tumbles. Be $l_{\mathrm{R},i}$ and $l_{\mathrm{T},i}$ the lengths of the ith step during a run or tumble, respectively. Further, be n_{R} (n_{T}) the total number of steps spent running (tumbling), $\langle n_{\mathrm{R}}\rangle$ ($\langle n_{\mathrm{T}}\rangle$) the average number of steps during a single run (tumble). Then we can write the time-averaged one-step MSD as

$$\begin{aligned}\mathrm{MSD}_{1-\mathrm{step}} &= \frac{1}{N}(\Sigma_i l_{\mathrm{R},i}^2 + \Sigma_k l_{\mathrm{T},k}^2) = \frac{n_{\mathrm{R}}}{N}\langle l_{\mathrm{R}}^2\rangle + \frac{n_{\mathrm{T}}}{N}\langle l_{\mathrm{T}}^2\rangle \\ &= \frac{N_0}{N}\big(\langle n_{\mathrm{R}}\rangle\langle l_{\mathrm{R}}^2\rangle + \langle n_{\mathrm{T}}\rangle\langle l_{\mathrm{T}}^2\rangle\big) = \frac{N_0}{\tau N}\big(\langle R\rangle\langle l_{\mathrm{R}}^2\rangle + \langle T\rangle\langle l_{\mathrm{T}}^2\rangle\big),\end{aligned}$$

with $\langle R\rangle = \tau\langle n_{\mathrm{R}}\rangle$ and $\langle T\rangle = \tau\langle n_{\mathrm{T}}\rangle$ the average run and tumble durations, and τ being the duration of one step. With this, we can compute the one-step MSD in terms of the speeds and the generalized diffusion constant D:

$$\mathrm{MSD}_{1-\mathrm{step}} = \frac{N_0}{N}\tau\big(\langle R\rangle\langle v_{\mathrm{R}}^2\rangle + \langle T\rangle\langle v_{\mathrm{T}}^2\rangle\big) = D\tau^2,$$

with

$$D = \frac{N_0}{\tau N}\big(\langle R\rangle\langle v_{\mathrm{R}}^2\rangle + \langle T\rangle\langle v_{\mathrm{T}}^2\rangle\big).$$

Note, that with fixed N and N_0, $\langle R\rangle$ and $\langle T\rangle$ are not independent of each other, and that D as a generalized diffusion constant [93] has the units of a squared velocity.

Parameter sampling Running/tumbling durations are drawn from distributions in the form of a combination of two power laws, respectively. For that, we use the inversion method of random variate generation [177]. First, we need to find the inverse of the two parts of the CDF individually. For the first part of the combination of power laws, with the CDF

$$F_1(x;\alpha,b) = \frac{x^{1-\alpha} - x_{\min}^{1-\alpha}}{(\alpha/b)^{1-\alpha} - x_{\min}^{1-\alpha}},$$

the inverse is

$$F_1^{-1}(x;\alpha,b) = \left[x\left(b^{1-\alpha} - x_{\min}^{1-\alpha}\right) + x_{\min}^{1-\alpha}\right]^{1/(1-\alpha)}.$$

For the second part, with the CDF

$$F_2(x;\chi,b) = b^{\chi-1}\left(b^{1-\chi} - x^{1-\chi}\right),$$

it is

$$F_2^{-1}(x;\chi,b) = b(1-x)^{1/(1-\chi)}.$$

We can now sample a combined power law distribution by first randomly choosing the part of the distribution we want to sample according to its weight and then plugging in for t the respective inverse CDF random variables drawn from a uniform distribution on the interval $[0,1]$.

Generating self-avoiding walks We construct the run-and-tumble self-avoiding walks in the following way: First, we draw a run duration from the respective power law distribution. Then, for each step of the run phase, we draw a turning angle from the respective exponential distribution and shift the current position by the walking speed times the time step of 4 minutes. If parts of the previous trajectory are encountered, we try a new direction according to the turning angle distribution. Then we draw a tumbling duration from the corresponding power law distribution and perform a diffusive motion with step lengths equal to the tumbling speed times the time step. In this way, walks can enter regions that are completely surrounded by previously visited areas, i.e. they can get trapped and have a finite length (Figure 25). Note, however, that "only walks much longer than the average walk length before trapping are representative for the true asymptotic behavior" for this type of self-avoiding walk [111, 178], which is why we only analyze long walks (Figure 25C). This type of self-avoiding walk is sometimes called a kinetic, genuine or growing self-avoiding walk [111, 178, 179].

3.3.3 Supplementary figures and tables

	Exp	Pow	WB	Gam	2Exp	3Exp	2Pow	BPow	PowExp
Plain agar, run durations									
AICc	7171.30	6947.80	7103.40	7150.00	6992.30	6996.30	6669.60	6789.70	6688.10
Delta	501.70	278.20	433.80	480.40	322.70	326.70	0.00	120.10	18.50
Akaike weight	6.17E-25	3.76E-14	1.45E-19	1.37E-21	9.67E-15	6.48E-15	1.00E+00	6.08E-06	1.57E-01
Plain agar, tumbling durations									
AICc	5234.90	5538.70	4902.50	4811.60	5238.90	5242.90	4764.70	5483.60	4790.00
Delta	470.20	774.00	137.80	46.90	474.20	478.20	0.00	718.90	25.30
Akaike weight	3.80E-21	2.43E-34	1.04E-06	9.19E-03	2.55E-21	1.71E-21	1.00E+00	6.01E-32	7.97E-02
Nutritious agar, run durations									
AICc	2410.40	2193.40	2270.50	2309.90	2223.50	2221.40	2140.20	2141.00	2138.60
Delta	271.80	54.80	131.90	171.30	84.90	82.80	1.60	2.40	0.00
Akaike weight	1.57E-12	4.17E-03	1.87E-06	3.64E-08	2.06E-04	2.54E-04	8.52E-01	7.87E-01	1.00E+00
Nutritious agar, tumble durations									
AICc	1381.40	1413.10	1335.80	1325.60	1385.50	1389.60	1279.20	1295.30	1271.20
Delta	110.20	141.90	64.60	54.40	114.30	118.40	8.00	24.10	0.00
Akaike weight	1.64E-05	6.88E-07	1.56E-03	4.34E-03	1.09E-05	7.21E-06	4.49E-01	8.98E-02	1.00E+00
Small plasmodia, run durations									
AICc	3968.60	3755.50	3917.30	3952.20	3838.20	3839.40	3632.10	3683.20	3647.20
Delta	336.50	123.40	285.20	320.10	206.10	207.30	0.00	51.10	15.10
Akaike weight	2.43E-15	4.37E-06	4.11E-13	1.25E-14	1.12E-09	9.93E-10	1.00E+00	6.04E-03	2.21E-01
Small plasmodia, tumble durations									
AICc	2957.10	3112.70	2782.20	2735.20	2961.10	2965.30	2656.30	2908.80	2706.40
Delta	300.80	456.40	125.90	78.90	304.80	309.00	0.00	252.50	50.10
Akaike weight	8.64E-14	1.51E-20	3.41E-06	3.74E-04	5.79E-14	3.80E-14	1.00E+00	1.08E-11	6.67E-03
Large plasmodia, run durations									
AICc	3199.90	3191.20	3183.90	3196.70	3150.80	3154.50	3033.30	3082.00	3035.60
Delta	166.60	157.90	150.60	163.40	117.50	121.20	0.00	48.70	2.30
Akaike weight	5.82E-08	1.39E-07	2.88E-07	8.01E-08	7.89E-06	5.45E-06	1.00E+00	7.67E-03	7.95E-01
Large plasmodia, tumble durations									
AICc	2279.80	2428.00	2123.80	2079.20	2283.90	2288.00	2046.60	2276.10	2087.40
Delta	233.20	381.40	77.20	32.60	237.30	241.40	0.00	229.50	40.80
Akaike weight	7.45E-11	2.73E-17	4.44E-04	3.84E-02	4.95E-11	3.28E-11	1.00E+00	1.08E-10	1.69E-02

Table 4: Corrected AIC values of several models computed via maximum-likelihood estimation, and their respective Akaike weights. Minimal AICc (best model) highlighted in red. The models are Exp=exponential, Pow=power law, WB=weibull, Gam=gamma, 2Exp=two exponentials, 3Exp=three exponentials, 2Pow=two power laws, BPow=bounded power law, PowExp=exponentially truncated power law.

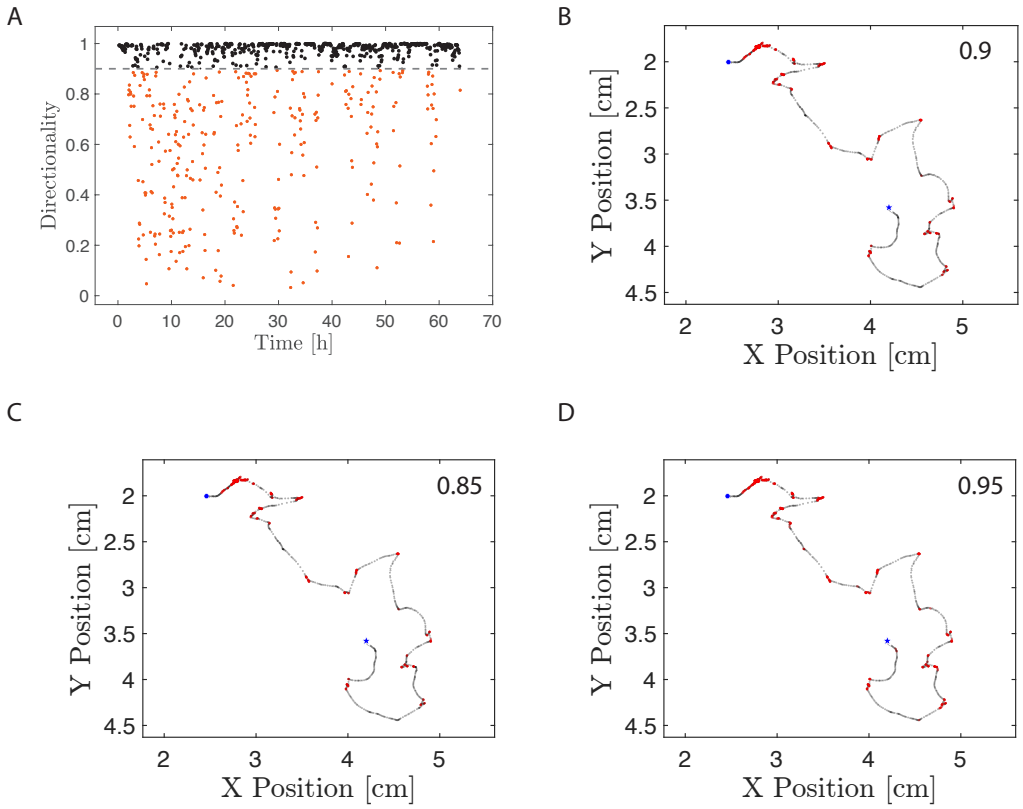

Figure 11: Detection of phases of running and tumbling via the directionality of the migration. (A) Directionality of an exemplary plasmodium over the course of its migration. Each scatter point corresponds to a time step, where black points signify a directionality above 0.9, so the running phase, and red dots signify lower directionality, so the tumbling phase. (B) Trajectory of the same plasmodium as in (A), with the same color code of running and tumbling phases. (C-D) Results for directionality thresholds of 0.85 and 0.95.

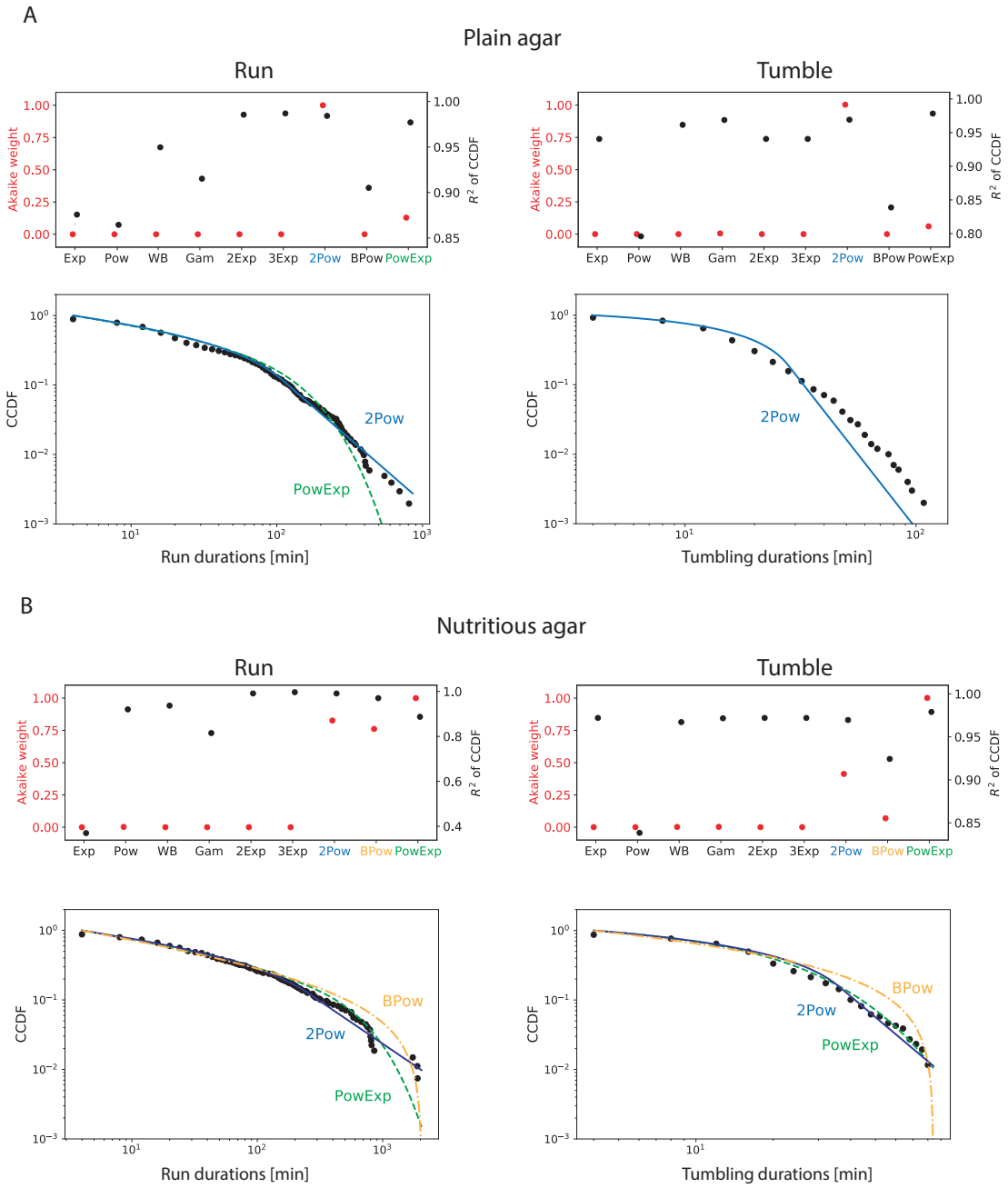

Figure 12: Akaike weights of the different tested models and the associated R-square values with respect to the complementary cumulative distribution function (CCDF) of the experimental data for plasmodia migrating on plain agar (A) and nutritious agar (B). The models are Exp=exponential, Pow=power law, WB=weibull, Gam=gamma, 2Exp=two exponentials, 3Exp=three exponentials, 2Pow=two power laws, BPow=bounded power law, PowExp=exponentially truncated power law.

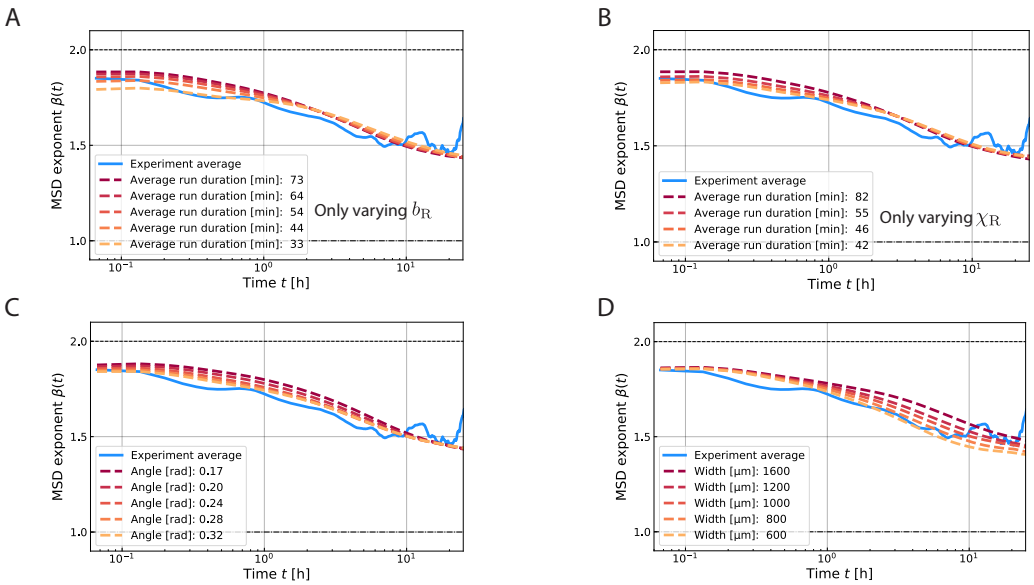

Figure 13: Parameter sweeps (5000 trajectories per simulation) reveal the control of the model parameters over the MSD exponent β. There are ten parameters in the model, four of which are investigated here as examples. One model parameter is varied, while the other parameters are kept constant. Experimental MSD exponent (plain agar) in blue solid line. Simulation MSD exponents in dashed lines. (A) The average run duration $\langle R \rangle$ is varied by changing the power law transition point b_R in the interval [52, 164] minutes. (B) The average run duration $\langle R \rangle$ is varied by changing the second power law exponent χ_R in the interval [2.4, 3.6]. (C) The average turning angle during runs ϕ_R is varied. (D) The median plasmodium width $\bar{w}$ corresponding to the self-avoidance is varied.

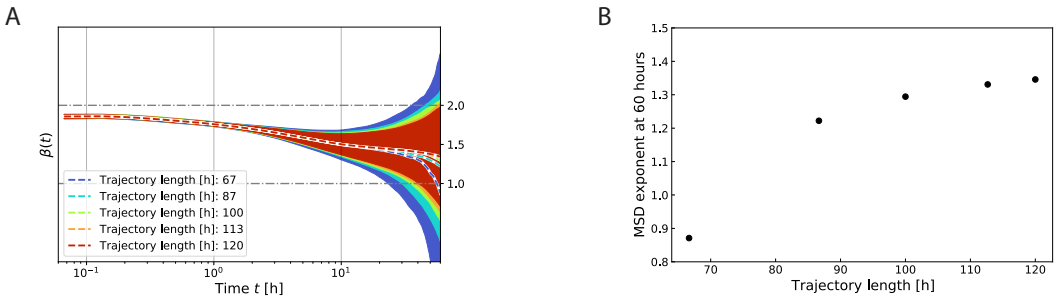

Figure 14: Long-time simulations approach an MSD exponent of $\beta = 1.5$. Instantaneous MSD exponent β depending on the simulated trajectory length for all times (A) and at 60 hours (B).

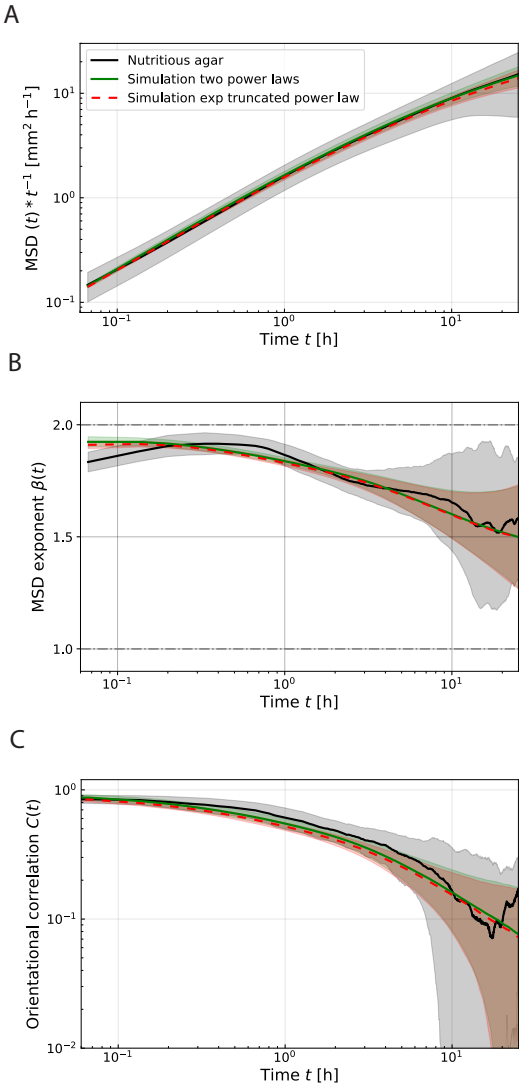

Figure 15: Simulation results are the same for two types of run duration distributions: A combination of two power laws (green solid line) and an exponentially truncated power law (dashed red line), compared to the data from nutritious agar (black solid line). (A) Log-log plot of the MSD for the experimental data on nutritious agar and for the simulations using the two different distributions of run durations. (B) Lin-log plot of the MSD exponent β. (C) Log-log plot of the orientational correlation C.

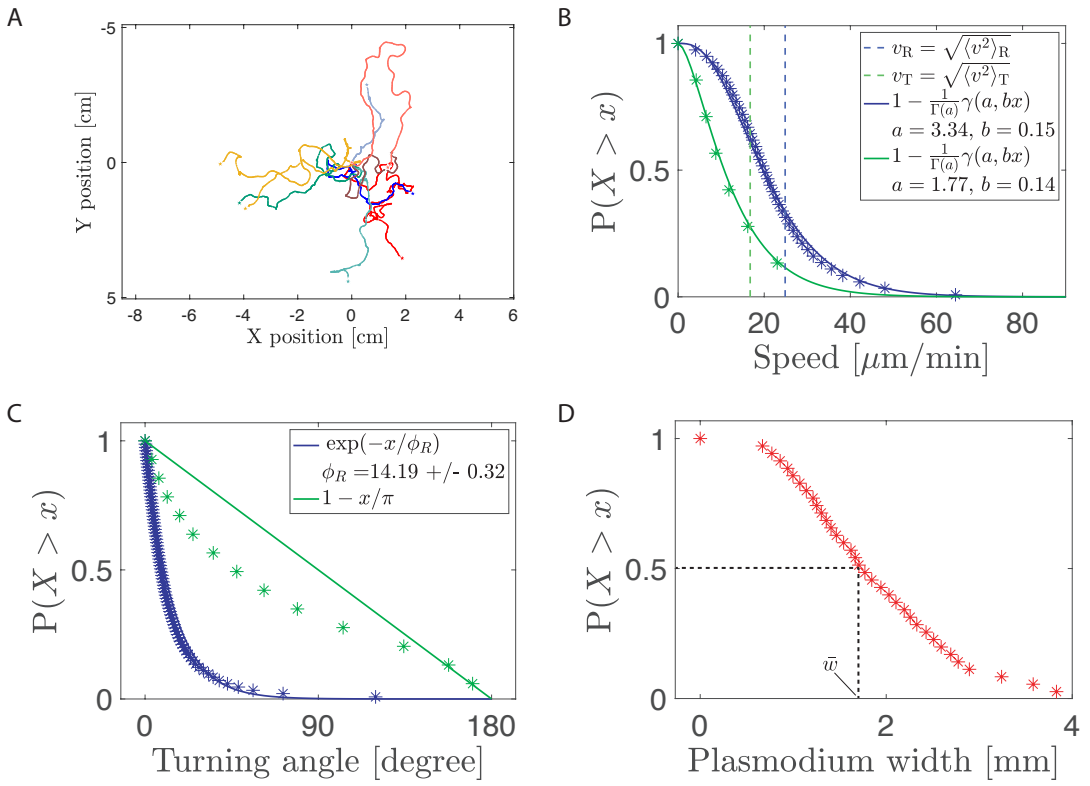

Figure 16: Parameter extraction for the migration of plasmodia on nutritious agar. (A) Trajectories of plasmodia migrating on nutritious agar. (B)-(D) Complementary cumulative distribution functions (CCDF), $P(X > x)$, of the analyzed variables, with X denoting the respective variable. Fits in solid lines. (B) Speeds during runs and tumbles with fitted gamma distributions (solid lines). Dashed lines: Root mean squared speeds. (C) Turning angles between consecutive steps during runs and tumbles. Run statistics fitted by an exponential distribution (blue solid line) and tumble statistics approximated by a homogeneous distribution (green solid line). (D) Widths of the plasmodia trails as a measure for the avoided space around the trajectories. The width is estimated as the width of an ellipse fitted to the plasmodium. The dashed line represents the median width of all plasmodia.

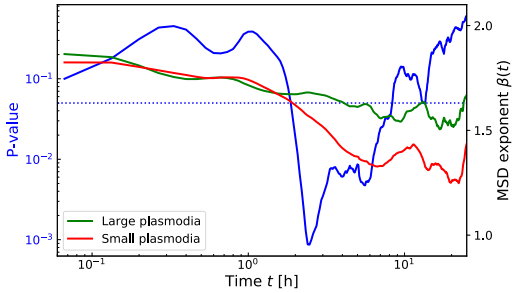

Figure 17: Small plasmodia have a lower MSD exponent than large plasmodia on time scales $> 2\,\mathrm{h}$. Left y-axis shows P-values obtained from a one-tailed Welch's t-test for different times t with the alternative hypothesis that the MSD exponent of small plasmodia is smaller than the MSD exponent of large plasmodia. Choosing a significance level of 5%, we can conclude that small plasmodia have a lower MSD exponent than large plasmodia on time scales $> 2\,\mathrm{h}$. For time scales larger than $10\,\mathrm{h}$, the experimental values become less and less reliable to make a statement.

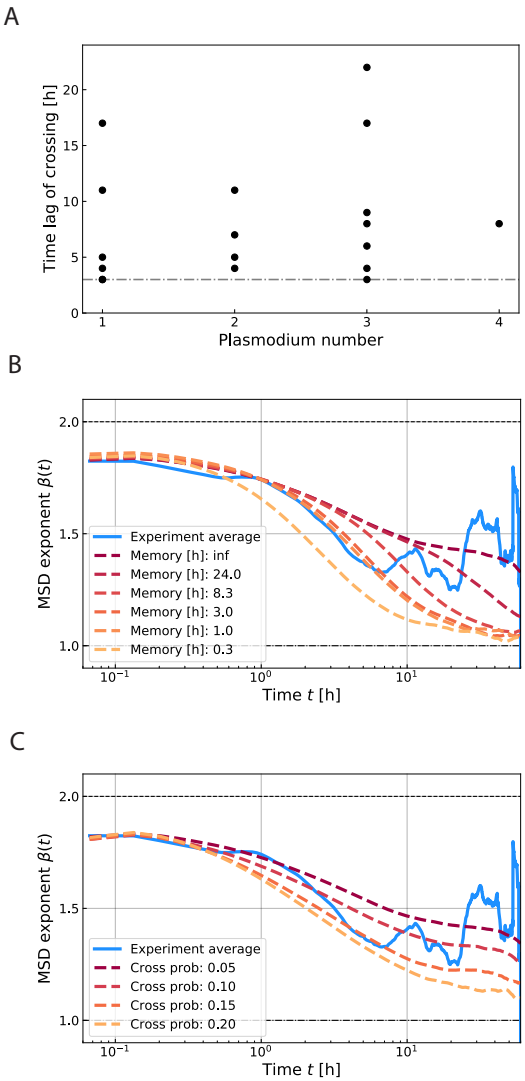

Figure 18: Small plasmodia start crossing their own trails after 3 hours. This can well be modeled by a memory-dependent trail. (A) Time lag after which some of the small plasmodia cross their own trail. (B) Changing the memory of the slime trail in simulations (5000 trajectories each) shows that this parameter controls the transition of the MSD exponent to a value of $\beta = 1$. Note that an infinite memory corresponds to a strictly self-avoiding walk. (C) Changing the probability to cross the slime trail in simulations (5000 trajectories each) shows that this parameter affects the MSD exponent on all time scales.

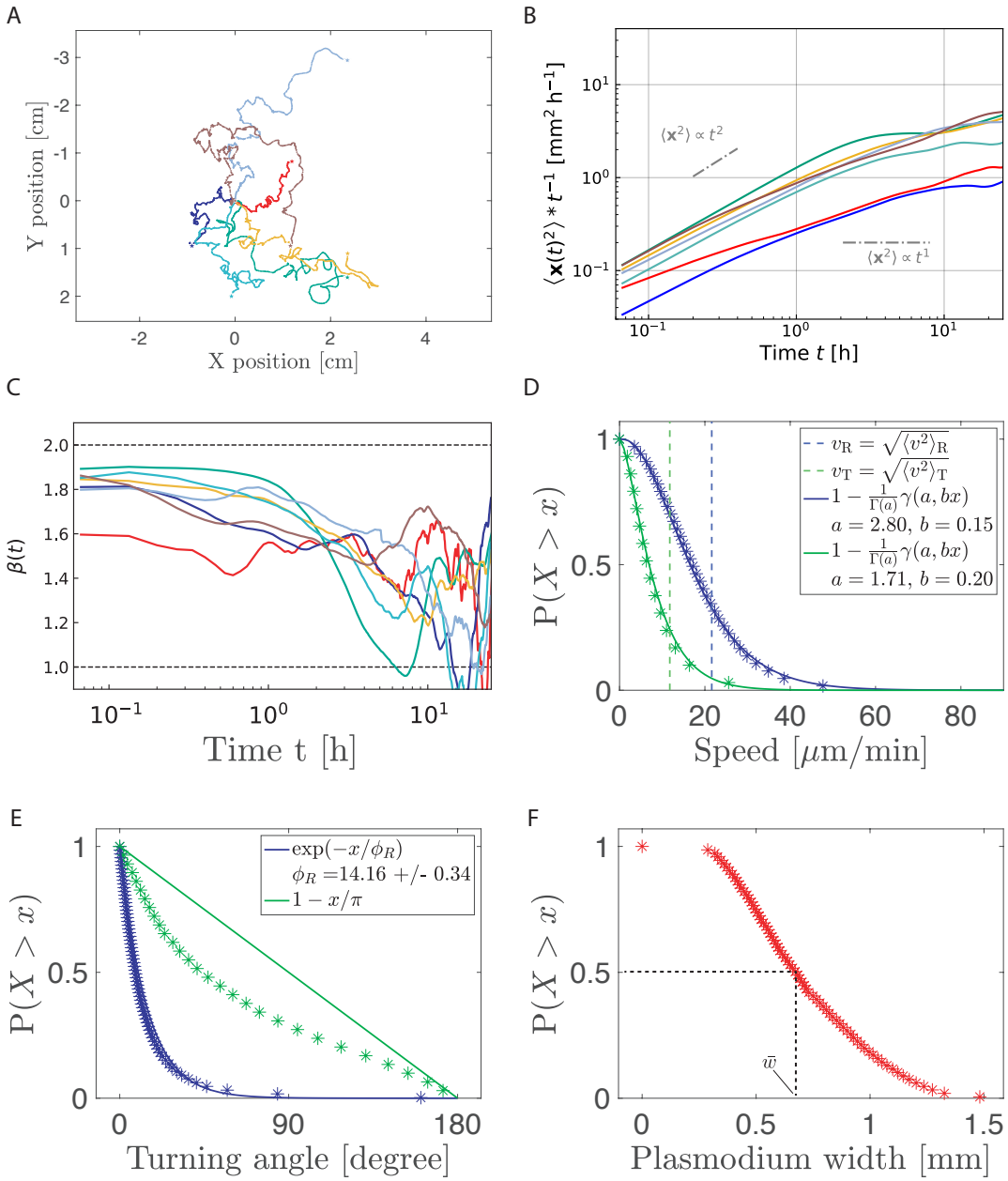

Figure 19: Trajectories, MSD and parameter extraction for the small plasmodia group. (A) Trajectories of the small plasmodia shifted to start at the same point. (B) Individual MSDs divided by time of the small plasmodia with colors corresponding to the trajectories in (A). (C) MSD exponents β of individual plasmodia. (D)-(F) Complementary cumulative distribution functions (CCDF), $P(X > x)$, of the analyzed variables, with X denoting the respective variable. Fits in solid lines. (D) Speeds during runs and tumbles with fitted gamma distributions (solid lines). Dashed lines: Root mean squared speeds. (E) Turning angles between consecutive steps during runs and tumbles. Run statistics fitted by an exponential distribution (blue solid line) and tumble statistics approximated by a homogeneous distribution (green solid line). (F) Widths of the plasmodia trails as a measure for the avoided space around the trajectories. The width is estimated as the width of an ellipse fitted to the plasmodium. The dashed line represents the median width of all plasmodia.

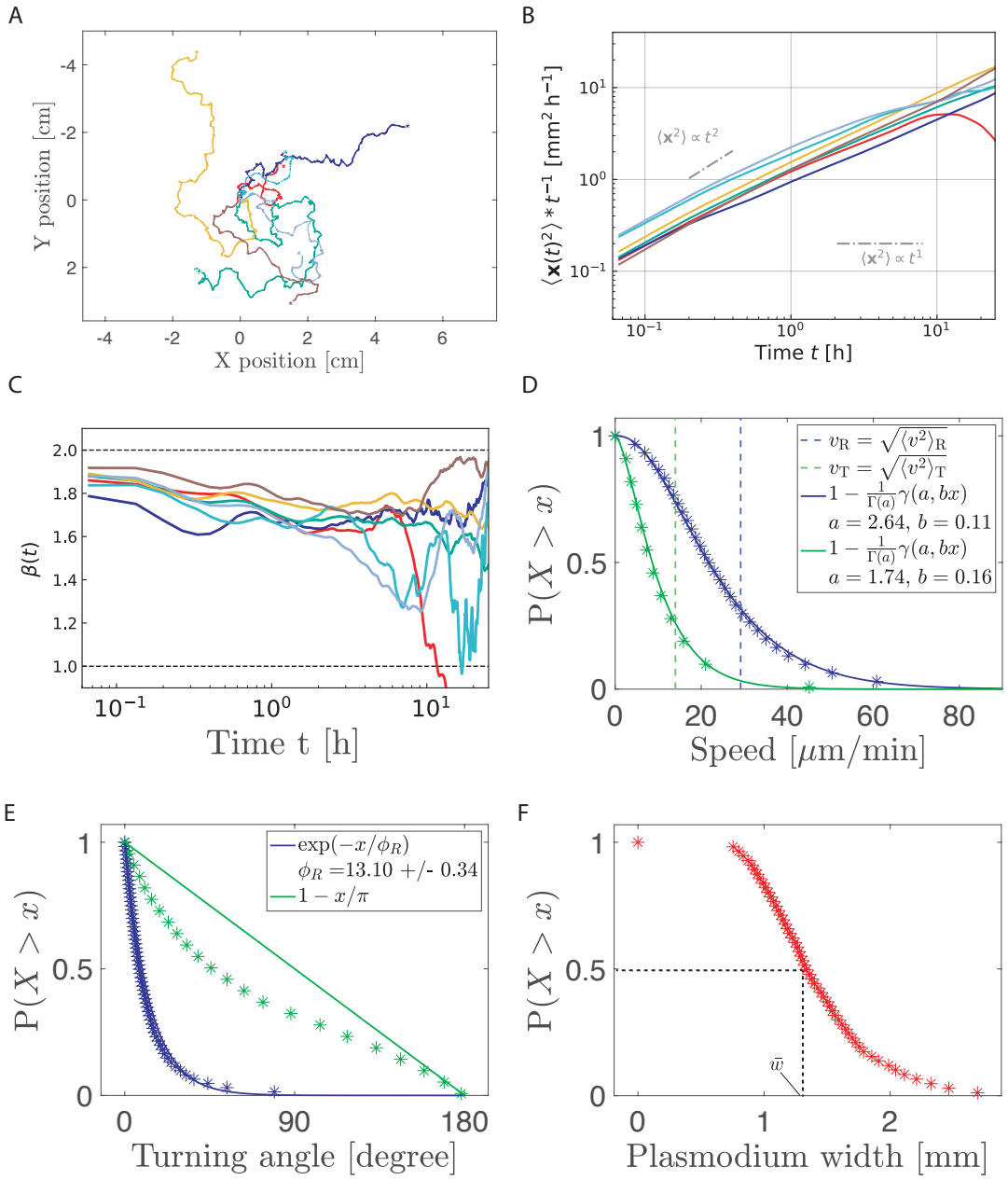

Figure 20: Trajectories, MSD and parameter extraction for the large plasmodia group. (A) Trajectories of the large plasmodia shifted to start at the same point. (B) Individual MSDs divided by time of the large plasmodia with colors corresponding to the trajectories in (A). (C) MSD exponents β of individual plasmodia. (D)-(F) Complementary cumulative distribution functions (CCDF), $P(X > x)$, of the analyzed variables, with X denoting the respective variable. Fits in solid lines. (D) Speeds during runs and tumbles with fitted gamma distributions (solid lines). Dashed lines: Root mean squared speeds. (E) Turning angles between consecutive steps during runs and tumbles. Run statistics fitted by an exponential distribution (blue solid line) and tumble statistics approximated by a homogeneous distribution (green solid line). (F) Widths of the plasmodia trails as a measure for the avoided space around the trajectories. The width is estimated as the width of an ellipse fitted to the plasmodium as in (A). The dashed line represents the median width of all plasmodia.

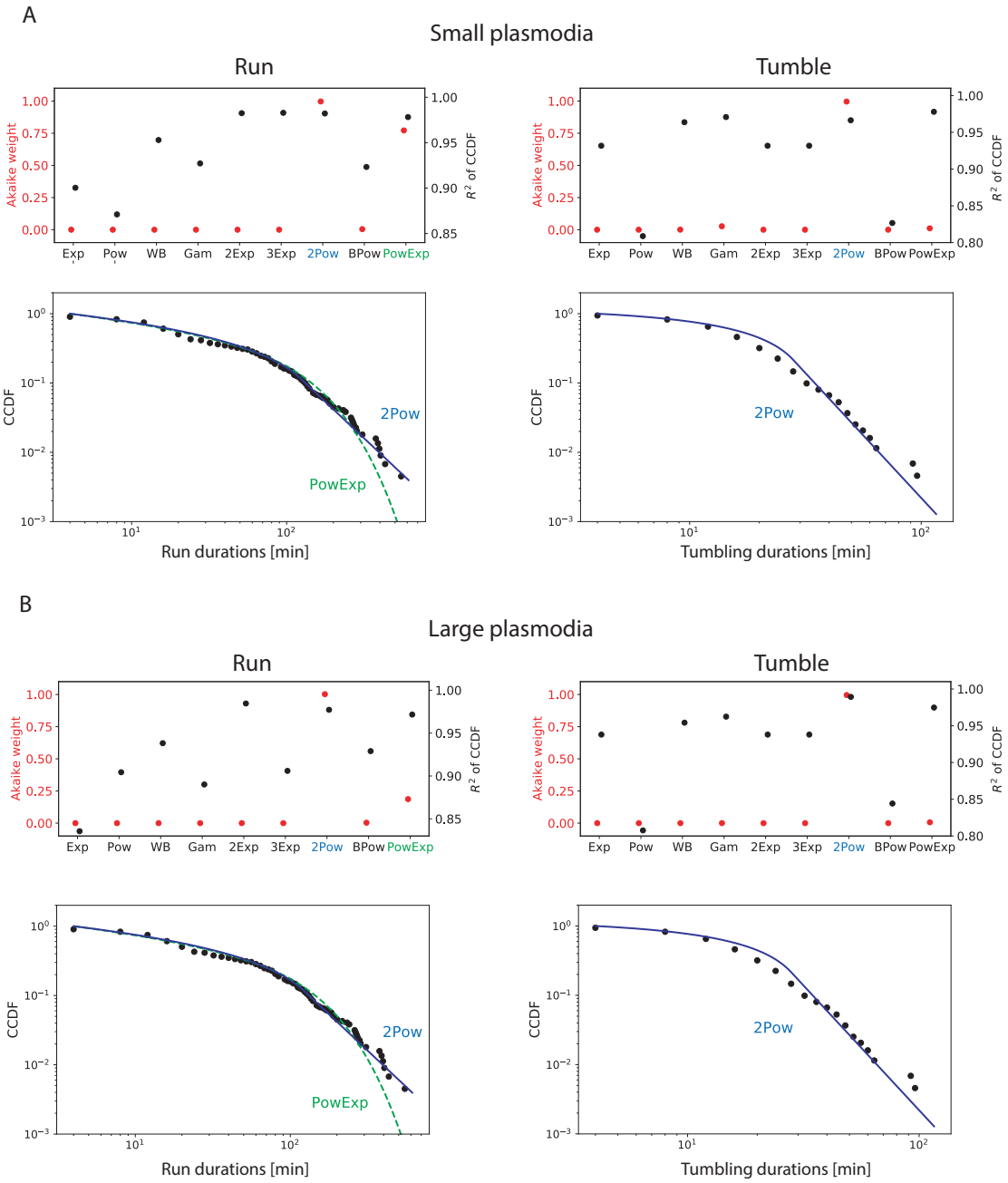

Figure 21: Akaike weights of the different tested models and the associated R-square values with respect to the complementary cumulative distribution function (CCDF) of the experimental data for small (A) and large (B) plasmodia. The models are Exp=exponential, Pow=power law, WB=weibull, Gam=gamma, 2Exp=two exponentials, 3Exp=three exponentials, 2Pow=two power laws, BPow=bounded power law, PowExp=exponentially truncated power law.

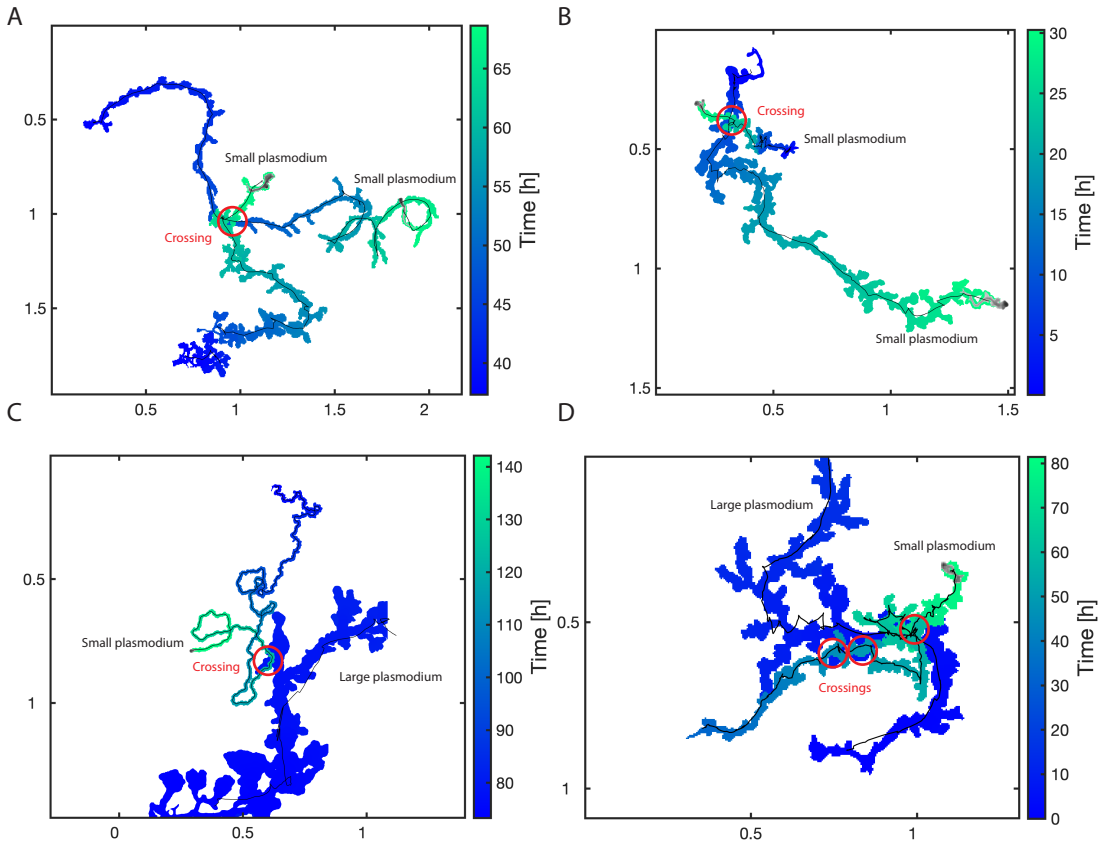

Figure 22: Small plasmodia avoid neither the slime trail of small plasmodia nor that of large plasmodia. (A-D) Examples of interaction events between two plasmodia. Plotted are the trails of the individual plasmodia, color coded with the time at which they explore certain areas. These are overlayed by the centroid trajectory (black lines). In case plasmodia are still within the region of interest at the latest time point, greyvalue images are overlayed, marking the position of the plasmodium in the last time frame. Events where plasmodia are crossing the trail of other plasmodia are highlighted by red circles. Ticks on axes in centimeters. (A) Small plasmodium (size: $0.55\,\mathrm{mm}^2$) crossing the slime trail of another small plasmodium (size: $0.28\,\mathrm{mm}^2$). (B) Small plasmodium (size: $0.12\,\mathrm{mm}^2$) crossing the slime trail of another small plasmodium (size: $0.49\,\mathrm{mm}^2$). (C) Small plasmodium (size: $0.03\,\mathrm{mm}^2$) crossing the slime trail of a large plasmodium (size: $2.9\,\mathrm{mm}^2$). (D) Small plasmodium (size: $0.14\,\mathrm{mm}^2$) crossing the slime trail of a large plasmodium (size: $0.77\,\mathrm{mm}^2$).

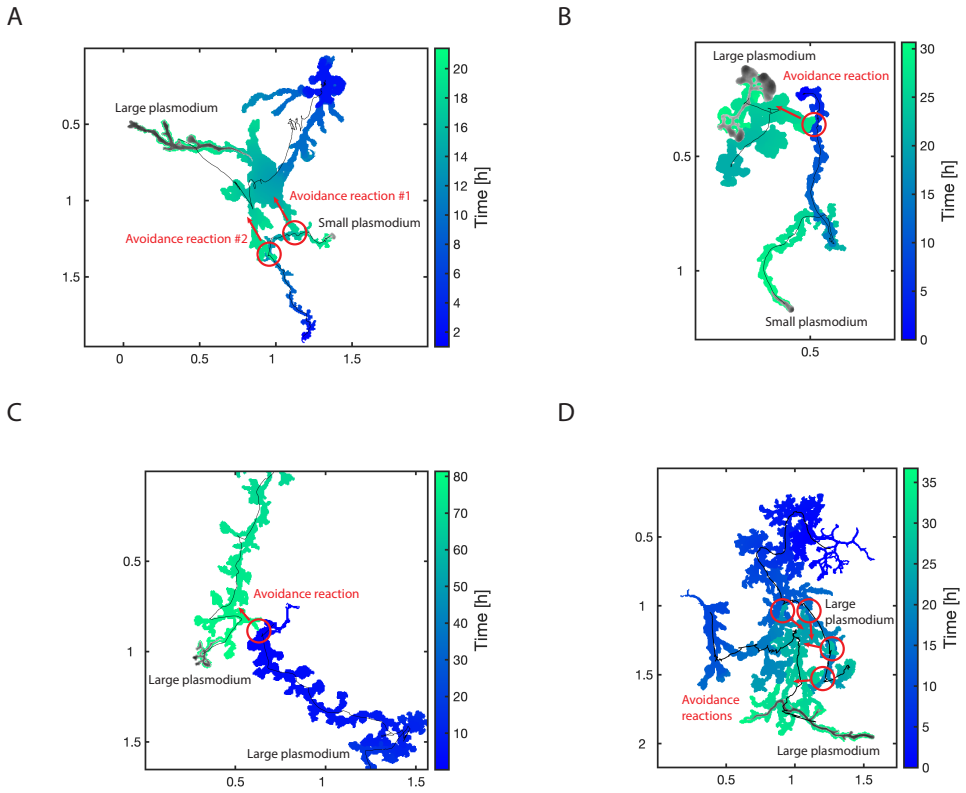

Figure 23: Large plasmodia avoid both the slime trail of small plasmodia and that of large plasmodia. (A-D) Examples of interaction events between two plasmodia. Plotted are the trails of the individual plasmodia, color coded with the time at which they explore certain areas. These are overlayed by the centroid trajectory (black lines). In case plasmodia are still within the region of interest at the latest time point, greyvalue images are overlayed, marking the position of the plasmodium in the last time frame. Events where plasmodia recognize the trail of other plasmodia and retract their protrusions as an avoidance reaction are highlighted by red circles. The retracting protrusions are highlighted by red arrows. Ticks on axes in centimeters. (A) Large plasmodium (size: 3.41 mm^2) avoiding the slime trail of a small plasmodium (size: 0.18 mm^2). (B) Large plasmodium (size: 1.40 mm^2) avoiding the slime trail of a small plasmodium (size: 0.24 mm^2). (C) Large plasmodium (size: 0.82 mm^2) avoiding the slime trail of another large plasmodium (size: 0.90 mm^2). (D) Large plasmodium (size: 1.46 mm^2) avoiding the slime trail of another large plasmodium (size: 1.85 mm^2).

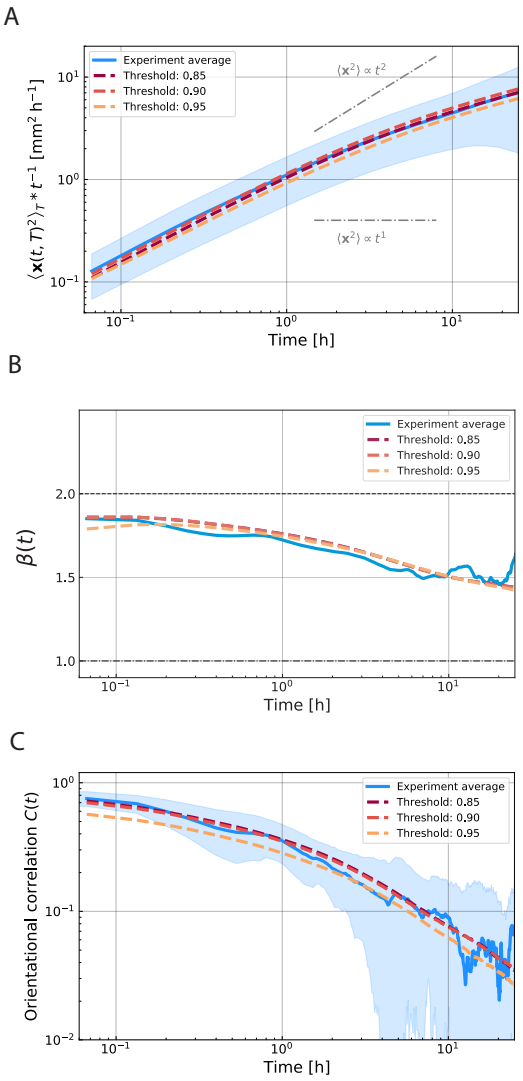

Figure 24: Parameter sweep (5000 trajectories per simulation) with respect to the directionality threshold reveals the robustness of the analysis with respect to simulation results, which are performed with model parameters extracted for different values of the directionality threshold (0.85, 0.9 and 0.95) used for the analysis of the run-and-tumble dynamics. Experimental results (plain agar) in blue solid lines. Simulation results in dashed lines. (A) Log-log plot of the MSD divided by time. (B) Lin-log plot of the MSD exponent β. (C) Log-log plot of the orientational correlation C.

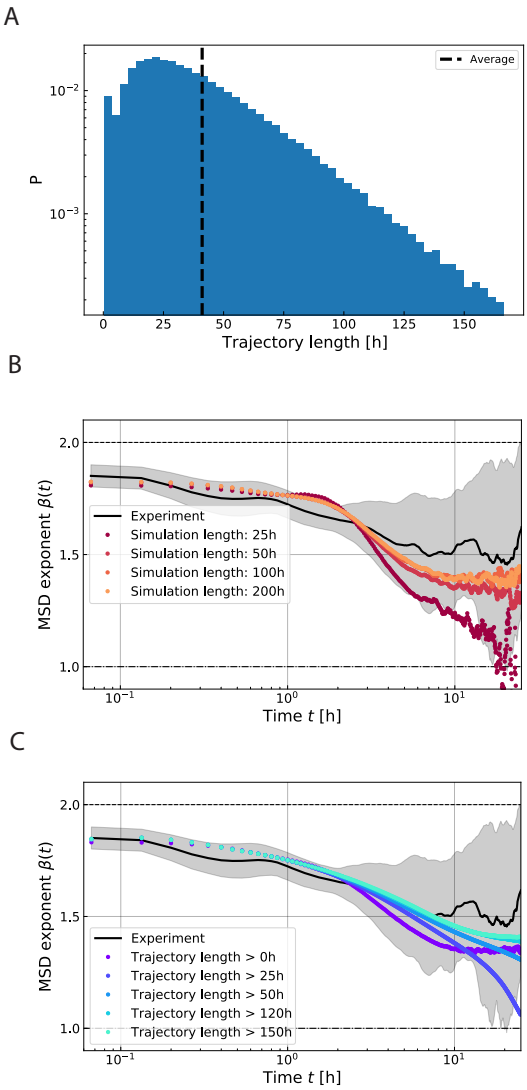

Figure 25: Only long trajectories of a length greater than 120 h approach the true long time behavior of the MSD exponent $\beta(t)$. (A) Probability distribution of the length of simulated trajectories (7×10^5 realizations of 2500 steps corresponding to 166 hours experimental time). (B) Dependence of $\beta(t)$ on the simulation length (10^5 realizations each). (C) Dependence of $\beta(t)$ on the criterion for selecting trajectories. Subsets are formed from the full set of trajectories in (A). The curve displaying the MSD exponent for trajectory lengths > 25 h exhibits a sampling bias around 25 h which leads to a drop of the value.

4 Migration of *Physarum polycephalum* in different environments

The following chapter is partly based on Diana Lenski's work, documented in Reference 180. Diana Lenski was jointly supervised by the author and Karen Alim.

4.1 Influence of the environment on cell behavior

The environment plays a crucial role for the behavior of living organisms [52, 181–185]. Even comparatively simple life forms like cells are very dynamic systems with self-regulating internal structures and processes that enable them to respond rapidly to environmental stimuli [186]. Slight changes in an organism's environment can therefore lead to strong changes in its behavior. For example, a change in the pH conditions can increase the metastasis of tumors [181] and lead to fruiting body formation of the slime mold *P. polycephalum* [187], but also perturb the functionality of the sensory system and the defense mechanisms of marine organisms [182, 183]. Of course, also the concentration of pH-conserving chemicals in the environment has an impact on cells. Salt, for example, has a pathogenic effect on T cells [188]. High concentrations of glucose inhibit cell migration of fibroblasts by impairing cell polarity and destabilizing protrusions [189], but enhance migration in endothelial cells due to unknown reasons [190].

How do single cell adapt their migration behavior to different environments? Microzooplankton, for example, changes the statistics of its swimming behavior depending on the presence of prey [12]. When prey is abundant, the distribution of durations of continuous swimming is exponential, so contains few long swimming events. When prey is scarce, they change they behavior and the distribution switches to a power-law with very long swimming events. This adaptation is beneficial since it was shown that, in low density scenarios, Lévy searching (characterized by a power law distribution) is more efficient than Brownian searching (characterized by an exponential distribution) [191, 192]. Fibroblasts change their speed of movement by a stronger cell polarization in the presence of chemicals, known as chemokinesis, which is to be distinguished from chemotaxis, where directional movement is decisive [193]. The migration speed of the cellular slime mold *Dictyostelium discoideum* decreases due to cell rounding for high

concentrations of cAMP, which functions as the chemoattractant during the aggregation phase *D. discoideum* [168]. Bacteria like Rhizobium meliloti and marine bacteria increase their swimming speed in the presence of some chemicals [167, 194]. The presence of a homogeneously distributed chemoattractant can also induce directed motion in groups of cells. Together, they break down the present chemoattractant and generate concentration differences, a self-generated gradient, which guides them to their aim [195–200].

The large unicellular organism *P. polycephalum* is also known to change its behavior depending on its environment [52, 184, 201]. Low concentrations of salt ($10\,\mathrm{milli/molar}$ KCl) act as an attractant for *P. polycephalum*, but it is repelled by high concentrations ($100\,\mathrm{milli/molar}$ KCl) [202]. In general, the presence of salt increases the period of the intracellular shuttle streaming [203], but decreases the migration speed of plasmodia [184]. The network structure also changes depending on the environmental conditions, such as the stiffness of the substrate, which is modulated by the agar concentration, and the concentration of attractants or repellents [52, 201]: in repellent environments, like a high KCl concentration or a soft substrate, it forms sparse networks with thin tubes, while in attractive environments, like a nutritious or stiff substrate, it forms dense networks with thick tubes. When given the choice between two environments, it migrates towards stiff and nutritious substrates.

The pH value also plays an important role for *P. polycephalum*. It is usually grown in acidic suspension culture and degenerates if the pH is higher than 6 [171], but its intracellular pH ranges between values of 7 and 7.5 [204]. Grown on agar substrate, it strives on a large range of pH values between 4.5 and 7, but migrates towards a value of around 5 when given the choice [205]. Also, the higher the pH value, the shorter the period a plasmodium will survive at high temperatures [187]. As said, the pH value also influences the fruiting body formation (spore formation) of *P. polycephalum*. At constant temperature, the highest percentage of fruiting occurs at a pH of 3 and decreases with increasing pH [187].

How do these different chemical compositions of its environment affect the migration of *P. polycephalum*? Does it modify its behavior? If yes, how? As stated above, it is known that it changes its morphology under different conditions. Can this change be a means of adapting the migration behavior? A connection between morphology and migration behavior has, for example, been shown on plain agar with large networks of *P. polycephalum*. It was found that networks in a so-called lightning morphology migrate faster [54]. In the following, we try to answer some of the above questions, focusing on the connection between environment, morphology and migration behavior.

4.2 Experimental setup and results

We observe small plasmodia migrating in 6 chemically different environments and compare them to the plain agar data from the previous chapter. They all consist of 1.5% agar substrates, but contain different chemicals: *glucose agar* containing 5.5 mM glucose and 2 mM leucine, *SDM agar* containing 10% semi-defined medium (resulting in a glucose concentration of 5.5 mM), *KCl agar* containing the salt KCl with concentrations of 20 mM and 50 mM, and *pH-adjusted agar* containing 20 mM KCl and additionally 0.8 mM HCl or 0.1 mM KOH to adjust the pH of the agar substrate from around 7 to values of 6 or 8, respectively. The complete list of experiments can be found in the Appendix, Table 6.

The protocols for the preparation these substrates can be found in the appendix. The inoculation of plasmodia to the substrate is done as described in the previous chapter: single microplasmodia from liquid culture are transferred to the substrates with a 1 mL pipet tip and deposited with a low cell density of 3 to 5 cells per petri dish with a diameter of 9 cm.

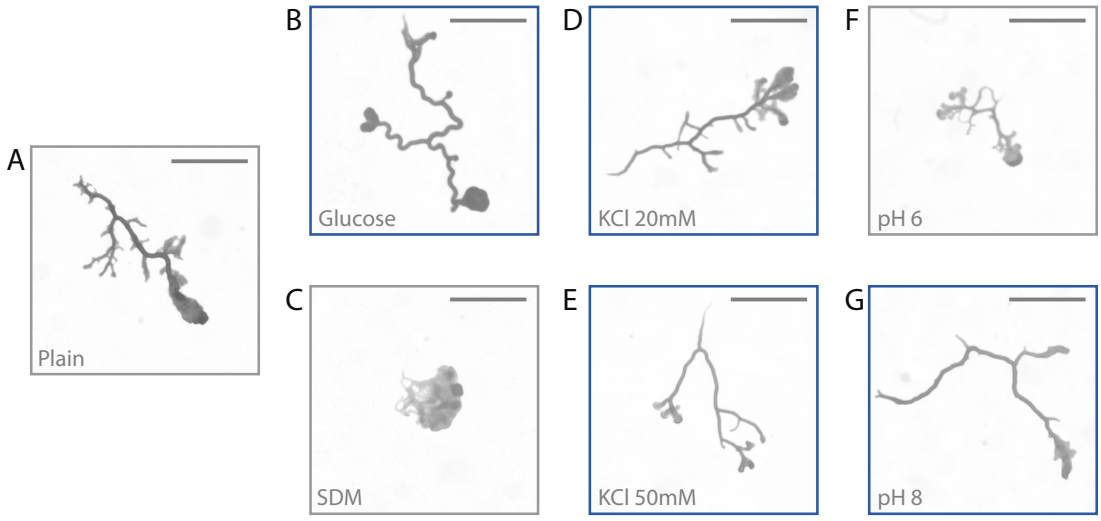

Figure 26: The chemical composition of the substrate affects the morphology of migrating plasmodia. All substrates consist of 1.5% agar with the indicated changes in chemical compositions. Blue frames indicate tubular morphologies. Scale bars: 2 mm.

After a few hours, the spherical microplasmodia start spreading out to form migrating plasmodia. The morphology differs for different migration substrates. On plain agar, plasmodia have a trailing tube at the cell rear, which transitions into a branched fan at the cell front (Figure 26A).

In contrast, plasmodia on agar containing glucose, on agar containing KCl, and on agar with a pH of 8 have more slender and elongated, tubular cell shapes, mainly consisting of a single main tube and few side branches (Figure 26B,D,E,G). The main tube of plasmodia on KCl agar has a diameter of around $70\,\mu m$ (Figure 26D,E), while the main tube on glucose agar is thicker with around $100\,\mu m$ diameter (Figure 26B). Plasmodia on agar with a pH value of 6 have a similar morphology as plasmodia on plain agar (Figure 26F). On agar containing SDM, the plasmodia have a very different morphology. They form a plasmodial sheet without any branches (Figure 26C). Due to the changed morphology, the slime trails left behind plasmodia have a different appearance. On agar with pH 6, slime trails are broader than on plain agar, while slime trails on agar with pH 8 and on agar containing glucose or KCl are narrower (Figure 27). On SDM agar, plasmodia leave a very broad trail.

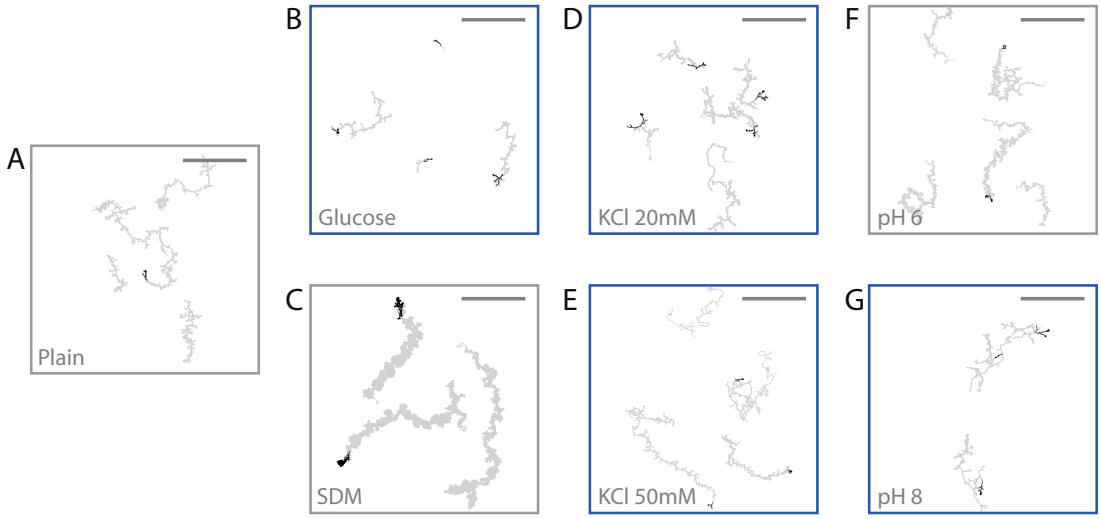

Figure 27: Deposited slime trails (here shown in gray) also depend on the chemical composition of the migration substrate due to its influence on the morphology. Still migrating plasmodia are shown in black. Substrates as in Figure 26, blue frames indicate tubular morphologies. Scale bars: $2\,cm$.

Plasmodia on agar containing glucose or $50\,mM$ KCl, or with a changed pH value show intermittent migration with pronounced stationary cell oscillations, in contrast to plasmodia on plain agar, SDM agar and $20\,mM$ KCl agar, which move continuously with few stopping or oscillations. For an example of a plasmodium with oscillating movement on agar with pH 8, see Figure 28. There seems to be a weak correlation between morphology and oscillations: 3 out of 4 tubular morphologies are connected with oscillations, while 2 out of 3 branched or sheet-like morphologies show no oscillations.

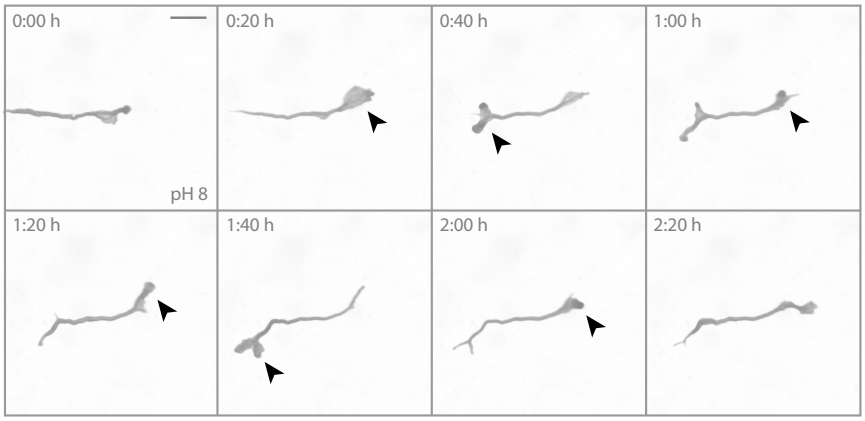

Figure 28: We observe stationary oscillations over hours on substrates which induce a tubular morphology. Here: time series of a plasmodium performing a stationary oscillation during migration on agar with a pH value of 8. Arrows indicate growing protrusions. Scale bar: 1 mm

To get some insights into their migration characteristics, we look again at the scaling of the MSD. We observe some differences between plasmodia migrating on modified substrates compared to plasmodia migrating on plain agar. Noticeably, the MSDs of plasmodia show a dip in the MSD exponent at around $t \approx 20\,\mathrm{min}$ for all substrates on which plasmodia show stationary cell oscillations: $5.5\,\mathrm{mM}$ glucose, pH 6, pH 8, and $50\,\mathrm{mM}$ KCl (Figure 29). This dip is not present for the control substrate plain agar nor for the substrate containing or SDM. $20\,\mathrm{mM}$ KCl agar is connected with only a slight dip.

There seems to be a connection between the stationary oscillations on one side and the reduced MSD exponent at around $t \approx 20\,\mathrm{min}$ on the other. To check this, we look at the time-dependent correlation or alignment of pairs of velocity vectors $\mathbf{v}$ separated in time,

$$\mathrm{Alignment}(T) = \frac{\mathbf{v}(T) \cdot \mathbf{v}(T+t)}{|\mathbf{v}(T)||\mathbf{v}(T+t)|},$$

with T the measurement time and t a certain time lag. When they are anti-aligned ($\mathrm{Alignment} < 0$) with a time lag of, for example, $t = 20\,\mathrm{min}$ between them, this corresponds to an oscillation with a period of $T_{\mathrm{oscillation}} = 40\,\mathrm{min}$ and can contribute to a dip in the MSD exponent at $t \approx 20\,\mathrm{min}$. Identifying these events along the trajectory (Figure 30B) matches the visual identification of oscillation events. We identify a phase of anti-alignment as an oscillation event if it persists for at least one oscillation period (twice the chosen value of $t = 20\,\mathrm{min}$ corresponding to the dip, so $40\,\mathrm{min}$), which we can also map on the trajectory (Figure 30C). This finding suggests that the oscillation is a distinct phase, which needs to be added to the model established in the previous chapter, in order to describe the migration behavior on different substrates

correctly. From visual inspection of the experimental recordings, this phase is morphologically often characterized by a single, long, mostly unbranched vein connecting two protrusions in most cases (Figure 28). Notably, oscillations are often detected as runs when performing the run-and-tumble analysis described in the previous chapter since they consist of persistent movement on short time scales (Figure 30A).

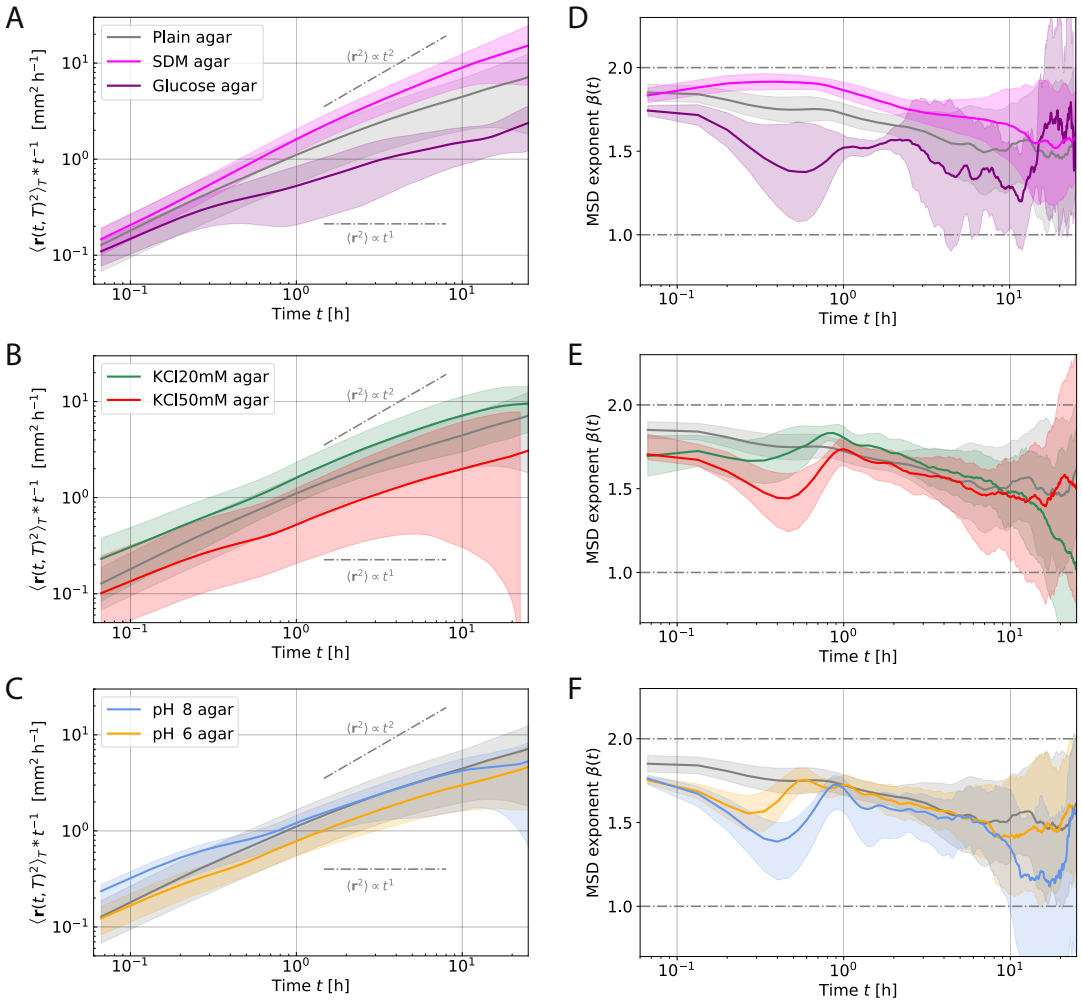

Figure 29: Migration characteristics are environment-dependent. (A-C) Log-log plot of the MSD divided by time of migrating plasmodia on plain agar (gray, 14 trajectories, from Chapter 2), SDM agar (pink, 9 trajectories), glucose agar (purple, 7 trajectories), 20 mM KCl agar (green, 9 trajectories), 50 mM KCl agar (red, 11 trajectories), ph 6 agar (orange, 8 trajectories) and ph 8 agar (blue, 12 trajectories). Shaded regions show the standard deviations. (D-F) Log-lin plot of the instantaneous MSD exponent $\beta(t)$ for the investigated environments.

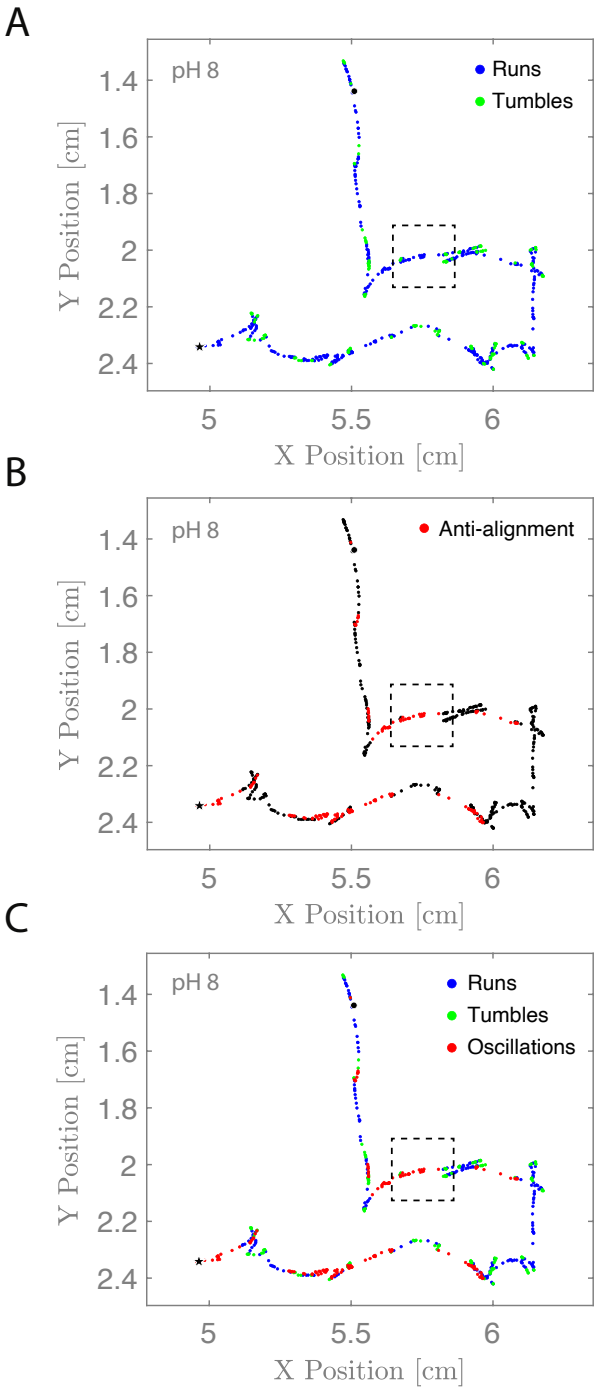

Figure 30: A part of the trajectory with anti-alignment in the motion on a time scale of $t = 20\,\text{min}$ is characterized as a new phase, the oscillation phase. (A) Run and tumble events in a centroid trajectory of a plasmodium migrating on pH 8 agar. (B) Same as in (A) but showing events of anti-alignment. (C) Same as in (A) but including the new phase, oscillations. The dashed square indicates the centroid positions of the plasmodium in Figure 28.

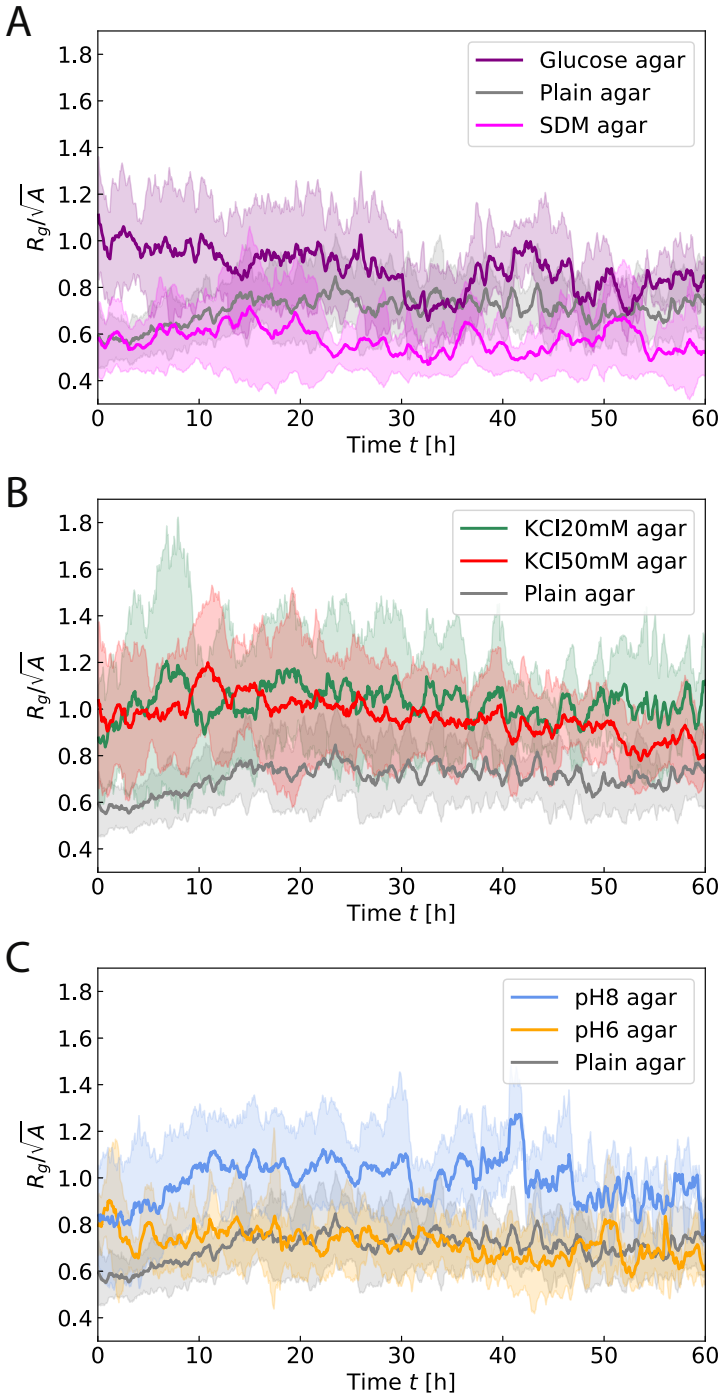

Figure 31: The scaled radius of gyration as a measure for the morphology is larger for plasmodia with a tubular morphology. (A-C) Time course of the ensemble average of the radius of gyration scaled by the square root of the plasmodium area for plasmodia migrating in the investigated environments (colored lines) compared to plain agar (gray line).

Given these findings, we suspect a connection between migration behavior and morphology, which we investigate further. To quantify the morphology of plasmodia, we use the radius of gyration, which we scale by the square root of the plasmodium area to remove a bias due to different plasmodium sizes [54]. We define the radius of gyration for the pixels that make up the two-dimensional shape of a plasmodium: it is given by a summation over all pixels' squared distances to the plasmodium's center and describes its mass distribution. We find that the scaled radius of gyration is large for plasmodia with tubular morphologies, namely plasmodia migrating on agar with glucose, pH 8 or KCl (Figure 31). The scaled radius of gyration is small for branched plasmodia (plain agar, pH 6 agar) or sheet-like plasmodia (SDM agar).

Using the alignment of the movement of plasmodia as a measure for the migration behavior and the scaled radius of gyration as a measure for the morphology, we find a connection between migration behavior and morphology: the alignment in the motion of plasmodia anticorrelates with the scaled R_g (Figure 32, r-value $= -0.56$). In other words, plasmodia with tubular morphologies show more phases of anti-alignment or oscillation in their motion, which reduces space exploration as seen from the MSD.

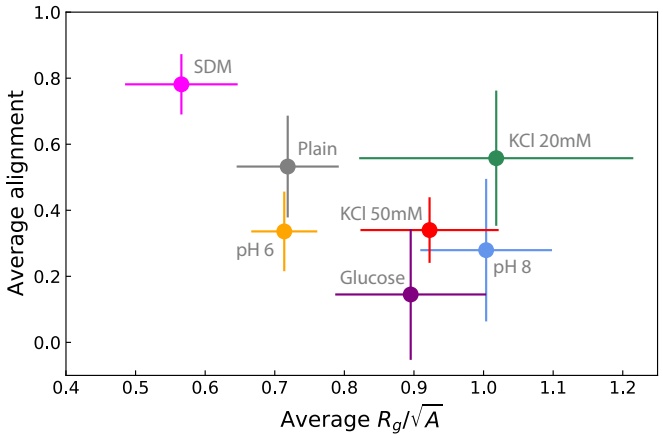

Figure 32: The average alignment during migration correlates negatively with the scaled radius of gyration. Plot of the average alignment against the scaled radius of gyration for the investigated environments. Error bars show the standard deviation.

4.3 Discussion

We have seen that migrating plasmodia take on very different morphologies depending on the chemical composition of the migration substrate. There is a crossover from sheet-like morphologies on SDM agar to branched plasmodia on plain agar or pH 6 agar, and tubular morphologies on agar containing glucose or KCl or on pH 8 agar, which can be quantified by the scaled radius of gyration, crossing over from small to large values, respectively. This relates to different migration statistics for different substrates. Certain environments lead to an anti-alignment of the movement on the 20-minute time scale associated with stationary cell oscillations. We connect this with the differences in morphology and find anti-correlation between alignment and the scaled radius of gyration, which teaches us that more tubular morphologies oscillate more often.

Oscillations are a fundamental property of *P. polycephalum*. Besides the shuttle streaming, there are several other intrinsic oscillations [41, 55, 56]. However, the pronounced oscillations described here seem to be unique to environments containing certain chemicals, being absent on plain agar. It remains unclear why *P. polycephalum* adapts its morphology and migration behavior in the way it does. Possibly, it changes its morphology to reduce the contact area with an unfavorable substrate and maybe this morphology induces oscillations. However, the oscillations seem to be counterproductive in leaving an unfavorable enviroment like high concentration KCl due to the reduced persistence. We have seen that on agar containing the growth medium SDM, *P. polycephalum* forms a dense plasmodial sheet without branches. This is optimal in the sense that the plasmodium maximizes its contact area with the substrate and, hence, can take up more nutrients from the substrate. The persistence of the plasmodia is the largest of all environments, with no oscillations present, supporting the hypothesis of a connection between migration and morphology. This is especially interesting because it does not seem necessary for the persistence to be higher in a more nutritive environment. However, plasmodia stop migrating at very high concentrations of SDM (50% SDM, data not shown) and instead just grow in size. It seems that the 10% SDM concentration used here is not high enough to sustain growth over a long period of time, for example because nutrients are quickly depleted and *P. polycephalum* needs to move on find new food. Therefore, the highly persistent migration strategy seems reasonable in this scenario. The low persistence of plasmodia with tubular morphology and oscillations seems to be counterproductive for space exploration. However, the oscillations could be part of a decision-making process, where *P. polycephalum* contemplates the best next migration di-

rection and searches for a chemical gradient it could follow. It has also been speculated that there might be a connection between oscillations and learning, with modulations of spontaneous oscillations sustaining the learning process in *P. polycephalum* [70].

In summary, we established that morphology and migration behavior of migrating plasmodia is environment-dependent and interconnected, but the reason for certain morphologies as adaptations to the environment remains unclear. We come back to this topic in the next chapter, where we expose *P. polycephalum* to a chemical gradient to test its search strategy in the presence of guiding cues.

5 Chemotaxis of *Physarum polycephalum*

In the previous chapter, we have seen that the morphology and the migratory behaviour of *P. polycephalum* is modified in different homogeneous environments. What happens when we expose it to an inhomogeneous environment and, more specifically, to a gradient of nutritive chemicals? This is the topic of the following chapter.

5.1 Chemical gradients and the chemoreception of *Physarum polycephalum*

Gradients are ubiquitous in nature. Also at small scales, natural environments tend to be very heterogeneous – microbes in the ocean, for example, are subject to many chemical and physical gradients; they "see a sea of gradients" [206]. Cells also experience gradients within organisms: chemical gradients guide neutrophils towards inflammation sites [207] and fibroblasts towards wounds [208], and sperm use chemical gradients to find the egg [3, 209]. Finally, chemical gradients also play a role in the chemical communication and the mating of microbes [210], and cells like, for example, bacteria are guided to their food by gradients [20, 211]. All these examples are known under the term chemotaxis, the directed motion of organisms in response to a gradient of chemicals. Of course, there are also other forms of *taxis*, such as phototaxis (in response to a light gradient) or mechanotaxis (in response to, for example, substrate stiffness gradients), which can also be achieved by simple cells [212, 213].

While bacterial chemotaxis is well understood [214], many unanswered questions remain about eukaryotic chemotaxis, such as how cells polarize along a gradient [215]. Despite that, some progress has been made in the last two decades with *D. discoideum* as the prominent model organism, highlighting the mechanism of a biased choice of protrusion retraction [144, 216–218]. The idea of this pseudo-pod centered mechanism [218] is that cell protrusions or pseudopods are self-generated more or less independent of the presence of chemoattractants. If chemoattractants are present, they bias, for example, the position at which new pseudopods grow or which pseudopod of two or more is retracted [218]. This could, for example, be regulated by intracellular signaling cycles, for example the LEGI system [143, 144], which is explained in

Section 2.5. Another possibility is that pseudopods compete for a finite pool of actin in such a way that a winning pseudopod takes all the available actin and determines the next direction of movement [219]. For an overview over other models of chemotaxis, see Reference 220.

The process of chemotaxis gets even more intricate if many cells are involved in the chemotactic process. In fact, cell clusters improve the accuracy of gradient sensing compared to individual cells, which might be mediated, for example, by measuring concentration differences across the cluster or by averaging the noisy, independent measurements of individual cells [221–224]. Also, groups of cells can generate gradients themselves in a homogenous environment, or steepen existing gradients, thereby enhancing chemotactic efficiency [195–200, 225].

Even though the details of gradient measuring and sensing are very diverse, using gradients as a sensory cue is a fundamental part of the search strategies of many different species, evoking the impression of convergent evolution [29]. As a remarkably large cell without central nervous system, what are the means by which *P. polycephalum* senses chemicals and performs chemotaxis? On the one hand, the large cell size seems to be advantageous since the spatial gradient can be measured with a higher accuracy. On the other hand, the directed motion up a gradient requires the coordination of its randomly forming protrusions over a large spatial distance, posing an intricate problem. How does the information transfer between distant protrusions work? And how is the sum of all information processed to coordinate the action of the protrusions? These are challenges not present in tiny bacteria or amoebas. How could the chemotactic process look like in *P. polycephalum*? All protrusions continuously receive some information about the chemical composition of the substrate at their location. This probably triggers a chemical pathway of signal sensing in a given protrusion and the information about the received chemical signal is somehow passed on. There could be, for example, an intracellular signaling molecule acting as a cue for protrusion growth or retraction that is transported through the whole cell between protrusions on different ends by diffusion or advection. In that case, large plasmodia should be slower in processing guiding information because the large size implies large spatial distances between the protrusions that need to be coordinated. This could lower the chemotactic performance. On the other hand, larger plasmodia span a larger portion of the gradient, so sense stronger concentration differences. This could increase chemotactic performance according to the Weber-Fechner law described in Section 2.5. Do plasmodia of different size show differences in how efficiently they follow a gradient? Also, do chemical gradients lead to changes in morphology, as seen in the previous chapter, and does this impact the migration behavior? Before we discuss the results of our chemotaxis experiments with *P. polycephalum*, we briefly summarize what is already known about its chemotaxis.

Different methods have been used to quantify the chemotactic response of *P. polycephalum*: measuring chemotaxis at the behavioral level of migration, pressure variations in the plasmod-

ium, the isometric tension in tubes, or the electrophoretic mobility of plasmodia [226]. Chemicals are only recognized above a certain threshold concentration, ranging from $0.1\,\mathrm{mM}$ for glucose to $1\,\mathrm{mM}$ for KCl and $10\,\mathrm{mM}$ for fructose [227]. Following the chemical detection, the tension of the network tubes changes. The tension decreases with the application of attractants like carbohydrates and increases with the application of repellents like inorganic salts [228]. Le-Verge-Serandour and Alim propose an electrophysiological feedback mechanism for the detection of chemicals and the migration as a response to that [160]: external concentrations hyperpolarize or depolarize the membrane potential, which in turn changes the amount of free calcium and ATP. This triggers locally either the tension or the relaxation of tubes or protrusions and results in locomotion, as explained later in this section. The idea is supported by the finding that the injection of ATP and calcium in a tube of *P. polycephalum* is known to cause a transient contraction [229].

At the behavioral level of chemotaxis, meaning the directed migration of *P. polycephalum* in response to chemicals, a number of experiments revealed the chemotactic performance of *P. polycephalum*. Carlile tested the ability of plasmodia to migrate towards a well filled with a test solution which was mirrored by a well filled with distilled water [230]. The test solution was allowed to diffuse for 1 to 4 days before the plasmodium was inoculated in the centre between the two wells. A test was counted as positive if the plasmodium had reached the well with the test solution but not the control well, and negative if vice versa. Glucose for example yielded 100% positive results for chemotaxis in 30 trials. Also, Carlile found that there is a correlation between the chemotactic effectiveness of a chemical and its ability to support cell growth of *P. polycephalum*. Interestingly, the response was most consistent if the agar substrate contained all nutrients required by *P. polycephalum* except the one being tested [230]. Another test of chemotaxis was performed by Chet and others with a 'star' chemotaxis test, a petri dish with four separate quadrants where only one quadrant contained the test solution and the three other quadrants a buffer as controls [231]. They found similar responses like Carlile for various substances and also determined that a gradient of 1 to 2 µg per ml and mm between 40 to 60 µg glucose per ml leads to a positive chemotactic response. In a scenario with both attractant and repellent substances as a mixed stimulus, *P. polycephalum* performs chemotaxis towards the test solution depending on the repellent concentration [202]: ranging from complete attraction for a low repellent concentration of $10\,\mathrm{mM}$ KCl to mixed attraction for intermediate concentrations and repulsion for high concentrations of more than $150\,\mathrm{mM}$ KCl.

The difference in cortex tension induced by the sensing of the chemicals affects the migration of *P. polycephalum*. It generates a pressure gradient, which leads to a flow of the cytoplasm from the tail to the front of the cell [232, 233], generating protrusions [160]. The exact process of protrusion formation in *P. polycephalum* has not yet been described. In eukaryotes, protrusions

are either formed by cell polarization due to cortex contraction at the tail and actin polymerization at the front of the cell [234], or by blebbing, which is the formation of spherical protrusions when a part of the cell membrane detaches from the cortex [235, 236]. The cellular slime mold *D. discoideum* employs both modes of migration [235]. Interestingly, its protrusions form randomly, even in a chemical gradient, but it still performs successful chemotaxis [216, 237]. This raises the question of how individual protrusions coordinate their growth and retraction on the level of the entire cell for directed migration. Insights from research on *D. discoideum* suggest that the cell front could communicate with the tail by transmitting a chemical protrusion inhibitor [237]. It is not known whether this signal would be transported by diffusion or by faster, directed transport mechanisms [238, 239]. A counter-proposal for a long-range inhibitor is membrane tension, based on experiments with neutrophils: it was shown that a tethered neutrophil with one extending pseudopod did only generate a new pseudopod when the tension was released by cutting away the old pseudopod from the cell body [238].

In *P. polycephalum*, contractions of the network tubes drive a shuttle flow [47]. Their dynamics are coordinated spatially in a peristaltic wave, which matches the organism's size, even for specimens up to 2 cm in size [47]. This long-range coordination can be explained by a model that involves the coupling of the tube contractions to a signaling molecule that is transported with the fluid flow [240]. On another note, Alim and others showed that the perception of a nutrient stimulus by the cell causes a local increase in the contraction amplitude which travels along the cell. This can be explained by the release of a signaling molecule in the cytoplasm of the cell which is advected by fluid flows and in turn influences the flow generation by causing local increases in contraction amplitude [241]. A recent study showed that a signaling molecule acting as a softening agent can explain the dynamic response of a tube network of *P. polycephalum* to a nutrient source [74]. These findings suggest that the advection of a signaling molecule could also play a role in protrusion coordination by flow during the chemotaxis of *P. polycephalum*.

5.2 Experimental setup and results

We let plasmodia of different sizes migrate on 1.5% agar substrates containing concentration gradients generated by diffusion (see also Appendix A.2 for the protocol and A.3 for estimations on the gradient shapes): part of the agar is cut out on one side and the cavity is filled with agar containing chemicals which will diffuse through the substrate. Symmetrically on the other side, agar is cut out and the cavity is filled with plain agar as a control stimulus. Plasmodia are placed in the middle of the $3.5\,\mathrm{cm}$-wide agar piece between the two cut-outs, around 3 to 4 hours after gradient initiation. After around 6 hours they start migrating and successfully move up the concentration gradient of SDM (semi-defined medium) within several hours (Figure 33). However, they do not move persistently towards the nutrient source, but we observe long phases of stationary cell oscillations as already described in the previous chapter.

Quantifying their centroid trajectories with a time resolution of $4\,\mathrm{min}$, we find that migration is mainly happening in the dimension of the gradient: the migration distance parallel to the gradient is much larger than the migration distance perpendicular to it (Figure 33C). The plasmodia show a high chemotactic index after 20 hours of migration (Figure 33C), which is defined as the ratio of the displacement in the gradient direction to the absolut displacement [162]. However, their directional persistence, defined as the ratio of the absolut displacement to the total distance traveled [162], appears rather low (Figure 33C). The reason for this discrepancy is that *P. polycephalum* does not move in one direction continuously, but shows back-and-forth movements as apparent from the oscillating time course of the migration distance (Figure 33C). This results in a large total distance traveled compared to the absolut displacement, so a low directional persistence.

To extract the migration characteristics, we compute again MSD and orientational correlation (Figure 34). We find that, compared to plain agar, the motion of plasmodia on gradient agar is more directed on long time scales, resulting in a larger MSD exponent β on these time scales (Figure 34A, inset), which aligns with their successful chemotaxis up and parallel to the concentration gradient. However, we find a strong dip in the MSD exponent and the orientational correlation towards zero at a time scale $t \approx 20\,\mathrm{min}$). This means that, on this time scale, plasmodia are effectively performing a diffusive motion.

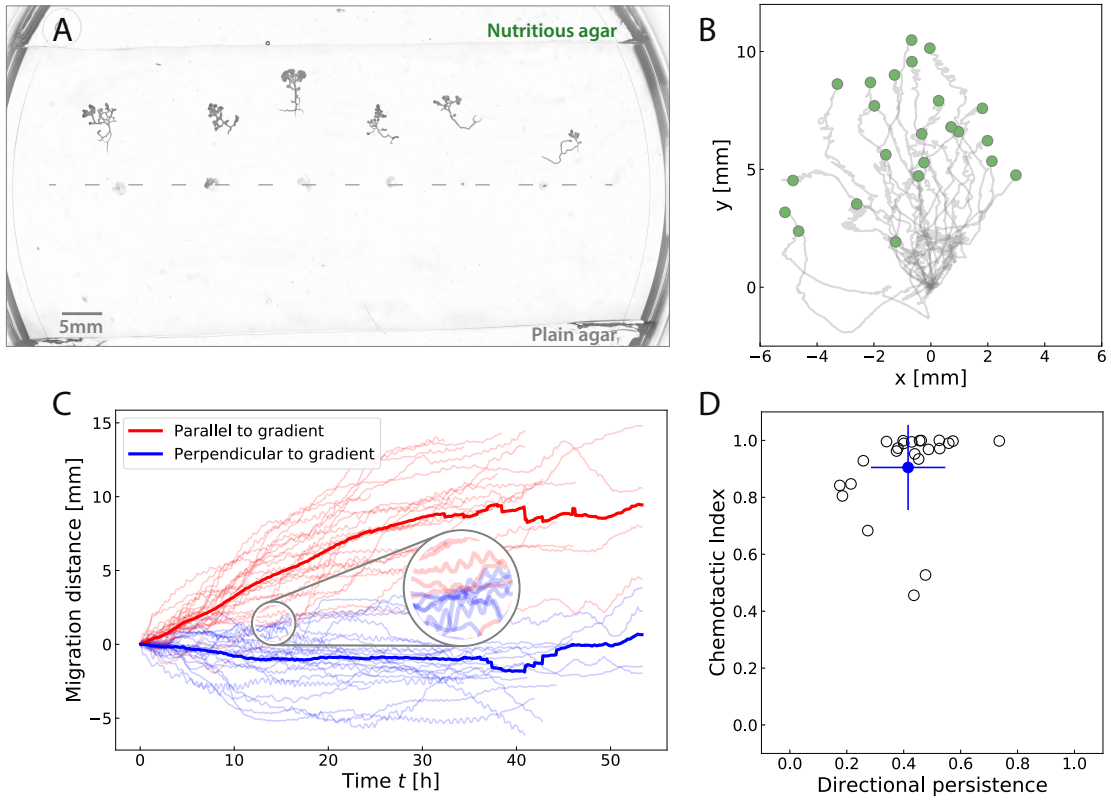

Figure 33: *P. polycephalum* successfully directs its motion towards a source of nutrients. (A) Background subtracted image of plasmodia of *P. polycephalum* on a petri dish with a gradient of nutrients in the migration substrate (1.5% agar). On the top and bottom, agar was cut out and replaced by agar containing nutritious medium (10% SDM mixed with 90% distilled water) and distilled water, respectively. The image was taken 28 h after inoculation of the plasmodia. Their initial positions lie on the gray dashed line. (B) Recentered trajectories of all 23 experimentally observed plasmodia. Green dots show end positions after 20 hours of migration. (C) Cumulative migration distance parallel to the gradient (red) and perpendicular to the gradient (blue) of individual plasmodia (thin lines) and of the mean (thick lines). The inset shows a zoom-in of the oscillating time course of the migration distance of individual plasmodia, present in both axes. (D) Chemotactic index (ratio of the displacement in the gradient direction to the absolut displacement) of plasmodia after 20 hours of migration against the corresponding directional persistence (ratio of the absolut displacement to the total distance traveled). In blue, the mean and standard deviation over all individuals.

Anti-persistent movement stems from protrusion oscillations To understand better what is going on, we have a closer look at the migration behavior: we perform an analysis of the run-tumble-and-oscillation dynamics as in Chapter 4. To quantify the orientation of migration steps in the three different phases, we compute histograms of the number of migration steps in a given direction.They show that runs are strongly oriented towards higher concentrations,

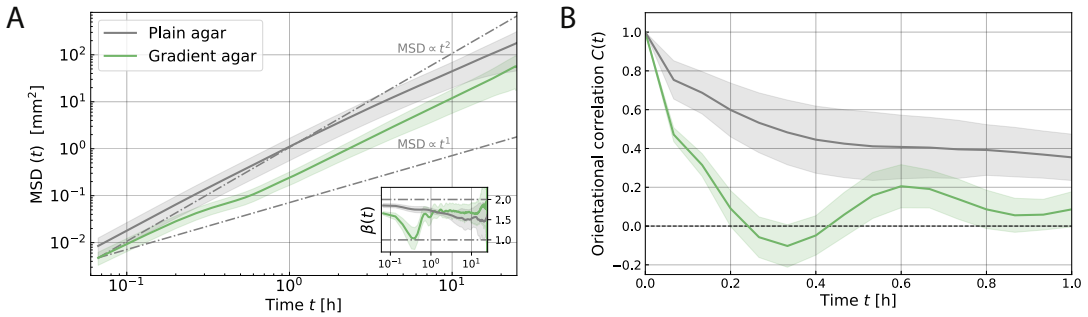

Figure 34: The chemotactic movement of *P. polycephalum* shows long-term directed motion and short-term anti-persistence. (A) Log–log plot of the superdiffusive MSD of migrating plasmodia on agar with a gradient generated by a 50% SDM agar source. The green line and shaded region represent the ensemble average over the time-averaged MSDs of 23 individual trajectories on gradient agar and the standard deviation, respectively. The gray line shows the result for plasmodia migrating on plain agar from Chapter 2. Dash-dotted lines show the MSDs of ballistic ($\propto t^2$) and diffusive motion ($\propto t^1$). Inset: Instantaneous MSD exponent $\beta(t)$. The migration is superdiffusive ($\beta > 1$), except for the dip at around $t \approx 20\,\mathrm{min}$. (B) Orientational correlation $C(t)$ with anticorrelation at $t \approx 20\,\mathrm{min}$.

whereas tumbles and oscillations are oriented randomly (Figure 35A). The average oscillation duration is approximately 70 minutes and we found no dependence on cell size. To find the dominant oscillation periods, we performed a Fourier analysis. We chose to perform a Fourier analysis of the time course of the speed projected in the direction of the gradient to look at oscillations in a given axis. To take out overtones, we consider the three strongest signals in the Fourier spectrum of the speed of a plasmodium and pick the one with the minimum period. We find that the dominant period computed in that way is independent of cell size and lies between between 30 and 47 minutes with an average of 35 minutes (Figure 35B). This explains the observed dip of the MSD exponent and orientational correlation at a time scale $t \approx 20\,\mathrm{min}$: it corresponds to approximately half the oscillation period.

Following the fate of two protrusions of a plasmodium during an oscillation event, we can explain the oscillations of the centroid speed: On a time scale of $t \approx 20\,\mathrm{min}$, a plasmodium is shifting its body mass from one protrusion to the other, resulting in a back-and-forth movement of the centroid position, which corresponds to anti-persistent movement. The two protrusions compete with each other until one wins and the plasmodium moves further up the gradient (Figure 36).

Where do these long-time oscillations originate and how can they be maintained? The oscillations can be explained by a model originally developed for cell shape oscillations during cytokinesis of HeLa cells and fibroblasts. It is based on a competition between the actin turnover dynamics and the contraction dynamics of the cell cortex [242]. To adapt the model to our case,

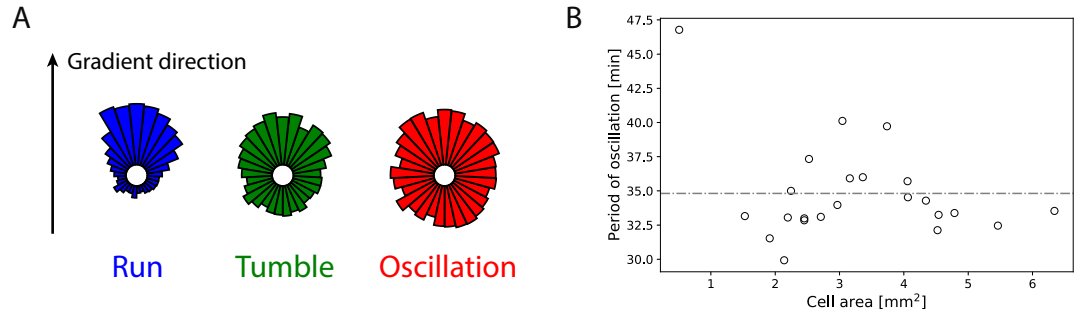

Figure 35: (A) *P. polycephalum* uses directed runs to climb the gradient, while tumbles and oscillations are oriented randomly. Histograms of the number of migration steps during a given phase (run, tumble, oscillation) in a certain direction. (B) Dominant period of the speed oscillations against cell area.

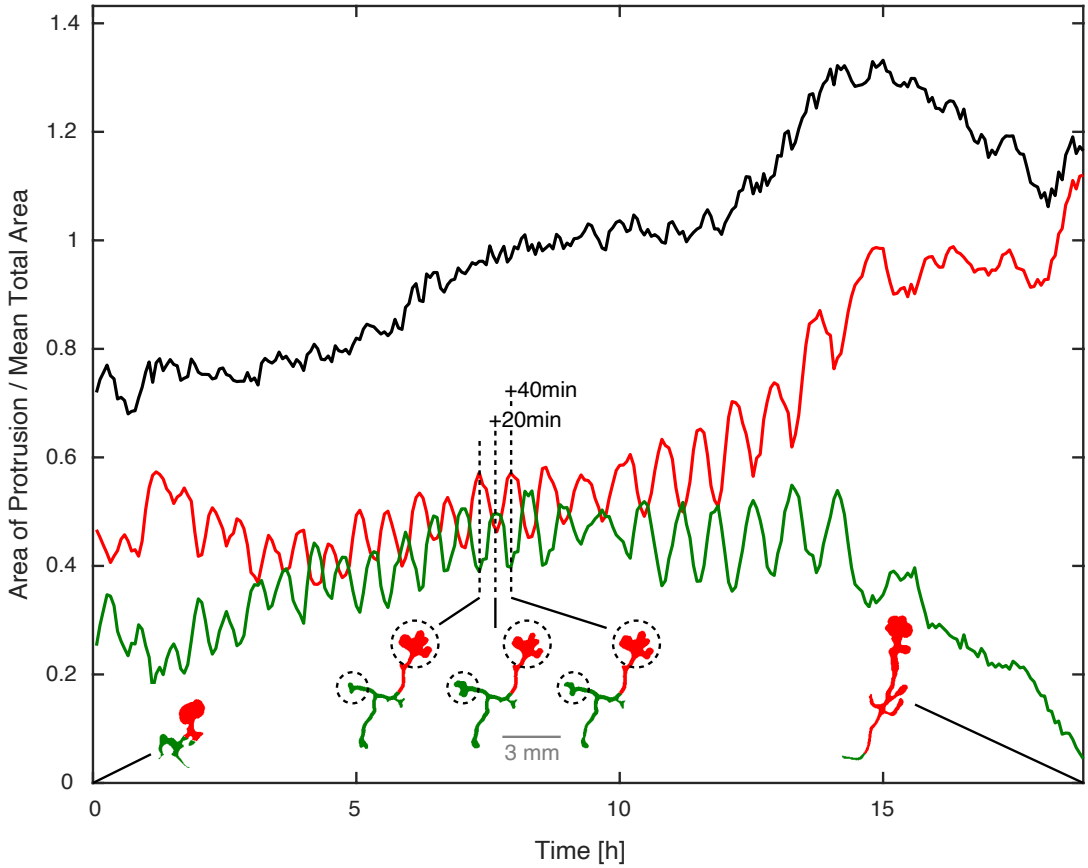

Figure 36: Plasmodia show long-time oscillations of protrusions. 18 h-long time course of the area of two competing protrusions (red and green). Protrusions are defined as shown in the insets. The black line represents the sum of the two areas.

we describe a plasmodium in the oscillation phase in a simplified manner: as two protrusions of radii R_1 and R_2 located at opposing ends of a single tube of radius a_0 (Figure 37). Each protrusion is modeled as a viscoelastic medium with bulk elastic modulus K and bulk viscosity η. Actin cortex tension T^* is parametrized as a function of actomyosin density [242], whose dynamics are determined by the actin turnover time τ. Cell mass can be transported from one protrusion to the other through the connecting tube, which is what we add to the model by Sedzinski and others. Fluid flows within the long slender tubes of *P. polycephalum* are laminar [43, 45] and characterized by a fluid viscosity μ.

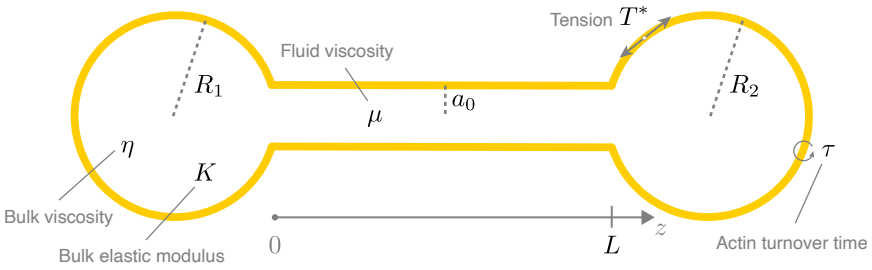

Figure 37: Schematic of the oscillation model with all parameters. Two protrusions with radii R_i are connected by a tube of length L and radius a_0.

Combining the contraction dynamics of the cell mediated by its elastic properties and the actin dynamics mediated by actin polymerization and depolymerization, Sedzinski and others arrive at a dynamic system with an instability. The stable system switches to oscillations at the threshold of the instability. The period of the oscillation is computed as

$$T_{\text{oscillation}} = \frac{2\pi\sqrt{\tau\tau_c}}{\sqrt{1-\epsilon h(r_*)}},$$

with the dominant time scale of the contraction dynamics τ_c, and two dimensionless parameters $\epsilon = T^*/(a_0 K)$ and $h(r_*)$ depending on some mechanical and geometrical properties of the plasmodium, where $r_* = a_0/R_*$ with R_* the rest radius of a protrusion [242]. The presence of the connecting tube in our case changes the value of τ_c due to the associated pressure drop along the tube, which can be computed solving the continuity equation. This leads to an additional term in $\tau_c = \frac{\eta}{2K} + \frac{16\mu L}{3r_*^3 a_0 K}$ compared to the $\tau_c = \frac{\eta}{2K}$ in the original model [242].

Moving *P. polycephalum* has actin turnover times in the range of 10 to 30 minutes [243], which is very slow compared to for example mammalian cells with turnover times of 20 to 25 seconds [244]. This increases the oscillation period $T_{\text{oscillation}}$ significantly. With literature values for cell mechanical properties and measurements of the dimensions of the plasmodia migrating in the gradient (Table 5), we find values for $T_{\text{oscillation}}$ in the range of 15 to 65 minutes.

Parameter	Value	Reference
τ	10-30 min	243
T^*	10^{-3} N/m	245
K	10 N/m^2	245
η	K * 24 s	240
μ	$6.4 * 10^{-3}$ Ns/m^2	241
L	5-10 mm	own measurements
R	500-800 µm	own measurements
a_0	100-150 µm	own measurements

Table 5: Mechanical and geometrical properties of plasmodia migrating in the gradient of nutrients.

This encloses the experimental oscillation periods of around 35 minutes and, hence, represents a possible mechanism for the observed cell shape oscillations.

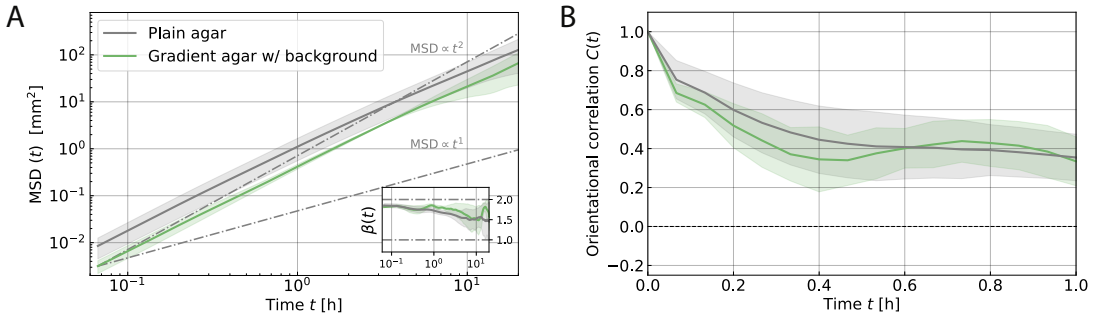

Figure 38: When a homogeneous background of SDM is superimposed on the chemotaxis setup, *P. polycephalum* shows no short-term anti-persistence. (A) Log–log plot of the superdiffusive MSD of migrating plasmodia on 5% SDM/BSS agar superimposed by a gradient generated by a 50% SDM/BSS agar source. The green line and shaded region represent the ensemble average over the time-averaged MSDs of 2 individual trajectories on gradient agar and the standard deviation, respectively. The gray line shows the result for plasmodia migrating on plain agar from reference 145. Dash-dotted lines show the MSDs of ballistic ($\propto t^2$) and diffusive motion ($\propto t^1$). Inset: Instantaneous MSD exponent $\beta(t)$. The migration is superdiffusive ($\beta > 1$) in both cases. (B) Orientational correlation $C(t)$.

To test if the morphology of plasmodia and hence the oscillations are introduced by this specific environment, we perform two additional experiments: one with a source containing 12.5% SDM and 12.5% basal salt solution (BSS), so a less steep gradient, and one with a low-concentration homogeneous background of SDM/BSS (2.5% each) in addition to the high-concentration SDM/BSS source (25% each). For the experiment with the less steep gradient, we still observe oscillations, but with a lower average duration of 56 min. However, for the experiment with additional background concentration, we observe two different behaviors of plasmodia: some do not leave their inoculation sites and display a tubular morphology connected with stationary oscillations. Another plasmodium takes on a sheet-like morphology after the initiation of migration and follows the gradient without oscillations. The last plasmodium

starts with tubular morphology and oscillations but then changes its morphology to sheet-like and moves up the gradient without oscillations. Looking at their MSD exponent and orientational correlation, we find them to be similar to the one observed for plain agar (Figure 38), only with a lower effective diffusion constant due to a lower speed, resulting in an offset in the MSD. This aligns well with our observation in the previous chapter that oscillations are connected with a tubular morphology but are absent in a sheet-like morphology.

Chemotactic efficiency depends on cell size Since the chemotactic index is very close to 1 for most plasmodia (Figure 33D), we introduce another measure to quantify chemotactic efficiency, the chemotactic drift velocity. It is defined as the mean velocity at which a cell moves up a chemoattractant gradient [246]. Since the speed of a plasmodium correlates with its size [41], we scale the chemotactic drift velocity with the average speed of a plasmodium. We find that this scaled chemotactic drift velocity correlates with cell size (Figure 39, $r\text{-value} = 0.69$), so larger plasmodia are more efficient in climbing the gradient.

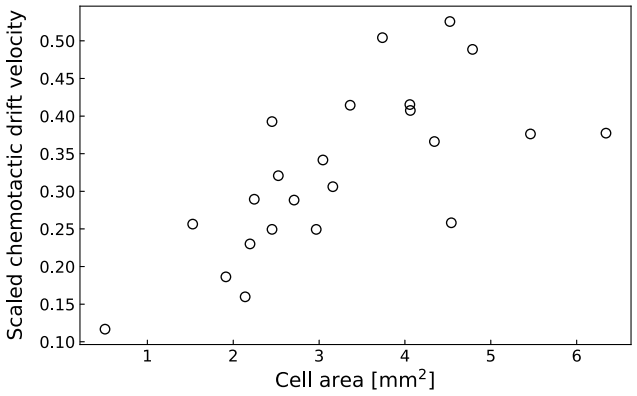

Figure 39: Larger plasmodia are more efficient in climbing the chemotactic gradient. We plot the average chemotactic drift velocity of individual plasmodia scaled by their average velocity against cell area.

A look at the migration phase statistics shows why: when we divide the number of 23 trajectories into two subgroups, one with a cell area smaller than $3\,\mathrm{mm}^2$ (11 plasmodia) and one with a larger cell area than $3\,\mathrm{mm}^2$ (12 plasmodia), we find that large plasmodia manage to orient their runs more towards the gradient direction (Figure 40). The overall time fraction of trajectories in the run phase is 23% for small plasmodia and 24% for large plasmodia, which is no significant difference. Also the average run duration is the same for both: about $17\,\mathrm{min}$. Therefore, the orientation of the runs along the gradient is the decisive factor in making the large plasmodia more efficient in climbing the gradient.

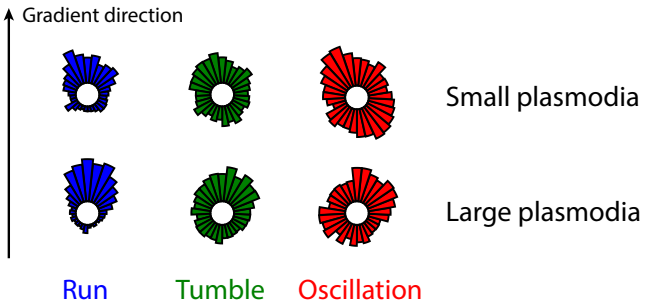

Figure 40: Large plasmodia are better at directing their runs towards the gradient source than small plasmodia. Histograms of the number of migration steps during a given phase (run, tumble, oscillation) in a certain direction for the two subgroups small plasmodia (11 individuals, cell area $< 3\,\mathrm{mm}^2$) and large plasmodia (12 individuals, cell area $< 3\,\mathrm{mm}^2$).

5.3 Discussion

We quantified the migration of *P. polycephalum* plasmodia in a concentration gradient of nutrients and showed that plasmodia perform successful chemotaxis. We find that during this process, plasmodia exhibit phases of anti-persistent cell oscillations and that larger plasmodia are more efficient in climbing the chemotactic gradient.

Our model gives a possible explanation for the origin of the oscillations. It highlights the competition between actin turnover dynamics and contraction dynamics as a likely mechanism for the emergence and maintenance of long-term oscillations in the system. To further test the model, one could quantify the perturbation of the mechanical properties of the plasmodia on the oscillation period. There are treatments that can alter the elastic properties of the plasmodial ectoplasm: phalloidin stabilizes actin filaments [247, 248], and Latrunculin A disrupts actin polymerization, leading to a dilation of the cell [53]. These treatments have been used before in a study investigating the traction stresses that plasmodia exert on the substrate. It has been shown that a treatment with phalloidin increases traction stresses, while Latrunculin A slightly decreases them [49]. In our case, it would be interesting to see the effect of these treatments on the period of the oscillation we have described. From the formula for the oscillation period, we predict that treatment with phalloidin, which stabilizes actin and probably increases the elastic modulus and decreases protrusion radii, will decrease the oscillation period, while treatment

with Latrunculin A will increase it. The model might explain what is happening during an oscillation event, but it does not account for the net motion observed before and after such a phase. It could perhaps be extended to explain the beginning and end of the oscillation phase by introducing different elastic moduli of the two protrusions, which could be induced, for example, by a softening agent released during nutrient sensing, biasing the oscillations and leading to a net movement of the cell. One could also try to simulate the movement of plasmodia up the gradient. If centroid-based simulations are employed, as in Chapter 3, it is reasonable to include the oscillations as an additional migration phase to simulate a run-tumble-and-oscillation movement. Finally, it would be interesting to study the existence and the characteristics of the oscillation phase also during the negative chemotaxis of *P. polycephalum* in response to a repellent stimulus such as KCl to see if the same dynamics appear.

The question remains as to why these oscillations are present during the migration on gradient agar since the anti-persistent nature of this migration phase makes the exploration behavior of *P. polycephalum* less efficient. The oscillations could also be a means of acquiring information about the environment. Do plasmodia maybe need the time of an oscillation event to process information about the gradient since information transfer is slow due to the large cell size, or are the oscillations even a mechanism to process the information by mechanical computation of softness differences in protrusions? Another possibility is a newly proposed model of protrusion growth as a directional decision-making process, which is mediated by the competition for a finite pool of actin [219], as described at the beginning of this chapter. The decision requires a certain decision-making time, which could be very long for *P. polycephalum* and connected with oscillations. Finally, the oscillations could just be morphology-induced, as suggested by the findings in the previous chapter that tubular morphology and oscillations are correlated. This is supported by the fact that sheet-like plasmodia perform successful chemotaxis without oscillation phases.

Regarding the influence of cell size on the chemotactic performance, we found that larger plasmodia are more efficient in climbing the gradient, quantified by the scaled chemotactic drift velocity. This finding is in favor for a membrane tension-induced inhibitor rather than a diffusing or advected signaling molecule since intracellular signal transport should take longer for larger cells, but not much longer if it's a mechanical signal [238]. In *E. coli*, the chemotactic drift velocity depends on the gradient of the logarithm of the concentration [138], a realization of the Weber-Fechner law [140] explained in Section 2.5. Larger cells of *P. polycephalum* sense larger concentration differences and hence receive a stronger cue, which could improve their chemotactic efficiency. This is supported by the fact that the runs of large plasmodia are more directed towards higher concentrations than the runs of small plasmodia.

6 (Self-)interacting random walks and aging

The analysis in this chapter was performed with input from Raphaël Voituriez as part of a collaboration.

6.1 Path marking and cell interaction

Some cells change their environment during migration by releasing signals to which they react as soon as they reencounter them - a mechanism that has been largely overlooked until now [164]. This process, known as self-interacting random walk, has strong consequences on the space exploration dynamics of such cells [114, 164, 249]. In particular, self-interacting random walks have aging properties, meaning that the dynamics of the random walk depend on the full trajectory of the random walker up to a time t, so show memory effects [114]. This is reflected by the fact that the MSD is not only a function of the time interval t but also of the observation time T:

$$\mathrm{MSD}(T,t) = 2D(T,t)t^{2/d_w},$$

where $D(T,t)$ is the effective time-dependent diffusion coefficient and d_w the fractal dimension of the random walk [114]. For example, MDCK epithelial cells deposit footprints on their path, facilitating adhesion and migration and having an attractive effect [164]. This leads to subdiffusive behavior (MSD exponent smaller than 1) on long time scales, and aging of the MSD on intermediate time scales because the cells deposit more signals, influencing the migration dynamics [164]. As described before, *P. polycephalum* leaves a slime trail and avoids it [79], so its migration also falls in the class of self-interacting random walks. The emerging features of self-interacting random walks become even more interesting when one considers not only one self-interacting random walker but a group of them. In this case, they will change the environment quicker, and individuals will receive more signals to which they will respond. There is no study investigating if a plasmodium reacts differently to its own slime trail than to the slime trail of another plasmodium. However, since we use clonemates, we assume that there should be no chemical difference between slime trails of different plasmodia.

Plasmodia might also interact with each other via other mechanisms than the slime trails. Few studies have investigated such interactions [250–252]. Vogel and others found that plasmodia also release so-called 'foraging stimuli' in the form of calcium to their environment, which are attractive to other plasmodia [250]. In a study by Briard and others, evidence was found supporting the hypotheses that *P. polycephalum* releases substances in its environment in response to stimuli and that other plasmodia can detect these substances and adapt their behavior [252]. When choosing between different substrates, plasmodia prefer agar previously explored by well-fed conspecifics over blank agar over agar previously explored by starved conspecifics.

Here, we want to investigate the effect of the path-marking by slime trails on the migration statistics of a group of plasmodia. More generally, how does a system of many path-marking agents evolve over time, with the agents interacting with the deposited paths as they encounter them?

6.2 Experimental setup and results

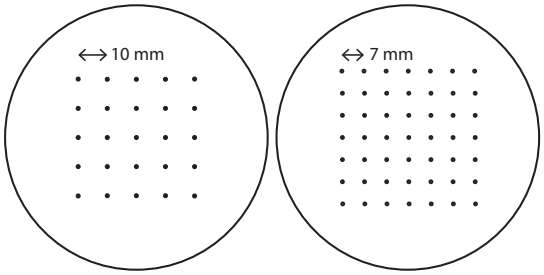

Figure 41: Arrangement of the cells on a 9 cm petri dish. Left: 5x5 cells, right: 7x7 cells.

We performed migration experiments on 1.5% agar substrate with many small plasmodia seeded in a grid arrangement of 5x5 (25) or 7x7 (49) cells, as shown in Figure 41. For this, single microplasmodia from liquid culture were placed on the agar surface using a 1 mL pipette tip and a grid pattern placed below the transparent petri dish. Imaging was started directly after, as described in chapter 2, and followed the migration of the plasmodia for 3 days. In the group of 25 plasmodia, migration started after 5 hours. Depending on the setup and the speed of the plasmodia, they encountered the slime trails of other plasmodia after another 5 to 15 hours and

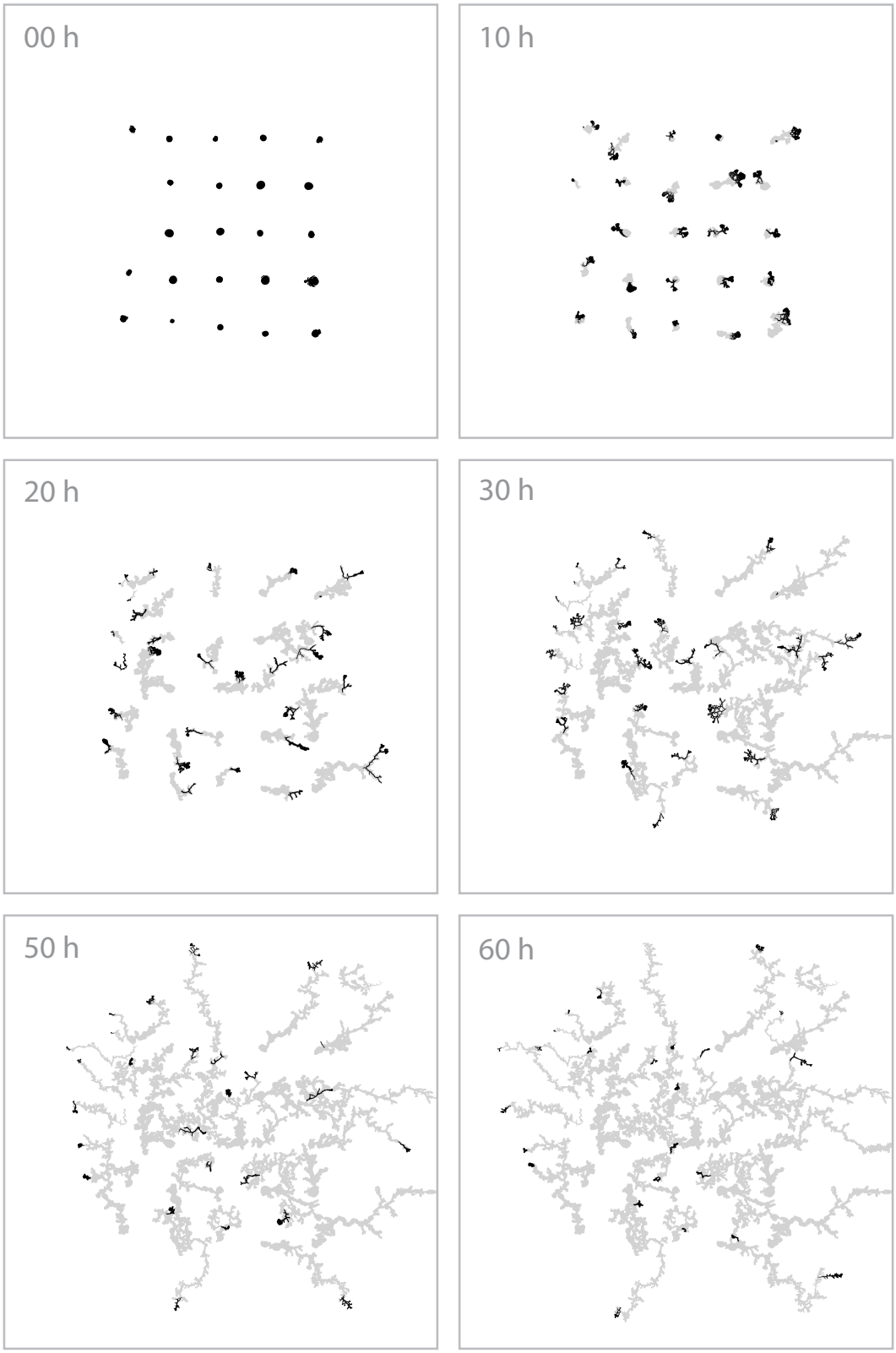

Figure 42: Time course of a group of 25 plasmodia migrating on 1.5% agar substrate. Plasmodia are displayed in black and slime trails in gray.

avoided them. Towards the end of the experiments (35 to 50 hours after inoculation), some cells stopped migrating and subsequently strongly decreased in size, turning into immobile, small, circular cells. The origin of this behavior is unclear. However, this phenomenon was not investigated further due to time constraints and is left for future studies. The data analysis for the following results was performed excluding these immobile states. First, we discuss the properties of the area covered by the plasmodia with slime, which define the aging of the environment. Afterward, we investigate the aging system's influence on the plasmodia's migration statistics.

Figure 42 shows a time evolution of the area covered by slime in a 5x5 grid scenario, which corresponds to the explored area. Plasmodia (black) explore their surrounding environment and simultaneously cover it with slime (gray), thereby changing the system and influencing their own and each other's migration due to the repellent property of the slime. We find that the time evolution of the covered area exhibits three regimes. After a lag time in the beginning where plasmodia are initiating migration, the area explored by the plasmodia and covered by slime grows about linearly in time (Figure 43A). Towards the end of the experiment, the growth flattens out. This is due to the mentioned immobilization of individual plasmodia which can be seen as plateaus in the time evolution of the areas explored by individual plasmodia (Figure 43B).

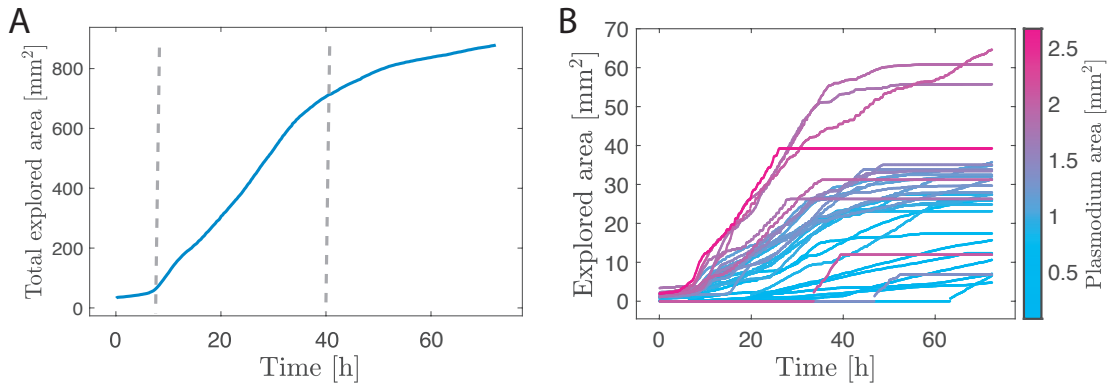

Figure 43: (A) Time evolution of the total area covered by all plasmodia shows three regimes (boundaries indicated by dashed lines). (B) Individually covered areas (color-coded by plasmodium area) plateau for long times.

The emerging shapes, especially towards the end of the experiment, resemble fractal structures (see last panels of Figure 42). We determined the fractal dimension of these shapes by the Minkowski–Bouligand dimension using the box-counting method implemented in MATLAB by Frederic Moisy [253]. We find fractal dimension between 1 and 2, revealing the fractal nature of the area covered by the slime. We find fractal dimensions of around 1.3 for individual trails and 1.7 for the group of trails (Figure 44).

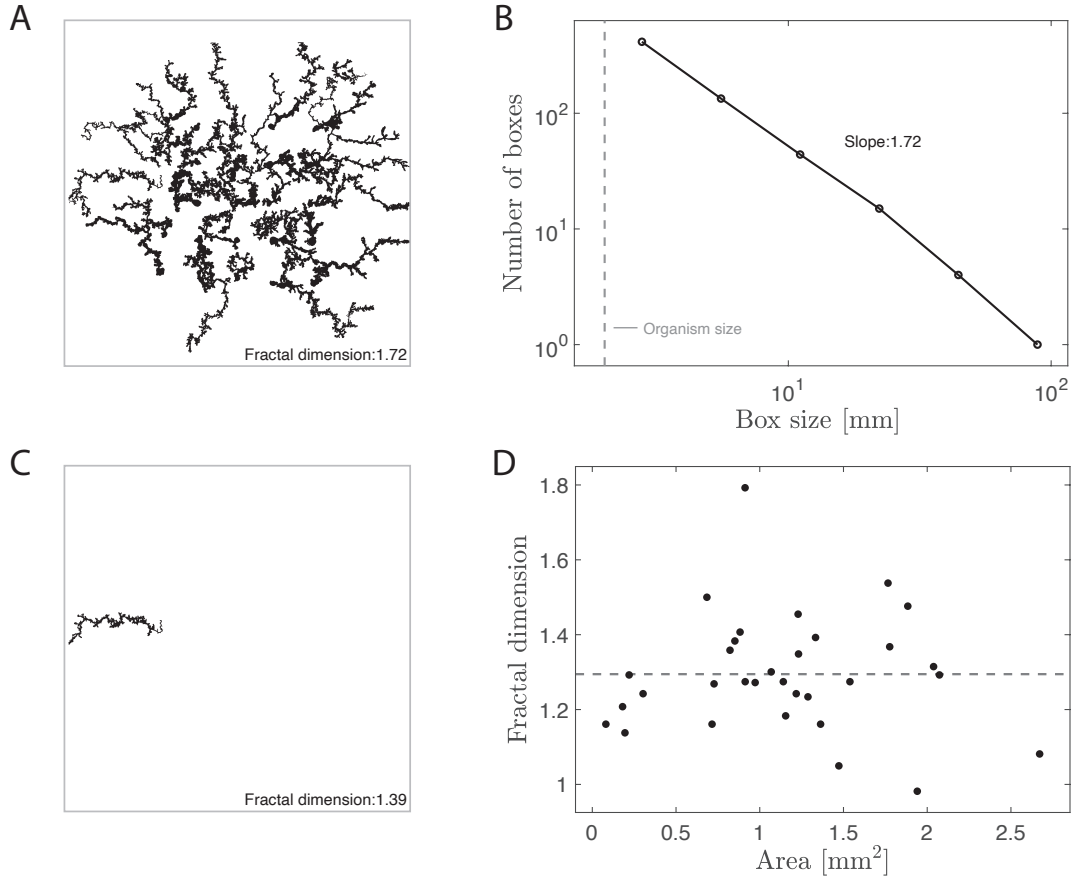

Figure 44: The area covered by the plasmodia with slime has a fractal structure. (A) Area covered after 3 days. The fractal dimension is the slope from (B). (B) Log-log plot of the number of quadratic boxes necessary to cover the area as a function of the box size. The slope gives the fractal dimension of the pattern. (C) Area covered by a single plasmodium. (D) Fractal dimensions of the slime tracks of the individual plasmodia with an average of 1.3 (dashed line).

Inspecting the experimental recordings, we observe differences between plasmodia migrating in the bulk of the cell group and plasmodia migrating at the periphery. While the latter are migrating radially outwards, the former remain mostly constrained to the inner part of the original grid arrangement. Therefore, analyzing these groups separately in terms of their migration characteristics is reasonable. Indeed, we find striking differences in the two groups. The outer plasmodia indeed exhibit a radial outward drift, which is not present for the inner plasmodia, where only one third moves radially outwards (Figure 45A,B). This drift cannot be explained by slime-trail interactions since it starts from the very beginning, when no trails have been deposited yet. Looking at MSD exponent and orientational correlation, we find that the plasmodia starting their migration at the group's periphery move more persistently on large time scales

than plasmodia starting in the bulk, but also more persistently than single plasmodia on plain agar (Figure 46), leading to a higher space exploration. This can be explained by the interaction of the plasmodia with slime trails. The plasmodia in the bulk are quickly surrounded by slime in all directions, which blocks their movement, while the plasmodia at the periphery escape radially outwards to still uncovered areas, resulting in a kind of collective superdiffusion.

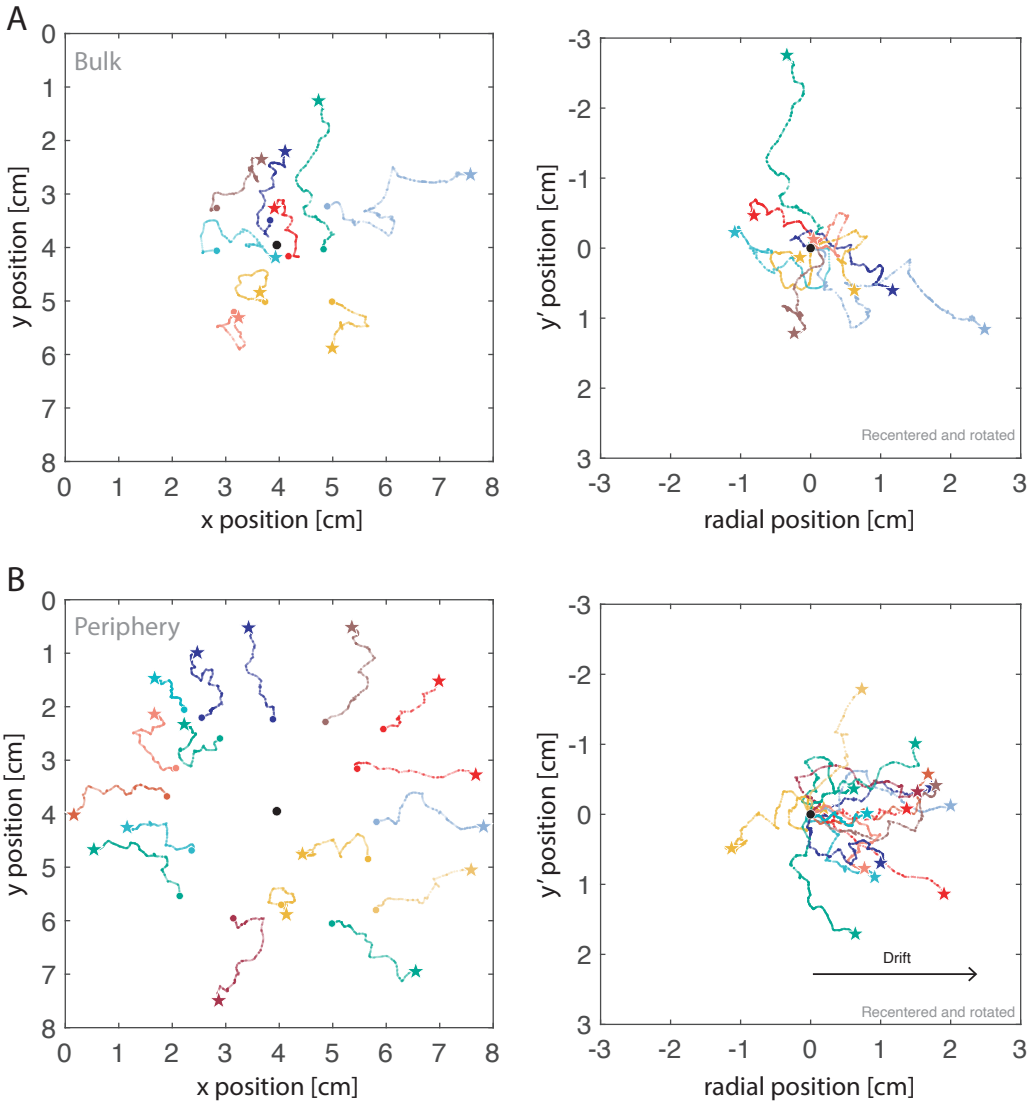

Figure 45: Plasmodia at the periphery show a radial drift outwards. (A) Left: trajectories of the bulk plasmodia. Right: trajectories rotated and recentered according to their relative position with respect to the center (black disk). (B) Left: trajectories of the peripheral plasmodia. Right: trajectories rotated and recentered according to their relative position with respect to the center (black disk).

Both peripheral and bulk plasmodia show a dip in the MSD exponent and the orientational correlation around $t \approx 20\,\mathrm{min}$ compared to plain agar (Figure 46), which indicates a lower persistence on this time scale. This is reminiscent of the behavior described in the previous chapters, where plasmodia show an oscillation phase when exposed to certain chemicals. Indeed, they sometimes show tubular morphologies connected with oscillations, especially when they are surrounded by slime trails. This suggests that the slime trail is containing chemicals to which plasmodia react by oscillations.

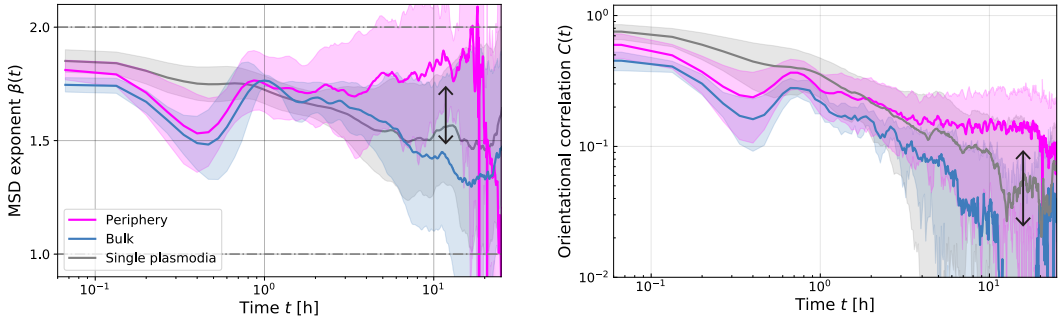

Figure 46: Plasmodia at the periphery show higher persistence than bulk plasmodia on long time scales. Left: Instantaneous MSD exponent of bulk plasmodia (blue) and peripheral plasmodia (pink). Right: Orientational correlation.

Next, we investigate how the migration statistics change depending on the observation time, which is known as aging. For that, we follow the aging-analysis procedure of D'Alessandro and coworkers [164]: we divide the experiments into time frames of 16 hours starting at experiment time $T \in [0, 8, 16, 24, 32, 40]\,\mathrm{h}$ and calculate the migration characteristics for these time frames individually. To improve the statistics, a sliding average over $t_0 \in [T, T + 16\,\mathrm{h}]$ is performed for the characterizing quantities. For the same reason, curves are cut at 16/3 = $5.3\,\mathrm{h}$. Looking again at MSD and orientational correlation, we find that they change with the observation time T, exhibiting strong aging effects for bulk plasmodia and slight aging effects for peripheral plasmodia (Figure 47). Note that the observation time $T = 0$ is not the inoculation time point like in Figure 42, but the time point where plasmodia start migrating. The MSD and orientational correlation reveal two aging effects: a general shift of the MSD to lower values and a change of the MSD and orientational correlation at a time interval $t \approx 20\,\mathrm{min}$. The general shift is due to a decrease of the effective time-dependent diffusion coefficient $D(T, t)$ with observation time T. The change at $t \approx 20\,\mathrm{min}$ is reminiscent of the dip discussed in the previous chapters, where it was related to chemical sensing. For bulk plasmodia, both effects can be explained by an increasing exposure to surrounding slime trails, which slow down the movement of plasmodia (shift of the the MSD) due to their repellent property and lead to anti-persistent protrusion oscil-

lations connected with chemical sensing (increasing dip in MSD and orientational correlation at $t \approx 20\,\mathrm{min}$). For peripheral plasmodia, the result is less clear. They also exhibit a slow down, but the dip in MSD and orientational correlation is slightly decreasing with observation time T. This could be the effect of the radial outward drift, resulting in more and more persistent movement due to the distance to other plasmodia.

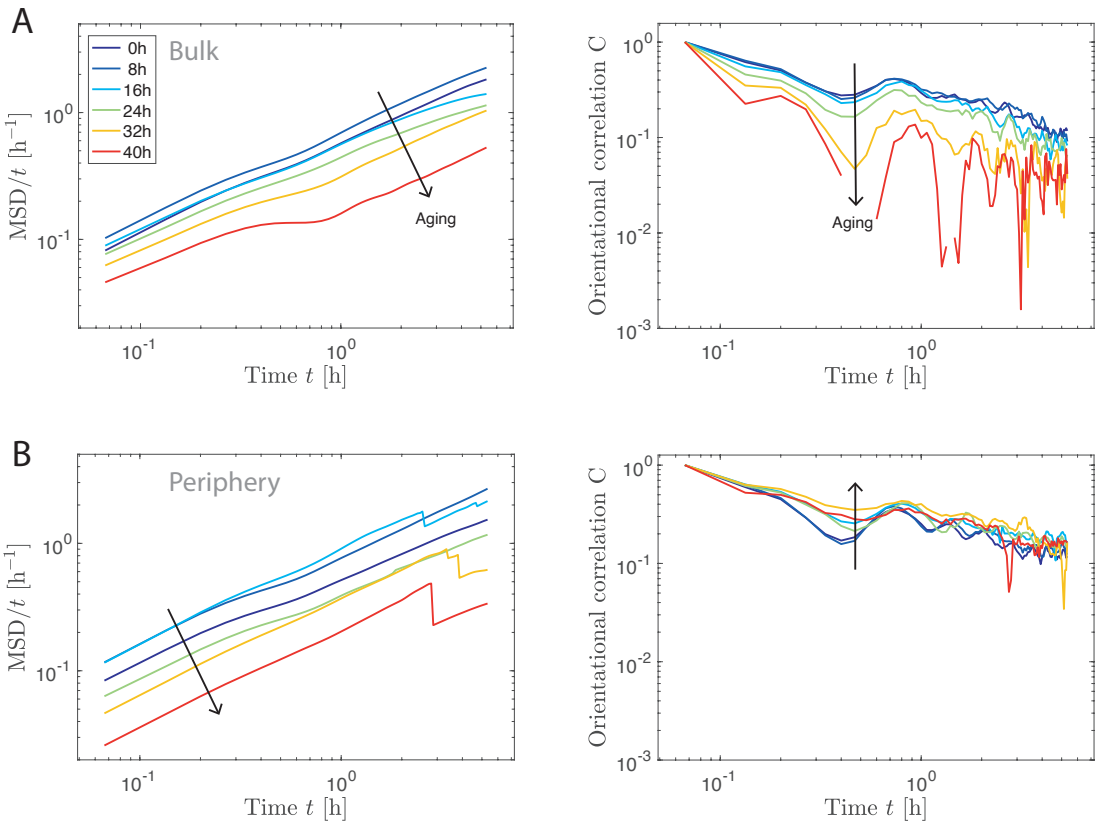

Figure 47: Plasmodia interacting with each other's slime trails show aging effects in their MSD and orientational correlation. (A) Left: MSD divided by time of bulk plasmodia for different observation times T. Right: Orientational correlation of bulk plasmodia. (B) Left: MSD divided by time of peripheral plasmodia for different observation times T. Right: Orientational correlation of peripheral plasmodia.

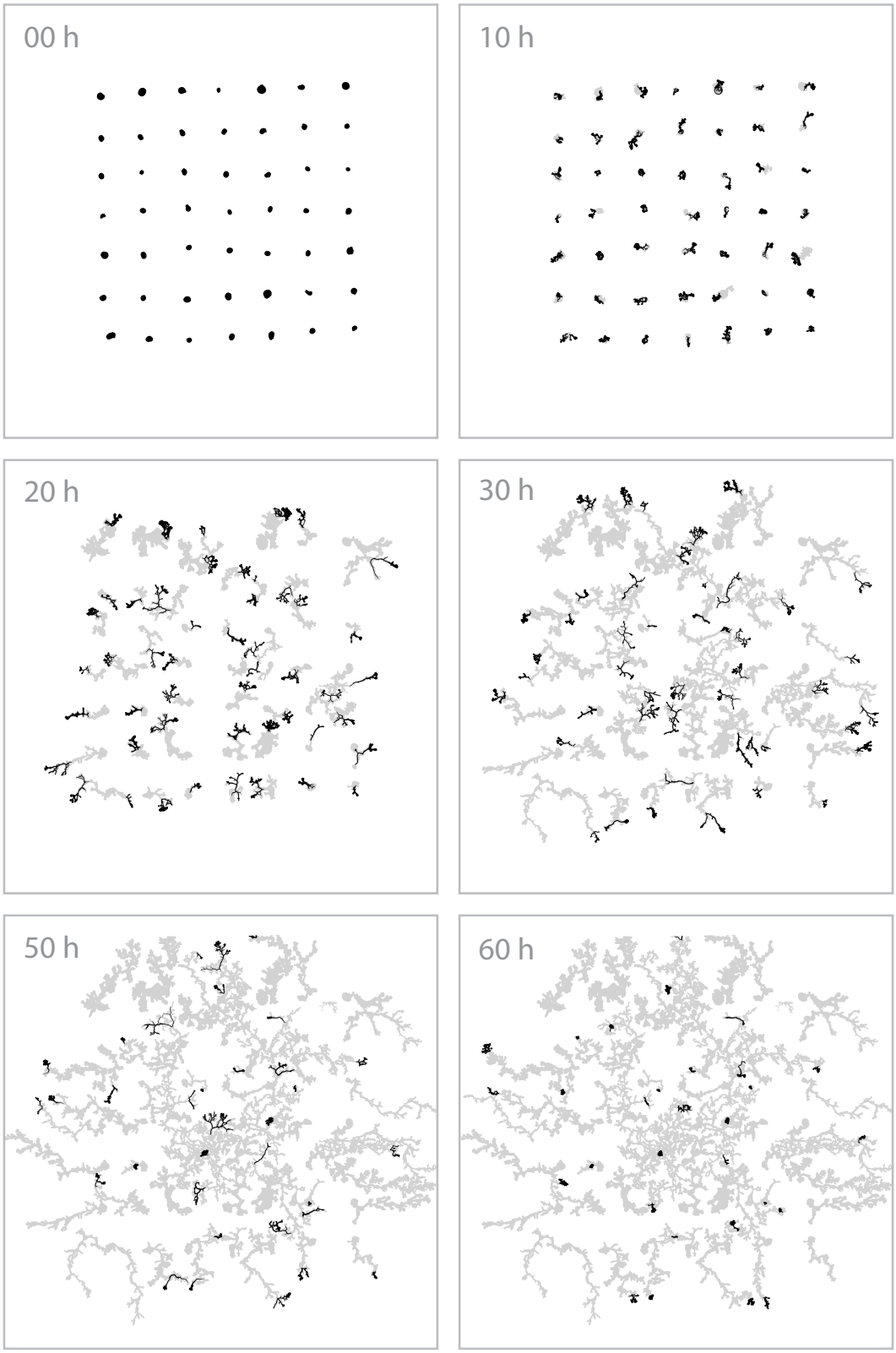

Figure 48: Time course of a group of 49 plasmodia migrating on 1.5% agar substrate. Plasmodia are displayed in black and slime trails in gray.

Finally, we shortly describe the outcome of the experiment with 49 plasmodia. They also covered the available space in a time frame of around 60 hours (Figure 48). The fractal dimension of the final structure is 1.78, which is close to the value for 25 plasmodia. Peripheral plasmodia also show a radial drift outwards (Figure 49). The remaining data analysis suffered from some problems. There were many plasmodia fusing with each other, as described in the discussion. Also, plasmodia started closer to the boundary of the observation area and quickly left it. All this lead to poor statistics, making it impossible to quantify any aging effects. Due to a lack of time, we could unfortunately not improve on this.

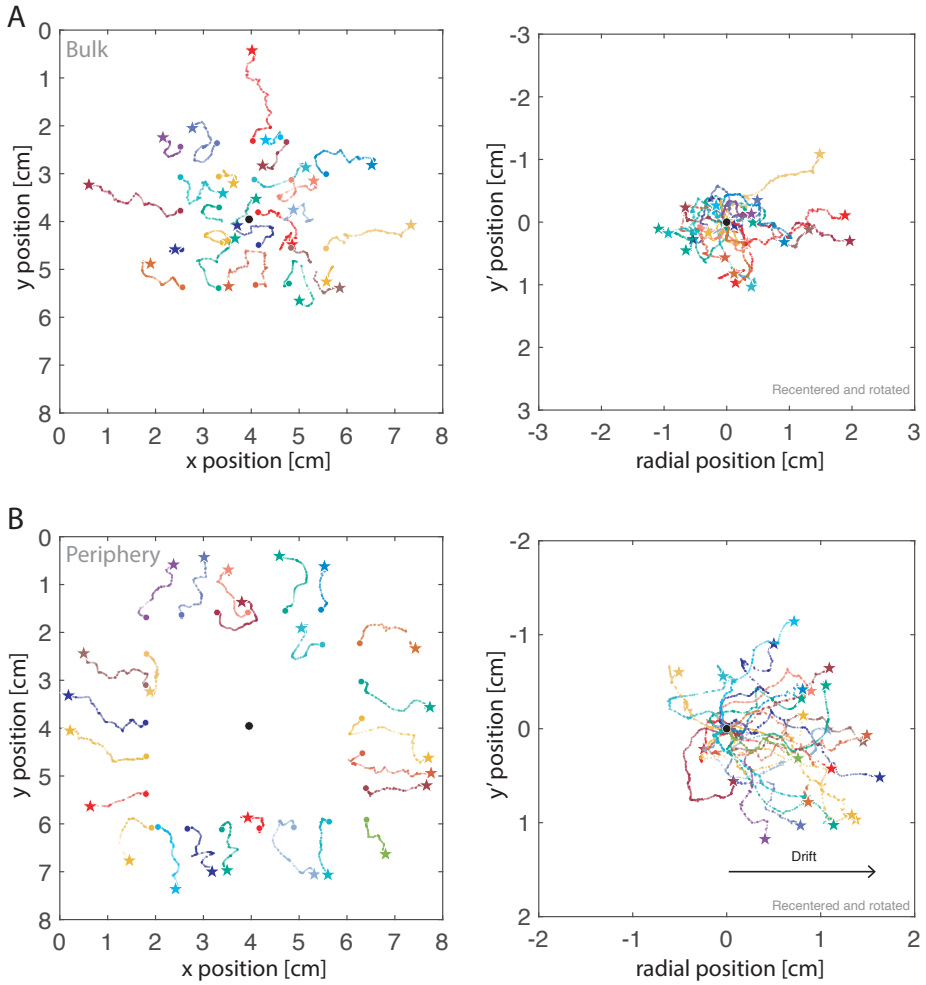

Figure 49: Plasmodia at the periphery show a radial drift outwards. (A) Left: trajectories of the bulk plasmodia. Right: trajectories rotated and recentered according to their relative position with respect to the center (black disk). (B) Left: trajectories of the peripheral plasmodia. Right: trajectories rotated and recentered according to their relative position with respect to the center (black disk).

6.3 Discussion

We found that a group of interacting agents with path-marking capabilities, in this case cells with a repellent trail, show complex dynamics in their migration behavior. Especially interesting is the different behavior of plasmodia depending on their position in the cell group: cells in the bulk show aging in the form of a general shift of the MSD to lower values and an increasing dip in the MSD exponent and the orientational correlation. Cells at the periphery exhibit a radial drift outwards.

The drift could be caused by substances that diffuse from the slime trails or that *P. polycephalum* releases into the agar directly, so they can be sensed by other plasmodia. This would align with previous findings that *P. polycephalum* releases substances into its environment [252]. The observed dip in the MSD exponent and the orientational correlation, and the presence of the oscillations described in the two previous chapters, where plasmodia were exposed to certain chemicals, also suggest the presence of some substances in the agar. Since no chemicals were introduced before the start of the experiment, they must have been secreted by the plasmodia themselves. It would be interesting to investigate this in more detail in future studies.

The described phenomenon of immobilization of the plasmodia towards the end of the experiments constrained the data analysis to a rather short time window, limiting the investigation of aging effects. A possible explanation for the immobilization could be that plasmodia sense the presence of other (starved) cells and estimate the environment as unfavorable. Another possibility is that plasmodia notice the presence of slime everywhere and, since it is used as a marker for already discovered and, hence, exploited territory with no food left, conclude that there is no possible direction to go and that sporulation is more reasonable to reach a new territory via flying spores. If the immobilization is due to the initiation of sporulation, this process could be impeded by using an agar substrate containing nutrients since sporulation is induced when plasmodia are starving [37, 254]. However, this would need to be tuned such that plasmodia do not grow and reduce the available migration area. The time window that could be analyzed was also shortened by plasmodia leaving the observation area at the borders of the petri dish. To deal with this, one could maybe use smaller plasmodia that move slower, or a larger petri dish. Another limitation in this study was the ability of two plasmodia to fuse due to their genetic identity, after which they form a single cell [66, 255, 256]. Somatic fusion is controlled at the plasmodium surface and can happen when two plasmodia touch each other [256]. However, fusion is not

necessary upon contact [88]. The fusion likely happens in a stochastic manner, as observed for a close relative [88]. It is unclear how such events should be treated in our data analysis, which is why we excluded plasmodia from the analysis once they fused, decreasing the statistics. To eliminate this problem, one would either need to think of a way of integrating fusion events in the analysis, or perform many experiments such that there will be more experiments without fusion events by chance.

In conclusion, despite the experimental problems we faced, which we think could be overcome with more time, we believe that migrating plasmodia of *P. polycephalum* are the model system of choice to study the collective dynamics of interacting self-avoiding random walkers. Theorists in the field of statistical physics show a growing interest in self-interacting random walks [114, 249], and the type of experiments shown here could provide them with data to test their theoretical predictions about how the dynamics of such a system evolve in time.

7 Conclusion and Outlook

The apparent smart behavior, flexible morphology and size variability of the slime mold *Physarum polycephalum* make this organism an interesting object of study regarding its migration behavior and search strategies. Although unicellular and, therefore, a relatively simple life form, it is known for its ability to process information without a nervous system. To tackle the problem of searching for food in an unexplored territory, it must self-organize its movement and integrate information about its environment in an efficient way. In this work, I presented detailed analysis, interpretation and modeling of its migration mechanisms and behavior in various environmental contexts, ranging from the absence of external signals to the presence of homogeneously distributed chemicals, and chemical gradients, and from individual to collective migration. We showed that the migration behavior of *P. polycephalum* can be captured by a self-interacting random process. The self-interacting character has strong consequences for the space exploration dynamics, both at the individual and collective level. Further, we found that *P. polycephalum*'s large cell size is advantageous in this process, as well as in the process of chemotaxis.

First, we statistically described the trajectories of migrating plasmodia in terms of their centroid positions. Our analysis in Chapter 3, treating the case of single plasmodia on a neutral substrate, revealed that a run-and-tumble behavior determines the short-term migration dynamics. Analysis of the long-term dynamics revealed superdiffusive behavior with a MSD exponent of $\beta \approx 1.5$, which we linked to the self-avoiding migration of plasmodia mediated by the deposited slime trails. We built a data-driven model that matches the experimental migration statistics of plasmodia, and explains the origins of the superdiffusive exponent. This highlights *P. polycephalum* as a model system for a self-avoiding random walker, falling in the class of self-interacting random walks, a topic that receives increasing interest in theoretical statistical physics. Investigating the interaction of plasmodia of different sizes with slime trails of plasmodia of different sizes, we showed that small plasmodia cannot always avoid slime trails, leading to frequent slime crossings, and that only large plasmodia reliably avoid slime trails. Therefore, only large plasmodia show real self-avoiding behavior leading to superdiffusive migration, while small plasmodia tend to diffusive migration. This highlights a potential evolutionary advantage for larger plasmodia, which may have driven *P. polycephalum* to evolve into one of the largest cells we know. This study laid the basis for further investigations of the short-term and long-term migration behavior of *P. polycephalum*.

In Chapter 4, we investigated the influence of the environment on its migration dynamics. We found a correlation between the environment-dependent morphology of plasmodia and their short-term migration behavior, while the long-term behavior is unaffected. Depending on the chemical composition of the migration substrate, plasmodia have tubular, branched, or sheet-like morphologies, which we quantified by the scaled radius of gyration. We determined the coupling of this measure with the alignment of the motion: on substrates inducing a tubular morphology with a large scaled radius of gyration, plasmodia perform more anti-aligned motion in the form of an oscillation phase not present in our run-and-tumble model. However, on substrates inducing a sheet-like morphology with a small scaled radius of gyration, plasmodia perform aligned motion without oscillations. This changes the short-term statistics of the movement: the MSD exponent shows a dip at around $t \approx 20\,\mathrm{min}$, indicating less persistent movement on this time scale. The oscillations are therefore counterproductive for space exploration, which is why we hypothesized that they could be part of a decision-making process for finding the next best migration direction.

In Chapter 5, we investigated how the search strategy of *P. polycephalum* changes in a chemical gradient of nutrients, where it has to align its motion with the gradient direction to reach higher concentrations, a process called chemotaxis. In agreement with the literature, plasmodia performed efficient chemotaxis by climbing the gradient we exposed it to. Surprisingly though, we found that larger plasmodia are more efficient in climbing the gradient than small plasmodia. That is because they more faithfully align their motion with the gradient, once more hinting at an advantage of larger cells. We also observed the presence of the oscillation phase, besides run and tumble phases, as in Chapter 4. Quantification of the direction of migration steps revealed that run phases are preferentially aligned with the gradient, while tumbles and oscillations are randomly oriented. This means that *P. polycephalum* can determine the direction of the gradient during the tumble and oscillation phases in between the run phases and subsequently move in this direction. This supports our hypothesis mentioned above that the oscillations could be part of a decision-making process. Therefore, we further studied these oscillations, as they seem to be an important behavior of *P. polycephalum*: we described a model of protrusion oscillations based on the competition between the actin turnover dynamics and the contraction dynamics of the cell cortex, which could explain the observed oscillations. The prediction of the model for the period of the oscillations matches our experimental data.

Bringing our attention back to the important effect of the slime trails deposited by *P. polycephalum*, in Chapter 6 we examined the effect of self-interactions on the migration dynamics of a dense group of plasmodia mediated by the emerging slime trail pattern. We found that the long-term migration behavior strongly depends on the position of plasmodia within the group: the MSD exponent and orientational correlation at long time scales are low for plasmodia in the bulk, meaning low persistence, and high for plasmodia at the periphery, meaning high per-

sistence. This shows how the collective effect can increase the space exploration efficiency of some individuals by sacrificing the space exploration by others. In addition, the MSD and orientational correlation of plasmodia surrounded by the trails of other plasmodia depend on the observation time, a property called aging. This means that the change in the migration environment that plasmodia create with their slime trails has a big impact on their migration behavior. *P. polycephalum* is, therefore, an intriguing model system to study the collective dynamics of interacting self-avoiding random walkers. The experiments presented here provide theorists working on the topic of self-interacting random walks with data to test their theoretical predictions about how the dynamics of such a system evolve in time.

Our findings open many doors, leading to possible new directions for future research. The mechanism of trail-deposition is a simple yet powerful trick to guide the migration and improve space exploration efficiency. From a biological perspective, it would be interesting to identify the substance in the slime that leads to the avoidance reaction. One could then generate artificial slime, which could be used to guide the cells, representing an easy tool for steering cell behavior. From a physics perspective, it is intriguing to study the trapping behavior of plasmodia by their slime trails in more detail. Trapping can change the dynamics of self-avoiding walks drastically [257]. When plasmodia migrate long enough, they will certainly be trapped by their own slime trail in finite time. In such a scenario, a plasmodium must cross the slime trail in order to survive or initiate sporulation. Indeed, we observed some events where trapped plasmodia escaped the trap by crossing the slime, assuming a lightning-like morphology, which has been shown to enable high migration speeds and optimize transport [54]. This hints at a very interesting ability of *P. polycephalum* to efficiently escape traps, which is worth investigating further. It would be interesting to understand the conditions under which plasmodia cross their slime and how they decide for or against doing so. The underlying crossing policy could exhibit optimality in terms of the trade-off between exploitation and space exploration.

Finally, two big questions remain to be answered: first, what are the intracellular mechanisms behind the self-avoiding behavior and the chemotaxis of *P. polycephalum*? Or more particular, how are the signals coming from a slime trail or a concentration gradient integrated to achieve a beneficial response? The two scenarios are related but not identical: while the response to the slime is an avoidance reaction, the chemotaxis is more complex since it requires the computation of the gradient direction based on concentration differences. To find an answer, one could quantify the intracellular dynamics of slime- or gradient-sensing plasmodia with high spatial and temporal resolution. For example, the actin dynamics could reveal how and when protrusions are forming to avoid slime or follow a gradient. Clarifying this question will likely also explain why larger plasmodia are better at avoiding slime trails and gradient climbing: larger cells must have an internal mechanism to compare concentrations at different ends of the cell

which is less effective in smaller cells. Second, why do plasmodia with certain morphologies oscillate, and what is the connection to the environmental conditions, like the presence of a gradient? Future studies could further validate the model for protrusion oscillations by altering cell properties like the elastic modulus of the cortex, which would influence the oscillation period. The aforementioned quantification of intracellular processes, such as actin dynamics, could also help to reveal what happens during an oscillation event, which is a putative decision-making process. In conclusion, *P. polycephalum* still holds some secrets about its surprising behavior and will keep scientists busy for many years to come.

Appendix

A Experimental methods

A.1 Media recipes

SDM (semi-defined medium)

Ingredients per liter:

10 g	(D+)-glucose anhydrous
10 g	Difco bacto-soytone
3.54 g	Citric acid monohydrate
2 g	Dipotassium phosphate
1.026 g	Calcium chloride dihydrate
0.6 g	Magnesium sulfate heptahydrate
0.034 g	Zinc sulfate heptahydrate
0.0424 g	Thiamine hydrochloride
0.0158 g	Biotin

Dissolve in distilled water. Adjust pH to 4.6 with 1M KOH or KOH pellets. Autoclave with liquid setting for 20 minutes and store at room temperature. Prior to use add 10 mL hemin solution per liter and 250 $\mu g\,mL^{-1}$ penicillin and streptomycin solution (-20°C) after autoclaving.

BSS medium (balanced salt solution)

Ingredients per liter:

3 g	Citric acid monohydrate
4.20 g	di-Potassium hydrogen phosphate trihydrate
0.25 g	Sodium chloride
0.21 g	Magnesium sulfate heptahydtrate
0.05 g	Calcium chloride dihydtrate

Dissolve in distilled water. Adjust pH to 5.0 with 1M KOH or KOH pellets. Autoclave with liquid setting for 20 minutes and store at room temperature.

A.2 Agar plates

Plates with homogeneous chemicals (50% SDM as example)

Recipe for 4 plates:

- Prepare a $250\,\mathrm{mL}$ bottle containing $50\,\mathrm{mL}$ VE water. Heat and stir them on the magnetic stirrer (full heat, 300 rpm) and add $1.5\,\mathrm{g}$ of agar.
- When it is boiling, move the bottle into the flow hood, let it cool down a bit and add $50\,\mathrm{mL}$ of SDM.
- Stir again for some seconds and put it back into the flow hood.
- As soon as you can hold the bottle without pain pour the agar into petri dishes.

Plates with a gradient of chemicals (50% SDM as example)

Recipe for up to 6 plates:

- Prepare two 100 $100\,\mathrm{mL}$ bottles containing $30\,\mathrm{mL}$ and $60\,\mathrm{mL}$ VE water, respectively. Heat and stir them on the magnetic stirrer (full heat, 300 rpm) and add 0.9 grams of agar into each of them.
- Remove two stripes of agar from an agar plate with a razor blade, see Figure 50.
- When the $30\,\mathrm{mL}$ are boiling, move the bottle to the flow hood and add $30\,\mathrm{mL}$ of SDM.
- Stir again for some seconds.
- Pipette around 5 mL of the liquid SDM agar, into one half of the plate.
- When the $60\,\mathrm{mL}$ are boiling, move the bottle to the flow hood and let cool down a minute.
- Pipette around $5\,\mathrm{mL}$ of the liquid water agar, into the other half of the plate.

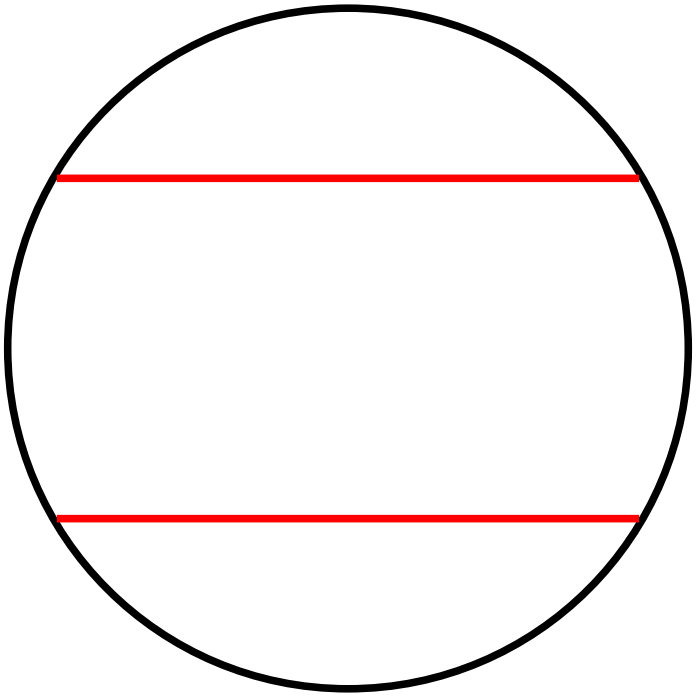

Figure 50: Template for the agar cut-out in its actual size, cutting lines in red.

Substrate (1.5% agar)	# Plasmodia	Date [yymmdd]	Duration [h]	Experimentalist
Plain	14	220204	71	Lucas Tröger
		220311	120	
		220414	96	
		220419	137	
		220610	168	
Plain (avoidance test)	8	210623	45	
		220414	115	
		240110	142	
		240116/8	72	
10% SDM	9	230105	312	
		230120	164	
		230130	162	
5.5 mM glucose, 2 mM leucine	7	221125	72	
		221202	48	
		221216	48	
SDM gradient: 50% – 0%	23	230731	48	
		230802	48	
		230804	64	
		230807	48	
SDM/BSS: 25% – 0%	4	240605	24	
SDM/BSS: 50% – 10%	2	240617	48	
Plain (many plasmodia)	75	230825	71.9	
		231215	46.6	
20 mM KCl	9	240502	93.6	Diana Lenski
		240506	96.0	
		240516	93.9	
		240520	75.1	
		240531	90.3	
		240606	93.1	
		240610	96.7	
50 mM KCl	11	230911	94.9	
		230922	98.2	
		231030	93.2	
pH 5.97	8	231114	71.6	
		231117	95.3	
		231123	94.4	
		231206	114.5	
pH 7.83	12	231106	46.9	
		231108	47.9	
pH 8.06		231211	95.5	
		231218	93.5	
		240209	118.5	

Table 6: Data sets analyzed in this thesis.

A.3 Gradient staining

To stain a gradient of glucose, one can use tetrazolium chloride (TTC) [57]. The staining solution contains:

$1.67\,\mathrm{g}$	TTC
$100\,\mathrm{mL}$	purified water
$3.54\,\mathrm{g}$	$1\,\mathrm{M}$ NaOH

Prepare agar plates a certain amount of time beforehand, e. g. 24 hours. Add $15\,\mathrm{mL}$ TTC solution to the agar plate, seal the agar plate with parafilm, and put it inside a bigger petri dish. Let it stain for 1 hour on the rocking shaker (40 rpm). Replace the solution by purified water and put it for $20\,\mathrm{min}$ on the rocking shaker. Warning: TTC solution needs to be put in special waste, ask your technician. Agar is very fragile now. Shortly dry. Image.

We let glucose diffusive in agar for 24 hours, stained it, and imaged it using a brightfield microscope. The result is seen in Figure 51A. From the image, we compute the gray level as a function of the vertical distance from the top of the image as the horizontal average over all pixels (Figure 51B). This can be converted into a relative intensity of the TTC stain (Figure 51C), which is proportional to the glucose concentration.

The concentration of glucose diffusing through agar can be estimated from its diffusion coefficient, which has a value of $D = 6{*}10^{-6}\,\mathrm{cm}^2\,\mathrm{s}^{-1}$ [258]. We compute the relative concentration in the agar according to the solution of Fick's law of diffusion

$$\frac{c(x,t)}{c_0} = \mathrm{erfc}\left(\frac{x}{\sqrt{4Dt}}\right),$$

with erfc the complementary error function, and where we assume one-dimensional diffusion from a source with constant concentration c_0 located at $x = 0$. We find good agreement with our data (Figure 52A) and can make estimates for various durations of diffusion (Figure 52B).

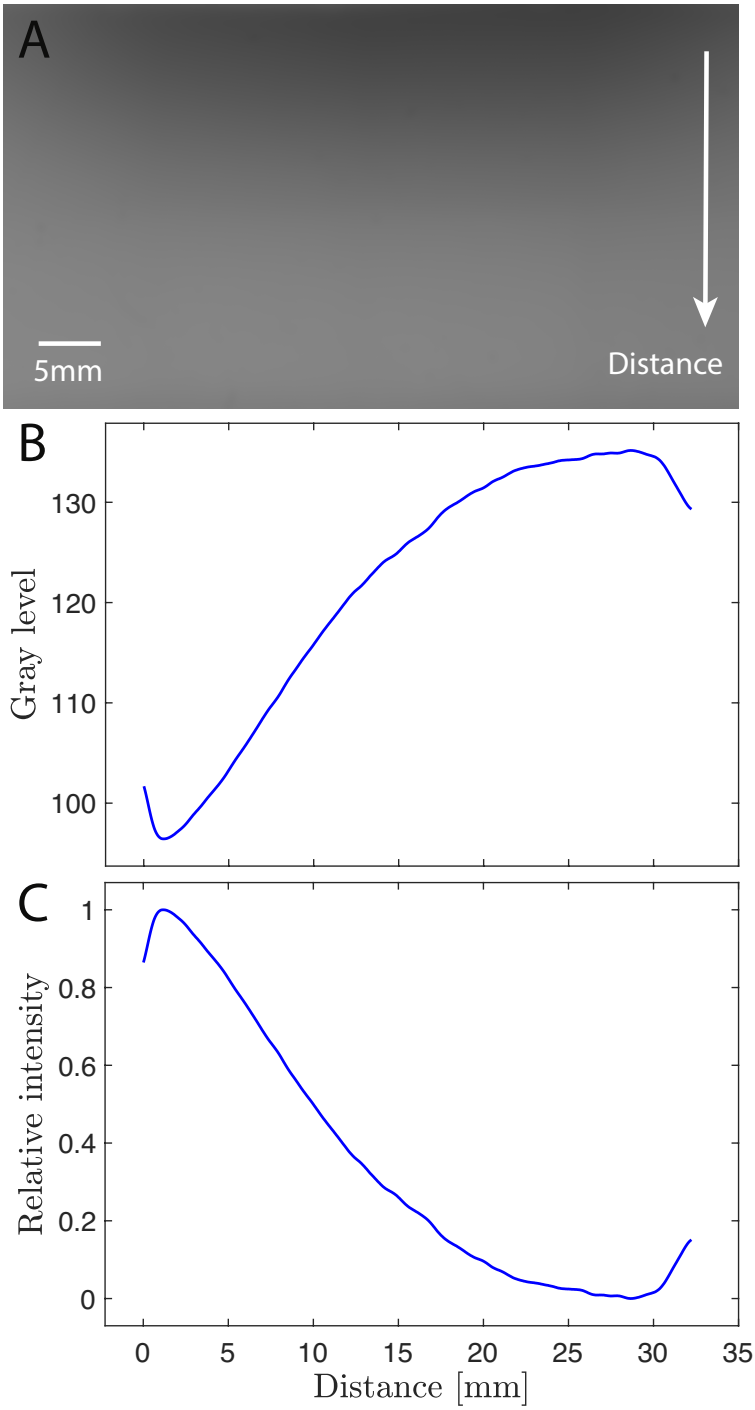

Figure 51: (A) Brightfield image of an agar plate diffused with glucose for 24 hours and stained with TTC. (B) Average vertical gray level of the image. (C) Relative intensity of the TTC stain.

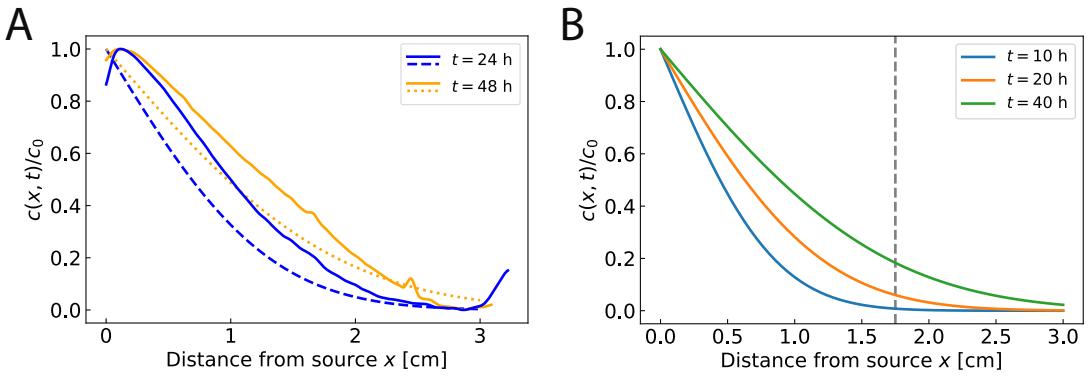

Figure 52: (A) Relative concentration of glucose estimated from staining (solid lines) and Fick's law (dashed and dotted lines) for glucose diffusing in one dimension from a source at $x = 0$. (B) Additional estimates from Fick's law. The dashed line indicates the initial distance of plasmodia from the source in our chemotaxis experiments.

Bibliography

1. Waharte S, Trigoni N (2010) Supporting search and rescue operations with UAVs. *Proceedings - EST 2010 - 2010 International Conference on Emerging Security Technologies, ROBOSEC 2010 - Robots and Security, LAB-RS 2010 - Learning and Adaptive Behavior in Robotic Systems*: 142–147.

2. Vilk O *et al.* (2022) Ergodicity Breaking in Area-Restricted Search of Avian Predators. *Physical Review X* **12**: 31005. ISSN: 21603308. `https://doi.org/10.1103/PhysRevX.12.031005`.

3. Abdelgalil M, Aboelkassem Y, Taha H (2021) Sea urchin sperm exploit extremum seeking control to find the egg. *Physical Review E* **106**: 1–6.

4. Mirny L *et al.* (2009) How a protein searches for its site on DNA: The mechanism of facilitated diffusion. *Journal of Physics A: Mathematical and Theoretical* **42**: 1–23. ISSN: 17518113.

5. Viswanathan G *et al.* (2001) Statistical physics of random searches. *Brazilian Journal of Physics* **31**: 102–108.

6. Viswanathan GM, Raposo EP, da Luz MG (2008) Lévy flights and superdiffusion in the context of biological encounters and random searches. *Physics of Life Reviews* **5**: 133–150. ISSN: 15710645. `http://dx.doi.org/10.1016/j.plrev.2008.03.002`.

7. Bartumeus F, Catalan J (2009) Optimal search behavior and classic foraging theory. *Journal of Physics A: Mathematical and Theoretical* **42**: 434002.

8. Charnov EL (1976) Optimal foraging, the marginal value theorem. *Theoretical population biology* **9**: 129–136.

9. Formaglio P *et al.* (2023) Plasmodium sporozoite search strategy to locate hotspots of blood vessel invasion. *Nature Communications* **14**. ISSN: 20411723.

10. Selmeczi D *et al.* (2008) Cell motility as random motion: A review. *European Physical Journal: Special Topics* **157**: 1–15. ISSN: 19516355.

11. Piipponen M, Li D, Landén NX (2020) The immune functions of keratinocytes in skin wound healing. *International Journal of Molecular Sciences* **21**: 1–26. ISSN: 14220067.

12. Bartumeus F, Peters F, Pueyo S, Marrasé C, Catalan J (2003) Helical Lévy walks: Adjusting searching statistics to resource availability in microzooplankton. *Proceedings of the National Academy of Sciences of the United States of America* **100**: 12771–12775. ISSN: 00278424.

13. Bénichou O, Coppey M, Moreau M, Suet PH, Voituriez R (2005) Optimal search strategies for hidden targets. *Physical Review Letters* **94**: 2–5. ISSN: 00319007. arXiv: `0504107 [cond-mat]`.

14. Faustino CL, Da Silva LR, Da Luz MG, Raposo EP, Viswanathan GM (2007) Search dynamics at the edge of extinction: Anomalous diffusion as a critical survival state. *EPL* **77**. ISSN: 02955075.

15. Tejedor V, Voituriez R, Bénichou O (2012) Optimizing persistent random searches. *Physical Review Letters* **108**: 1–5. ISSN: 00319007. arXiv: `1111.1881`.

16. Przibram K (1913) Über die ungeordnete Bewegung niederer Tiere. *Archiv für Entwicklungsmechanik der Organismen* **43**: 20–27. ISSN: 0949944X.

17. Przibram K (1917) Über die ungeordnete Bewegung niederer Tiere. II. *Archiv für Entwicklungsmechanik der Organismen* **43**: 20–27.

18. Fürth R (1920) Die Brownsche Bewegung bei Berücksichtigung einer Persistenz der Bewegungsrichtung. Mit Anwendungen auf die Bewegung lebender Infusorien. *Zeitschrift für Physik* **2**: 244–256. ISSN: 14346001.

19. Bartumeus F, Da Luz MG, Viswanathan GM, Catalan J (2005) Animal search strategies: A quantitative random-walk analysis. *Ecology* **86**: 3078–3087. ISSN: 00129658. `https://esapubs.org/archive/ecol/E086/168/appendix-A.htm`.

20. Berg HC, Brown DA (1972) Chemotaxis in E coli analysed by 3D tracking. *Nature* **239**: 500–504.

21. Li L, Nørrelkke SF, Cox EC (2008) Persistent cell motion in the absence of external signals: A search strategy for eukaryotic cells. *PLoS ONE* **3**. ISSN: 19326203.

22. Bénichou O, Coppey M, Moreau M, Voituriez R (2006) Intermittent search strategies: When losing time becomes efficient. *Europhysics Letters* **75**: 349–354. ISSN: 02955075.

23. Palyulin VV, Chechkin AV, Metzler R (2014) Lévy flights do not always optimize random blind search for sparse targets. *Proceedings of the National Academy of Sciences of the United States of America* **111**: 2931–2936. ISSN: 00278424.

24. Wosniack ME, Raposo EP, Viswanathan GM, Da Luz MG (2015) Efficient search of multiple types of targets. *Physical Review E - Statistical, Nonlinear, and Soft Matter Physics* **92**: 1–10. ISSN: 15502376.

25. Shaebani MR, Piel M, Lautenschläger F (2022) Distinct Speed and Direction Memories of Migrating Cells Diversify Their Possible Search Strategies: 1–10. arXiv: 2205.10555. http://arxiv.org/abs/2205.10555.

26. Rupprecht JF, Bénichou O, Voituriez R (2016) Optimal search strategies of run-and-tumble walks. *Physical Review E* **94**: 1–9. ISSN: 24700053. arXiv: 1603.03544.

27. Moreau M, Bénichou O, Loverdo C, Voituriez R (2009) Chance and strategy in search processes. *Journal of Statistical Mechanics: Theory and Experiment* **2009**: P12006.

28. Bénichou O, Loverdo C, Moreau M, Voituriez R (2011) Intermittent search strategies. *Reviews of Modern Physics* **83**: 81–129. ISSN: 00346861. arXiv: 1104.0639.

29. Hein AM, Carrara F, Brumley DR, Stocker R, Levin SA (2016) Natural search algorithms as a bridge between organisms, evolution, and ecology. *Proceedings of the National Academy of Sciences of the United States of America* **113**: 9413–9420. ISSN: 10916490.

30. Le Verge-Serandour M, Alim K (2024) Physarum polycephalum : Smart Network Adaptation. *Annual Review of Condensed Matter Physics* **15**: 263–289. ISSN: 1947-5454. arXiv: 2306.09063.

31. Oettmeier C, Brix K, Döbereiner HG (2017) Physarum polycephalum - A new take on a classic model system. *Journal of Physics D: Applied Physics* **50**. ISSN: 13616463.

32. Bonner JT (1998) The origins of multicellularity. *Integrative Biology: Issues, News, and Reviews* **1**: 27–36. ISSN: 10934391.

33. Alexopoulos CJ (1982) Morphology, taxonomy, and phylogeny. *Cell Biology of Physarum and Didymium*: 1.

34. Kauffman S, Wille JJ (1975) The mitotic oscillator in Physarum polycephalum. *Journal of theoretical biology* **55**: 47–93.

35. Ueda T. in *Networks Of Interacting Machines: Production Organization In Complex Industrial Systems And Biological Cells* 221–255 (2005). ISBN: 9789812703248.

36. Sachsenmaier W, Remy U, Plattner-Schobel R (1972) Initiation of synchronous mitosis in Physarum polycephalum. A model of the control of cell division in eukariots. *Experimental Cell Research* **73**: 41–48. ISSN: 00144827.

37. Starostzik C, Marwan W (1995) A photoreceptor with characteristics of phytochrome triggers sporulation in the true slime mould Physarum polycephalum. *FEBS* **370**: 146–148.

38. Burland TG, Solnica-Krezel L, Bailey J, Cunningham DB, Dove WF (1993) Patterns of inheritance, development and the mitotic cycle in the protist Physarum polycephalum. *Advances in Microbial Physiology* **35**: 1–69. ISSN: 00652911.

39. Kessler D (1982) Plasmodial structure and motility. *Cell biology of Physarum and Didymium*: 145–208.

40. McCormick J, Blomquist J, Rusch H (1970) Isolation and characterization of an extracellular polysaccharide from Physarum polycephalum. *Carbohydrate Polymers* **56**: 423–427. ISSN: 01448617.

41. Kuroda S, Takagi S, Nakagaki T, Ueda T (2015) Allometry in Physarum plasmodium during free locomotion: Size versus shape, speed and rhythm. *Journal of Experimental Biology* **218**: 3729–3738. ISSN: 00220949.

42. Seifriz W (19377) A theory of protoplasmic streaming. *Science* **86**: 397–398. ISSN: 0003049X.

43. Kamiya N (1950) The Rate of the Protoplasmic Flow in the Myxomycete Plasmodium. I. *Cytologia*.

44. Rieu JP, Delanoë-Ayari H, Takagi S, Tanaka Y, Nakagaki T (2015) Periodic traction in migrating large amoeba of Physarum polycephalum. *Journal of the Royal Society Interface* **12**. ISSN: 17425662.

45. Bykov AV, Priezzhev AV, Lauri J, Myllylä R *Doppler OCT imaging of cytoplasm shuttle flow in Physarum polycephalum* 2009.

46. Matsumoto K, Takagi S, Nakagaki T (2008) Locomotive mechanism of Physarum plasmodia based on spatiotemporal analysis of protoplasmic streaming. *Biophysical Journal* **94**: 2492–2504. ISSN: 15420086. `http://dx.doi.org/10.1529/biophysj.107.113050`.

47. Alim K, Amselem G, Peaudecerf F, Brenner MP, Pringle A (2013) Random network peristalsis in Physarum polycephalum organizes fluid flows across an individual. *Proceedings of the National Academy of Sciences of the United States of America* **110**: 13306–13311. ISSN: 00278424.

48. Cavalier-Smith T (2009) Megaphylogeny, cell body plans, adaptive zones: Causes and timing of eukaryote basal radiations. *Journal of Eukaryotic Microbiology* **56**: 26–33. ISSN: 10665234.

49. Zhang S, Lasheras JC, del Álamo JC (2019) Symmetry breaking transition towards directional locomotion in Physarum microplasmodia. *Journal of Physics D: Applied Physics* **52**: 494004. https://dx.doi.org/10.1088/1361-6463/ab3ec8.

50. Brix K, Stockem W (1987) Studies on microplasmodia of Physarum polycephalum. VII. Adhesion-dependent changes in the organization of the fibrillar actin system. *Cell biology international reports* **11**: 529–536.

51. Latty T, Beekman M (2009) Food quality affects search strategy in the acellular slime mould, Physarum polycephalum. *Behavioral Ecology* **20**: 1160–1167.

52. Patino-Ramirez F, Arson C, Dussutour A (2021) Substrate and cell fusion influence on slime mold network dynamics. *Scientific Reports* **11**: 1–20. ISSN: 20452322. https://doi.org/10.1038/s41598-020-80320-2.

53. Oettmeier C, Lee J, Döbereiner HG (2018) Form follows function: Ultrastructure of different morphotypes of Physarum polycephalum. *Journal of Physics D: Applied Physics* **51**. ISSN: 13616463.

54. Schick L, Kramar M, Alim K (2024) Dynamic cost allocation allows network-forming forager to switch between search strategies. *PRX Life* **2**: 033005.

55. Satoh H, Ueda T, Kobatake Y (1985) Oscillations in cell shape and size during locomotion and in contractile activities of Physarum polycephalum, Dictyostelium discoideum, Amoeba proteus and macrophages. *Experimental Cell Research* **156**: 79–90. ISSN: 00144827.

56. Kakiuchi Y, Ueda T (2006) Multiple oscillations in changing cell shape by the plasmodium of Physarum polycephalum : general formula governing oscillatory phenomena by the Physarum plasmodium. *Biological Rhythm Research* **37**: 137–146. ISSN: 0929-1016.

57. Westendorf C, Gruber CJ, Schnitzer K, Kraker S, Grube M (2018) Quantitative comparison of plasmodial migration and oscillatory properties across different slime molds. *Journal of Physics D: Applied Physics* **51**. ISSN: 13616463.

58. Nakagaki T, Yamada H, Ueda T (2000) Interaction between cell shape and contraction pattern in the Physarum plasmodium. *Biophysical Chemistry* **84**: 195–204. ISSN: 03014622.

59. Nakagaki T *et al.* (2007) Minimum-risk path finding by an adaptive amoebal network. *Physical Review Letters* **99**: 1–4. ISSN: 00319007.

60. Tero A *et al.* (2010) Rules for Biologically Inspired Adaptive Network Design. *Science* **1**: 439–442.

61. Zhu L, Kim SJ, Hara M, Aono M (2018) Remarkable problem-solving ability of unicellular amoeboid organism and its mechanism. *Royal Society Open Science* **5**. ISSN: 20545703.

62. Reid CR *et al.* (2016) Decision-making without a brain: how an amoeboid organism solves the two-armed bandit. *Journal of The Royal Society Interface* **13**: 20160030.

63. Latty T, Beekman M (2011) Speed – accuracy trade-offs during foraging decisions in the acellular slime mould Physarum polycephalum: 539–545.

64. Dussutour A, Latty T, Beekman M, Simpson SJ (2010) Amoeboid organism solves complex nutritional challenges. *Proceedings of the National Academy of Sciences of the United States of America* **107**: 4607–4611. ISSN: 00278424.

65. Saigusa T, Tero A, Nakagaki T, Kuramoto Y (2008) Amoebae anticipate periodic events. *Physical Review Letters* **100**. ISSN: 00319007.

66. Vogel D, Dussutour A (2016) Direct transfer of learned behaviour via cell fusion in non-neural organisms. *Proceedings of the Royal Society B: Biological Sciences* **283**. ISSN: 14712954.

67. Boisseau RP, Vogel D, Dussutour A (2016) Habituation in non-neural organisms: Evidence from slime moulds. *Proceedings of the Royal Society B: Biological Sciences* **283**: 2–8. ISSN: 14712954.

68. Boussard A, Delescluse J, Pérez-Escudero A, Dussutour A (2019) Memory inception and preservation in slime moulds: The quest for a common mechanism. *Philosophical Transactions of the Royal Society B: Biological Sciences* **374**. ISSN: 14712970.

69. Smith-Ferguson J, Beekman M (2020) Who needs a brain? Slime moulds, behavioural ecology and minimal cognition. *Adaptive Behavior* **28**: 465–478. ISSN: 17412633.

70. Boussard A *et al.* (2021) Adaptive behaviour and learning in slime moulds: the role of oscillations. *Philosophical Transactions of the Royal Society B: Biological Sciences* **376**: 20190757. ISSN: 0962-8436.

71. Dussutour A (2021) Biochemical and Biophysical Research Communications Learning in single cell organisms. *Biochemical and Biophysical Research Communications*. ISSN: 0006-291X. https://doi.org/10.1016/j.bbrc.2021.02.018.

72. Reid CR (2023) Thoughts from the forest floor: a review of cognition in the slime mould Physarum polycephalum. *Animal Cognition*. ISSN: 14359456. https://doi.org/10.1007/s10071-023-01782-1.

73. Chen S, Alim K (2022) Network topology enables efficient response to environment in Physarum polycephalum. *Physical Biology*: 9–14.

74. Kramar ME, Alim K (2021) Encoding memory in tube diameter hierarchy of living flow network - SI. *Proceedings of the National Academy of Sciences of the United States of America* **118**: 1–11. ISSN: 10916490.

75. Shirakawa T, Sato H, Nishida M (2016) A power law in the exploratory behavior of the Physarum plasmodium. *Artificial Life and Robotics* **21**: 195–200. ISSN: 16147456.

76. Rodiek B, Takagi S, Ueda T, Hauser MJ (2015) Patterns of cell thickness oscillations during directional migration of Physarum polycephalum. *European Biophysics Journal* **44**: 349–358. ISSN: 14321017.

77. Rodiek B, Hauser MJ (2015) Migratory behaviour of Physarum polycephalum microplasmodia. *European Physical Journal: Special Topics* **224**: 1199–1214. ISSN: 19516401.

78. Shirakawa T, Niizato T, Sato H, Ohno R (2019) Biased Lévy-walk pattern in the exploratory behavior of the Physarum plasmodium. *BioSystems* **182**: 52–58. ISSN: 18728324. https://doi.org/10.1016/j.biosystems.2019.103985.

79. Reid CR, Latty T, Dussutour A, Beekman M (2012) Slime mold uses an externalized spatial "memory" to navigate in complex environments. *Proceedings of the National Academy of Sciences of the United States of America* **109**: 17490–17494. ISSN: 00278424.

80. Reid CR, Beekman M, Latty T, Dussutour A (2013) Amoeboid organism uses extracellular secretions to make smart foraging decisions. *Behavioral Ecology* **24**: 812–818. ISSN: 10452249.

81. Smith-Ferguson J, Reid CR, Latty T, Beekman M (2017) Hänsel, Gretel and the slime mould - How an external spatial memory aids navigation in complex environments. *Journal of Physics D: Applied Physics* **50**. ISSN: 13616463.

82. Huynh TT, Phung TV, Stephenson SL, Tran HT (2017) Biological activities and chemical compositions of slime tracks and crude exopolysaccharides isolated from plasmodia of Physarum polycephalum and Physarella oblonga. *BMC Biotechnology* **17**: 1–10. ISSN: 14726750.

83. Sesaki H, Ogihara S (1997) Protrusion of cell surface coupled with single exocytotic events of secretion of the slime in Physarum plasmodia. *Journal of Cell Science* **110**: 809–818. ISSN: 00219533.

84. Sesaki H, Ogihara S (1997) Secretion of Slime , the Extracellular Matrix of the Plasmodium , as Visualized with a Fluorescent Probe and Its Correlation with Locomotion on the Substratum. **289**: 279–289.

85. Rhea RP (1966) Electron microscopic observations on the slime mold Physarum polycephalum with specific reference to fibrillar structures. *Journal of Ultrasructure Research* **15**: 349–379. ISSN: 00225320.

86. Wolf KV, Hoffmann HU, Stockem W (1981) Studies on microplasmodia of Physarum polycephalum: II. Fine structure and function of the mucous layer. *Protoplasma* **107**: 345–359. ISSN: 0033183X.

87. Henney HR, Asgari M (1975) The function of slime from Physarum flavicomum in the control of cell division. *Canadian Journal of Microbiology* **21**: 1866–1876. ISSN: 00084166.

88. Masui M, Satoh S, Seto K (2018) Allorecognition behavior of slime mold plasmodium - Physarum rigidum slime sheath-mediated self-extension model. *Journal of Physics D: Applied Physics* **51**. ISSN: 13616463.

89. Masui M, Yamamoto PK, Kono N (2024) Allorecognition behaviors in Myxomycetes respond to intraspecies factors. *Biology Open* **13**.

90. Sims M, Kiverstein J (2022) Externalized memory in slime mould and the extended (non-neuronal) mind. *Cognitive Systems Research* **73**: 26–35. ISSN: 13890417.

91. Sethna JP *Statistical mechanics: entropy, order parameters, and complexity* (Oxford University Press, USA, 2021).

92. Berg HC *Random Walks in Biology Princeton University Press* 1993.

93. Metzler R, Jeon JH, Cherstvy AG, Barkai E (2014) Anomalous diffusion models and their properties: Non-stationarity, non-ergodicity, and ageing at the centenary of single particle tracking. *Physical Chemistry Chemical Physics* **16**: 24128–24164. ISSN: 14639076.

94. Pearson K (1905) The problem of the random walk. *Nature* **72**: 342–342.

95. Friedrich BM (2008) Search along persistent random walks. *Physical Biology* **5**. ISSN: 14783975.

96. Selmeczi D, Mosler S, Hagedorn PH, Larsen NB, Flyvbjerg H (2005) Cell motility as persistent random motion: Theories from experiments. *Biophysical Journal* **89**: 912–931. ISSN: 00063495.

97. Ornstein L *On the Brownian motion* in *Proc. Amst* **21** (1919): 96–108.

98. Uhlenbeck GE, Ornstein LS *On the theory of Brownian motion* 1930.

99. Madras N, Slade G *The self-avoiding walk* (Springer Science & Business Media, 2013).

100. Mandelbrot BB (2000) Some Mathematical Questions Arising in Fractal Geometry. *Development of Mathematics, 1950–2000*: 795–811.

101. Sims DW *et al.* (2014) Hierarchical random walks in trace fossils and the origin of optimal search behavior. *Proceedings of the National Academy of Sciences of the United States of America* **111**: 11073–11078. ISSN: 10916490.

102. Madras N, Sokal AD (1988) The pivot algorithm: A highly efficient Monte Carlo method for the self-avoiding walk. *Journal of Statistical Physics* **50**: 109–186. ISSN: 00224715.

103. Slade G (1994) Self-avoiding walks. *The Mathematical Intelligencer* **16**: 29–35.

104. Flory PJ (1949) The configuration of real polymer chains. *The Journal of Chemical Physics* **17**: 303–310.

105. Pietronero L (1985) Survival probability for kinetic self-avoiding walks. *Physical Review Letters* **55**: 2025.

106. De Gennes PG *Scaling concepts in polymer physics* (Cornell university press, 1979).

107. Coniglio A, Jan N, Majid I, Stanley HE (1987) Conformation of a polymer chain at the theta'point: Connection to the external perimeter of a percolation cluster. *Physical Review B* **35**: 3617.

108. Majid I, Jan N, Coniglio A, Stanley HE (1984) Kinetic growth walk: A new model for linear polymers. *Physical review letters* **52**: 1257.

109. Hemmer S, Hemmer P (1984) An average self-avoiding random walk on the square lattice lasts 71 steps. *The Journal of Chemical Physics* **81**: 584–585.

110. Lyklema J, Kremer K (1986) Monte Carlo series analysis of irreversible self-avoiding walks. II. The growing self-avoiding walk. *Journal of Physics A: Mathematical and General* **19**: 279.

111. Hemmer PC, Hemmer S (1986) Trapping of genuine self-avoiding walks. *Physical Review A* **34**: 3304–3308. ISSN: 10502947.

112. Amit DJ, Parisi G, Peliti L (1983) Asymptotic behavior of the" true" self-avoiding walk. *Physical Review B* **27**: 1635.

113. Grassberger P (2017) Self-trapping self-repelling random walks. *Physical review letters* **119**: 140601.

114. Barbier-Chebbah A, Bénichou O, Voituriez R (2022) Self-Interacting Random Walks: Aging, Exploration, and First-Passage Times. *Physical Review X* **12**: 1–15. ISSN: 21603308. arXiv: `2109.13127`.

115. Malakis A (1976) The trail problem on the square lattice. *Journal of Physics A: Mathematical and General* **9**: 1283.

116. Guttmann A, Byrnes C, Frankel N (1984) A generalised self-avoiding walk. *Journal of Physics A: Mathematical and General* **17**: L457.

117. Cira NJ *et al.* (2024) Structure , motion , and multiscale search of traveling networks.

118. Visser AW, Kiørboe T (2006) Plankton motility patterns and encounter rates. *Oecologia* **148**: 538–546.

119. Reynolds A (2015) Liberating Lévy walk research from the shackles of optimal foraging. *Physics of Life Reviews* **14**: 59–83. ISSN: 15710645. `http://dx.doi.org/10.1016/j.plrev.2015.03.002`.

120. Bénichou O, Loverdo C, Moreau M, Voituriez R (2006) Two-dimensional intermittent search processes: An alternative to Lévy flight strategies. *Physical Review E—Statistical, Nonlinear, and Soft Matter Physics* **74**: 020102.

121. Pyke GH (1984) Optimal foraging theory: a critical review. *Annual review of ecology and systematics* **15**: 523–575.

122. Hughes RN *Behavioural Mechanisms of Food Selection* ISBN: 9783642751202 (1990).

123. Celani A, Vergassola M (2010) Bacterial strategies for chemotaxis response. *Proceedings of the National Academy of Sciences of the United States of America* **107**: 1391–1396. ISSN: 00278424.

124. Simon HA (1956) Rational choice and the structure of the environment (reprint from 1956). *Psychological Review* **63**.

125. Carmel Y, Ben-haim Y (2005) Info - Gap Robust - Satisficing Model of Foraging Behavior : Do Foragers Optimize or Satisfice ? Published by : The University of Chicago Press for The American Society. *The American Naturalist* **166**: 633–641.

126. Bonner JT *First signals: the evolution of multicellular development* (Princeton University Press, 2009).

127. Wicher D, Marion-Poll F (2018) Editorial: Function and regulation of chemoreceptors. *Frontiers in Cellular Neuroscience* **12**: 10–12. ISSN: 16625102.

128. Parent CA, Devreotes PN (1999) A cell's sense of direction. *Science* **284**: 765–770.

129. Janetopoulos C, Firtel RA (2008) Directional sensing during chemotaxis. *FEBS Letters* **582**: 2075–2085. ISSN: 00145793.

130. Segall JE, Block SM, Berg HC (1986) Temporal comparisons in bacterial chemotaxis. *Proceedings of the National Academy of Sciences of the United States of America* **83**: 8987–8991. ISSN: 00278424.

131. Dusenbery DB (1998) Spatial sensing of stimulus gradients can be superior to temporal sensing for free-swimming bacteria. *Biophysical Journal* **74**: 2272–2277. ISSN: 00063495.

132. Thar R, Kühl M (2003) Bacteria are not too small for spatial sensing of chemical gradients: An experimental evidence. *Proceedings of the National Academy of Sciences of the United States of America* **100**: 5748–5753. ISSN: 00278424.

133. Wheeler JHR, Foster KR, Durham WM (2024) Bacteria use spatial sensing to direct chemotaxis on surfaces Author list. *bioRxiv*: 2024.02.13.580113. `https://doi.org/10.1101/2024.02.13.580113`.

134. Wan KY, Jékely G (2021) Origins of eukaryotic excitability. *Philosophical Transactions of the Royal Society B: Biological Sciences* **376**: 0–2. ISSN: 14712970. arXiv: `2007.13388`.

135. Alonso A, Kirkegaard JB (2024) Learning optimal integration of spatial and temporal information in noisy chemotaxis. *PNAS nexus*: 5–6.

136. Rode J, Novak M, Friedrich BM (2024) Information Theory of Chemotactic Agents Using Both Spatial and Temporal Gradient Sensing. **023012**: 1–11.

137. Lackie JM. in *Cell Movement and Cell Behaviour* 219–251 (Springer Netherlands, Dordrecht, 1986). ISBN: 978-94-009-4071-0. https://doi.org/10.1007/978-94-009-4071-0_9.

138. Kalinin YV, Jiang L, Tu Y, Wu M (2009) Logarithmic sensing in Escherichia coli bacterial chemotaxis. *Biophysical Journal* **96**: 2439–2448. ISSN: 15420086. http://dx.doi.org/10.1016/j.bpj.2008.10.027.

139. Brus J, Heng JA, Polanía R (2019) Weber's Law: A Mechanistic Foundation after Two Centuries. *Trends in Cognitive Sciences* **23**: 906–908. ISSN: 1879307X.

140. Fechner GT (1948) Elements of psychophysics, 1860.

141. Arumugam G, Tyagi J (2021) Keller-Segel chemotaxis models: A review. *Acta Applicandae Mathematicae* **171**: 1–82.

142. Thomas MA, Kleist AB, Volkman BF (2018) Decoding the chemotactic signal. *Journal of leukocyte biology* **104**: 359–374.

143. Xiong Y, Huang CH, Iglesias PA, Devreotes PN (2010) Cells navigate with a local-excitation, global-inhibition-biased excitable network. *Proceedings of the National Academy of Sciences of the United States of America* **107**: 17079–17086. ISSN: 00278424.

144. Insall RH (2013) The interaction between pseudopods and extracellular signalling during chemotaxis and directed migration. *Current Opinion in Cell Biology* **25**: 526–531. ISSN: 09550674. http://dx.doi.org/10.1016/j.ceb.2013.04.009.

145. Tröger L, Goirand F, Alim K (2024) Size-dependent self-avoidance enables superdiffusive migration in macroscopic unicellulars. *Proceedings of the National Academy of Sciences* **121**: e2312611121.

146. Jackson DE, Ratnieks FL (2006) Communication in ants. *Current biology* **16**: R570–R574.

147. Sims DW *et al.* (2008) Scaling laws of marine predator search behaviour. *Nature* **451**: 1098–1102. ISSN: 14764687.

148. Raichlen DA *et al.* (2014) Evidence of Lévy walk foraging patterns inhuman hunter-gatherers. *Proceedings of the National Academy of Sciences of the United States of America* **111**: 728–733. ISSN: 00278424.

149. Wu PH, Giri A, Sun SX, Wirtz D (2014) Three-dimensional cell migration does not follow a random walk. *Proceedings of the National Academy of Sciences of the United States of America* **111**: 3949–3954. ISSN: 10916490.

150. Dieterich P, Klages R, Preuss R, Schwab A (2008) Anomalous dynamics of cell migration. *Proceedings of the National Academy of Sciences of the United States of America* **105**: 459–463. ISSN: 00278424.

151. Harris TH *et al.* (2012) Generalized Lévy walks and the role of chemokines in migration of effector CD8 + T cells. *Nature* **486**: 545–548. ISSN: 00280836.

152. Huda S *et al.* (2018) Lévy-like movement patterns of metastatic cancer cells revealed in microfabricated systems and implicated in vivo. *Nature Communications*: 1–11. ISSN: 2041-1723. http://dx.doi.org/10.1038/s41467-018-06563-w.

153. Upadhyaya A, Rieu JP, Glazier JA, Sawada Y (2001) Anomalous diffusion and non-Gaussian velocity distribution of Hydra cells in cellular aggregates. *Physica A: Statistical Mechanics and its Applications* **293**: 549–558. ISSN: 03784371.

154. Miramontes O, DeSouza O, Paiva LR, Marins A, Orozco S (2014) Lévy flights and self-similar exploratory behaviour of termite workers: Beyond model fitting. *PLoS ONE* **9**: 1–9. ISSN: 19326203. arXiv: 1410.0930.

155. Viswanathan GM *et al.* (1996) Lévy flight search patterns of wandering albatrosses. *Nature* **381**: 413–415. ISSN: 00280836.

156. Ariel G *et al.* (2015) Swarming bacteria migrate by Lévy Walk. *Nature Communications* **6**. ISSN: 20411723.

157. Slade G (2019) Self-avoiding walk, spin systems and renormalization. *Proceedings of the Royal Society A: Mathematical, Physical and Engineering Sciences* **475**. ISSN: 14712946. arXiv: 1808.04476.

158. Li L, Cox EC, Flyvbjerg H (2011) 'Dicty dynamics': Dictyostelium motility as persistent random motion. *Physical Biology* **8**. ISSN: 14783967.

159. Shaebani MR, Rieger H (2019) Transient Anomalous Diffusion in Run-and-Tumble Dynamics. *Frontiers in Physics* **7**: 1–9. ISSN: 2296424X. arXiv: 2107.07329.

160. Verge-Serandour ML, Alim K (2024) Annual Review of Condensed Matter Physics Physarum polycephalum: Smart Network Adaptation. *Annual Review of Condensed Matter Physics* **15**: 263–289. ISSN: 19475462.

161. Viswanathan GM, Raposo EP, Bartumeus F, Catalan J, Da Luz MG (2005) Necessary criterion for distinguishing true superdiffusion from correlated random walk processes. *Physical Review E - Statistical, Nonlinear, and Soft Matter Physics* **72**: 1–6. ISSN: 15393755.

162. Varennes J, ran Moon H, Saha S, Mugler A, Han B (2019) Physical Constraints On Accuracy and Persistence During Breast Cancer Cell Chemotaxis. *arXiv*: 1–20. ISSN: 23318422.

163. Zhao K *et al.* (2013) Psl trails guide exploration and microcolony formation in Pseudomonas aeruginosa biofilms. *Nature* **497**: 388–391. ISSN: 00280836.

164. D'Alessandro J *et al.* (2021) Cell migration guided by long-lived spatial memory. *Nature Communications* **12**: 1–10. ISSN: 20411723.

165. Robinson EJ, Jackson DE, Holcombe M, Ratnieks FL (2005) 'No entry'signal in ant foraging. *Nature* **438**: 442–442.

166. Kranz WT, Gelimson A, Zhao K, Wong GC, Golestanian R (2016) Effective Dynamics of Microorganisms That Interact with Their Own Trail. *Physical Review Letters* **117**: 1–6. ISSN: 10797114. arXiv: 1504.06814.

167. Barbara GM, Mitchell JG (2003) Marine bacterial organisation around point-like sources of amino acids. *FEMS Microbiology Ecology* **43**: 99–109. ISSN: 01686496.

168. Varnum B, Soll DR (1984) Effects of cAMP on Single Cell Motility. *J Cell Biol.* 1–5.

169. Tweedy L *et al.* (2020) Seeing around corners: Cells solve mazes and respond at a distance using attractant breakdown. *Science* **369**. ISSN: 10959203.

170. Gerber T *et al.* (2022) Spatial transcriptomic and single-nucleus analysis reveals heterogeneity in a gigantic single-celled syncytium. *Elife* **11**: e69745.

171. Daniel JW, Rusch HP (1961) The pure culture of Physarum polycephalum on a partially defined soluble medium. *Microbiology* **25**: 47–59.

172. Daniel JW, Kelley J, Rusch HP, P H (1962) Hematin-requiring plasmiodial myxomycete: 1104–1110. http://jb.asm.org/.

173. Hato M, Ueda T, Kurihara K, Kobatake Y (1976) Phototaxis in True Slime Mold Physarum polycephalum. *Cell Structure and Function* **1**: 269–278. ISSN: 13473700.

174. Blattner T *et al. A hybrid CPU-GPU system for stitching large scale optical microscopy images* in *2014 43rd International Conference on Parallel Processing* (2014): 1–9.

175. Chalfoun J *et al.* (2017) MIST: Accurate and Scalable Microscopy Image Stitching Tool with Stage Modeling and Error Minimization. *Scientific Reports* **7**: 1–10. ISSN: 20452322.

176. Anderson D, Burnham K (2004) Model selection and multi-model inference. *Second. NY: Springer-Verlag* **63**: 10.

177. Devroye L, Devroye L (1986) General principles in random variate generation. *Non-uniform random variate generation*: 27–82.

178. Pietronero L (1985) Survival Probability for Kinetic Self-Avoiding Walks. *Physical Review Letters* **55**: 2025–2027. ISSN: 00319007.

179. Lyklema J. in *Fractals in Physics* 93–96 (Elsevier, 1986).

180. Lenski D *The influence of external conditions on the migration of small plasmodia of Physarum polycephalum* MA thesis (2024).

181. Bloom AB, Zaman MH (2014) Influence of the microenvironment on cell fate determination and migration. *Physiological genomics* **46**: 309–314.

182. Roggatz CC *et al.* (2022) Becoming nose-blind—Climate change impacts on chemical communication. *Global Change Biology* **28**: 4495–4505. ISSN: 13652486.

183. Roggatz CC, Hardege JD, Saha M (2022) Modelling Antifouling compounds of Macroalgal Holobionts in Current and Future pH Conditions. *Journal of Chemical Ecology* **48**: 455–473. ISSN: 15731561.

184. Patino-Ramirez F, Boussard A, Arson C, Dussutour A (2019) Substrate composition directs slime molds behavior. *Scientific Reports* **9**: 1–14. ISSN: 20452322.

185. Costa AC, Sridhar G, Wyart C, Vergassola M (2024) Fluctuating landscapes and heavy tails in animal behavior. *PRX Life* **2**: 023001.

186. Nicholson DJ (2019) Is the cell really a machine? *Journal of theoretical biology* **477**: 108–126.

187. Gray WD (1939) The Relation of pH and Temperature to the Fruiting of Physarum polycephalum. *American Journal of Botany* **26**: 709. ISSN: 00029122.

188. Willebrand R, Kleinewietfeld M (2018) The role of salt for immune cell function and disease. *Immunology* **154**: 346–353. ISSN: 13652567.

189. Lamers ML, Almeida ME, Vicente-Manzanares M, Horwitz AF, Santos MF (2011) High glucose-mediated oxidative stress impairs cell migration. *PLoS ONE* **6**: 1–9. ISSN: 19326203.

190. Hayashi JN *et al.* (1991) Effects of glucose on migration, proliferation and tube formation by vascular endothelial cells. *Virchows Archiv B Cell Pathology Including Molecular Pathology* **60**: 245–252. ISSN: 00426431.

191. Viswanathan GM *et al.* (1999) Optimizing the success of random searches. *Nature* **401**: 911–914.

192. Bartumeus F, Catalan J, Fulco UL, Lyra ML, Viswanathan GM (2002) Optimizing the Encounter Rate in Biological Interactions: Lévy versus Brownian Strategies. *Physical Review Letters* **88**: 4. ISSN: 10797114.

193. Wilkinson PC (1990) How do leucocytes perceive chemical gradients? *FEMS Microbiology Letters* **64**: 303–311. ISSN: 15746968.

194. Sourjik V, Schmitt R (1996) Different roles of CheY1 and CheY2 in the chemotaxis of Rhizobium meliloti. *Molecular Microbiology* **22**: 427–436. ISSN: 0950382X.

195. Scherber C *et al.* (2012) Epithelial cell guidance by self-generated EGF gradients. *Integrative biology : quantitative biosciences from nano to macro* **4**: 259–269. ISSN: 17579708.

196. Donà E *et al.* (2013) Directional tissue migration through a self-generated chemokine gradient. *Nature* **503**: 285–289. ISSN: 00280836.

197. Tweedy L, Susanto O, Insall RH (2016) Self-generated chemotactic gradients - cells steering themselves. *Current Opinion in Cell Biology* **42**: 46–51. ISSN: 18790410. `http://dx.doi.org/10.1016/j.ceb.2016.04.003`.

198. Clark AG *et al. Self-generated gradients steer collective migration on viscoelastic collagen networks* **10:** 1200–1210. ISBN: 4156302201259 (Springer US, 2022).

199. Stock J, Kazmar T, Schlumm F, Hannezo E, Pauli A (2022) A self-generated Toddler gradient guides mesodermal cell migration. *Science Advances* **8**: 1–14. ISSN: 23752548.

200. Alanko J *et al.* (2023) CCR7 acts as both a sensor and a sink for CCL19 to coordinate collective leukocyte migration. *Science immunology* **8**: eadc9584.

201. Takamatsu A, Takaba E, Takizawa G (2009) Environment-dependent morphology in plasmodium of true slime mold Physarum polycephalum and a network growth model. *Journal of Theoretical Biology* **256**: 29–44. ISSN: 00225193.

202. Shirakawa T, Gunji YP, Sato H, Tsubakino H (2020) Diversity in the chemotactic behavior of physarum plasmodium induced by bi-modal stimuli. *International Journal of Unconventional Computing* **15**: 275–285. ISSN: 15487202.

203. Miyake Y, Tada H, Yano M, Shimizu H (1994) Relationship between Intracellular Period Modulation and External Environment Change in Physarum Plasmodium. *Cell Structure and Function* **19**: 363–370. ISSN: 13473700.

204. Morisawa M, Steinhardt R (1982) Changes in intracellular pH of Physarum plasmodium during the cell cycle and in response to starvation. *Experimental cell research* **140**: 341–351.

205. Anderson JD (1951) Galvanotaxis of slime mold. *The Journal of general physiology* **35**: 1–16.

206. Stocker R (2012) Marine microbes see a sea of gradients. *Science* **338**: 628–633. ISSN: 10959203.

207. Dieterich P *et al.* (2022) Anomalous diffusion and asymmetric tempering memory in neutrophil chemotaxis. *PLOS Computational Biology* **18**: e1010089. `http://dx.doi.org/10.1371/journal.pcbi.1010089`.

208. Albini A, Adelmann-Grill BC, Müller PK (1985) Fibroblast chemotaxis. *Collagen and related research* **5**: 283–296.

209. Gagnon C, de Lamirande E (2006) Controls of sperm motility. *The Sperm Cell: Production, Maturation, Fertilization, Regeneration*: 108–133.

210. Chet I, Mitchell R (1976) Ecoological Aspects of Microbial Chemotactic Behavior. *Ann. Rev. Microbiol.* **30**: 221–239. ISSN: 01302906.

211. Kojadinovic M, Armitage JP, Tindall MJ, Wadhams GH (2013) Response kinetics in the complex chemotaxis signalling pathway of Rhodobacter sphaeroides. *Journal of the Royal Society Interface* **10**. ISSN: 17425662.

212. Jékely G (2009) Evolution of phototaxis. *Philosophical Transactions of the Royal Society B: Biological Sciences* **364**: 2795–2808. ISSN: 14712970.

213. Roca-Cusachs P, Sunyer R, Trepat X (2013) Mechanical guidance of cell migration: Lessons from chemotaxis. *Current Opinion in Cell Biology* **25**: 543–549. ISSN: 09550674. `http://dx.doi.org/10.1016/j.ceb.2013.04.010`.

214. Vladimirov N, Sourjik V (2009) Chemotaxis: How bacteria use memory. *Biological Chemistry* **390**: 1097–1104. ISSN: 14316730.

215. Swaney KF, Huang CH, Devreotes PN (2010) Eukaryotic chemotaxis: A network of signaling pathways controls motility, directional sensing, and polarity. *Annual Review of Biophysics* **39**: 265–289. ISSN: 1936122X.

216. Andrew N, Insall RH (2007) Chemotaxis in shallow gradients is mediated independently of PtdIns 3-kinase by biased choices between random protrusions. *Nature Cell Biology* **9**: 193–200. ISSN: 14657392.

217. Kay RR, Langridge P, Traynor D, Hoeller O (2008) Changing directions in the study of chemotaxis. *Nature Reviews Molecular Cell Biology* **9**: 455–463. ISSN: 14710072.

218. Insall RH (2010) Understanding eukaryotic chemotaxis: A pseudopod-centred view. *Nature Reviews Molecular Cell Biology* **11**: 453–458. ISSN: 14710072.

219. Alonso A, Kirkegaard JB, Endres RG (2024) Persistent pseudopod splitting is an effective chemotaxis strategy in shallow gradients. *arXiv preprint arXiv:2409.09342*.

220. Iglesias PA, Devreotes PN (2008) Navigating through models of chemotaxis. *Current Opinion in Cell Biology* **20**: 35–40. ISSN: 09550674.

221. Malet-Engra G *et al.* (2015) Collective cell motility promotes chemotactic prowess and resistance to chemorepulsion. *Current Biology* **25**: 242–250.

222. Camley BA, Zimmermann J, Levine H, Rappel WJ (2016) Emergent Collective Chemotaxis without Single-Cell Gradient Sensing. *Physical Review Letters* **116**: 1–6. ISSN: 10797114. arXiv: 1506.06698.

223. Camley BA (2018) Collective gradient sensing and chemotaxis: modeling and recent developments. *Journal of Physics: Condensed Matter* **30**: 223001. https://dx.doi.org/10.1088/1361-648X/aabd9f.

224. Ipiña EP, Camley BA (2022) Collective gradient sensing with limited positional information. *Physical Review E* **105**: 1–16. ISSN: 24700053. arXiv: 2110.10260.

225. LeFebre R, Landsittel JA, Stone DE, Mugler A (2024) Role of signal degradation in directional chemosensing. *Physical Review Letters* **133**: 138402.

226. Ueda T, Kobatake Y (1982) Chemotaxis in plasmodia of Physarum polycephalum. *Cell biology of Physarum and Didymium*: 111–143.

227. Ueda T, Terayama K, Kurihara K, Kobatake Y (1975) Threshold phenomena in chemoreception and taxis in slime mold Physarum polycephalum. *Journal of General Physiology* **65**: 223–234. ISSN: 15407748.

228. Ueda T, Muratsugu M, Kurihara K, Kobatake Y (1976) Chemotaxis in Physarum polycephalum. Effects of chemicals on isometric tension of the plasmodial strand in relation to chemotactic movement. *Experimental Cell Research* **100**: 337–344. ISSN: 00144827.

229. Ueda T, Hirose T, Kobatake Y (1980) Membrane biophysics of chemoreception and taxis in the plasmodium of physarum polycephalum. *Biophysical Chemistry* **11**: 461–473. ISSN: 03014622.

230. Carlile MJ (1970) Nutrition and chemotaxis in the myxomycete Physarum polycephalum: the effect of carbohydrates on the plasmodium. *Journal of general microbiology* **63**: 221–226. ISSN: 00221287.

231. Chet I, Naveh A, Henis Y (1977) Chemotaxis of Physarum polycephalum towards carbohydrates, amino acids and nucleotides. *Journal of General Microbiology* **102**: 145–148. ISSN: 00221287.

232. Lewis OL, Zhang S, Guy RD, Del Álamo JC (2015) Coordination of contractility, adhesion and flow in migrating Physarum amoebae. *Journal of the Royal Society Interface* **12**. ISSN: 17425662.

233. Ueda KI, Takagi S, Nishiura Y, Nakagaki T (2011) Mathematical model for contemplative amoeboid locomotion. *Physical Review E—Statistical, Nonlinear, and Soft Matter Physics* **83**: 021916.

234. Ridley AJ *et al.* (2003) Cell migration: integrating signals from front to back. *Science* **302**: 1704–1709.

235. Yoshida K, Soldati T (2006) Dissection of amoeboid movement into two mechanically distinct modes. *Journal of Cell Science* **119**: 3833–3844. ISSN: 00219533.

236. Charras G, Paluch E (2008) Blebs lead the way: how to migrate without lamellipodia. *Nature reviews Molecular cell biology* **9**: 730–736.

237. Lange M, Prassler J, Ecke M, Müller-Taubenberger A, Gerisch G (2016) Local Ras activation, PTEN pattern, and global actin flow in the chemotactic responses of oversized cells. *Journal of Cell Science* **129**: 3462–3472. ISSN: 14779137.

238. Houk AR *et al.* (2012) Membrane tension maintains cell polarity by confining signals to the leading edge during neutrophil migration. *Cell* **148**: 175–188. ISSN: 00928674. `http://dx.doi.org/10.1016/j.cell.2011.10.050`.

239. Maiuri P *et al.* (2015) Actin flows mediate a universal coupling between cell speed and cell persistence. *Cell* **161**: 374–386. ISSN: 10974172.

240. Julien JD, Alim K (2018) Oscillatory fluid flow drives scaling of contraction wave with system size. *Proceedings of the National Academy of Sciences of the United States of America* **115**: 10612–10617. ISSN: 10916490. arXiv: `1806.05933`.

241. Alim K, Andrew N, Pringle A, Brenner MP (2017) Mechanism of signal propagation in Physarum polycephalum. *Proceedings of the National Academy of Sciences of the United States of America* **114**: 5136–5141. ISSN: 10916490.

242. Sedzinski J *et al.* (2011) Polar actomyosin contractility destabilizes the position of the cytokinetic furrow. *Nature* **476**: 462–468. ISSN: 00280836.

243. Stockem W, Brix K (1994) Analysis of Microfilament Organization and Contractile Activities in Physarum. *International Review of Cytology* **149**: 145–215. ISSN: 00747696.

244. Fritzsche M, Lewalle A, Duke T, Kruse K, Charras G (2013) Analysis of turnover dynamics of the submembranous actin cortex. *Molecular Biology of the Cell* **24**: 757–767. ISSN: 10591524.

245. Robinson DN, Kee YS, Luo T, Surcel A (2012) Understanding how dividing cells change shape. *Comprehensive Biophysics* **7**: 48–72.

246. Locsei JT (2007) Persistence of direction increases the drift velocity of run and tumble chemotaxis. *Journal of mathematical biology* **55**: 41–60.

247. Löw I, Dancker P, Wieland T (1975) Stabilization of F-actin by phalloidin reversal of the destabilizing effect of cytochalasin B. *FEBS letters* **54**: 263–265.

248. Kukulies J, Stockem W (1985) Function of the microfilament system in living cell fragments of Physarum polycephalum as revealed by microinjection of fluorescent analogs. *Cell and tissue research* **242**: 323–332.

249. Brémont J, Bénichou O, Voituriez R (2024) Exact propagators of one-dimensional self-interacting random walks. *Physical Review Letters* **133**: 157101.

250. Vogel D *et al.* (2015) Phenotypic variability in unicellular organisms: From calcium signalling to social behaviour. *Proceedings of the Royal Society B: Biological Sciences* **282**. ISSN: 14712954.

251. Reid CR, Latty T (2016) Collective behaviour and swarm intelligence in slime moulds. *FEMS Microbiology Reviews* **40**: 798–806. ISSN: 15746976.

252. Briard L, Goujarde C, Bousquet C, Dussutour A (2020) Stress signalling in acellular slime moulds and its detection by conspecifics: Stress detection in slime moulds. *Philosophical Transactions of the Royal Society B: Biological Sciences* **375**. ISSN: 14712970.

253. Moisy F *boxcount* `https://www.mathworks.com/matlabcentral/fileexchange/13063-boxcount`. Accessed: 2024-08-28. 2024.

254. Nakagaki T, Umemura S, Kakiuchi Y, Ueda T (1996) Action Spectrum for Sporulation and Photoavoidance in the Plasmodium of Physarum polycephalum, as Modified Differentially by Temperature and Starvation. *Photochemistry and Photobiology* **64**: 859–862. ISSN: 00318655.

255. Rusch H, Sachsenmaier W, Behrens K, Gruter V (1966) Synchronization of mitosis by the fusion of the plasmodia of Physarum polycephalum. *The Journal of cell biology* **31**: 204.

256. Jeffery WR, Rusch HP (1974) Induction of somatic fusion and heterokaryosis in two incompatible strains of Physarum polycephalum. *Developmental Biology* **39**: 331–335. ISSN: 00121606.

257. Albers T, Delnoij S, Schramma N, Jalaal M (2024) Billiards with Spatial Memory. *Physical Review Letters* **132**: 157101.

258. Schantz EJ, Lauffer MA (1962) Diffusion Measurements in Agar Gel. *Biochemistry* **1**: 658–663. ISSN: 15204995.